Fakultät für Medizin, Translationale Immuntherapie der III. Medizinischen Klinik am Klinikum rechts der Isar, Technische Universität München

Characterization of T-cell receptors for clinical translation

Stefan Audehm

Vollständiger Abdruck der von der Fakultät für Medizin der Technischen Universität München zur Erlangung des akademischen Grades eines Doktors der Naturwissenschaften (Dr. rer. nat.) genehmigten Dissertation.

Vorsitzender: Prof. Dr. Dirk Busch

Prüfende der Dissertation:

1. Prof. Dr. Angela Krackhardt
2. Prof. Dr. Aphrodite Kapurniotu

Die Dissertation wurde am 25.09.2019 bei der Technischen Universität München eingereicht und durch die Fakultät für Medizin am 10.03.2020 angenommen.

Summary

Among the immunotherapies, the adoptive T-cell transfer with immunoreceptor transgenic T cells has demonstrated high efficacy in tumor diseases. This becomes clear primarily through the use of chimeric antigen receptors (CAR) used to target B cell-derived tumors. While there are only a small number of different CARs is available, due to the lack of suitable target structures on various tumor cells, classic T-cell receptor (TCR) therapies have a great advantage. The working principle of TCR recognition of endogenously processed peptides derived from cellular proteins presented to the immune system by cell-surface major histocompatibility complexes (MHCs), allows a much higher number of potentially available TCRs compared to CARs. However, one of the biggest challenges is finding a TCR that is both highly effective and safe to use. To achieve this, both the TCRs and the corresponding target peptides on the MHCs have been assigned to a variety of characteristics, that might allow selecting TCRs potentially suitable for clinical translation. Since most of these characteristics were identified in the autologous system, this work aims to evaluate them by the most common and sophisticated methods applied for the allogeneic system. In order to propose a set of relevant and time-efficient preclinical methods to select for the most suitable allogeneic receptors, two TCRs recognizing different peptides derived from the differentiation antigen myeloperoxidase (MPO) with the same MHC restriction were compared to each other. Special attention was laid on surface expression, functional avidity, cytokine secretion, cytotoxicity, and TCR-peptide-MHC dissociation rates. Furthermore, the restricted peptide-MHC complexes (p-MHC) were examined in-vitro by stability experiments such as UV-mediated peptide exchange, differential fluorometry and by mass spectrometry. Finally, the p-MHC complexes were studied using sequence- and structure-based in-silico analyses. In summary, TCR-trans-

genic T cells showed considerable differences in their anti-tumor efficacy in mouse experiments which was not predictable by the displayed similar functional avidity, TCR-p-MHC dissociation rate, and cytotoxicity in-vitro. Substantial differences, however, were found in surface expression between both TCRs as well as cytokine secretion and cross-reactivity of TCR-transgenic T cells. Besides these three attributes, the p-MHC complex studies identified low peptide flexibility within the MHC binding pocket and high p-MHC affinity as the most important criteria for the selection of p-MHC combinations with the potential of clinical utility.

Zusammenfassung

Unter den Immuntherapien hat der adoptive T-Zelltranfer mit Immunrezeptor-transgenen T-Zellen bei Tumorerkrankungen eine hohe Wirksamkeit bewiesen. Dies ist vor allem durch den Einsatz von Chimären Antigen Rezeptoren (CAR) gegen B-Zell abgeleitete Tumorerkrankungen deutlich geworden. Während es hier, aufgrund fehlender geeigneter Zielstrukturen auf den Tumorzellen, nur eine geringe Zahl wirksamer CARs zur Bekämpfung von unterschiedlichsten Krebsarten gibt, haben klassische T-Zellrezeptoren (TCR) einen großen Vorteil. Durch ihr Funktionsprinzip, endogen prozessierte Peptide, die von zelleigenen Proteinen stammen und von Haupt-Histokompatibilitäts-Komplexen (MHC) auf der Zelloberfläche dem Immunsystem präsentiert werden, zu erkennen, ist die Anzahl potenziell möglicher TCRs im Vergleich zu den CARs um ein Vielfaches höher. Eine der größten Herausforderungen liegt jedoch darin, einen TCR zu finden, der gleichzeitig hoch wirksam und sicher in der Anwendung ist. Um dies zu erreichen, wurden sowohl den TCRs als auch den entsprechenden Zielpeptiden auf den MHCs in den letzten Jahrzehnten eine Vielzahl an Charakteristika zugewiesen, auf Basis derer ein TCR als potenziell erfolgreich für die klinische Translation eingeschätzt werden kann. Da diese Erkenntnisse überwiegend aus dem autologen System stammen, wurde in dieser Arbeit die Gültigkeit im allogenen System überprüft und ein Set geeigneter Methoden vorgeschlagen, mit deren Hilfe eine zielgerichtete und zeiteffiziente präklinische Charakterisierung von TCRs aus dem allogenen Repertoire durchgeführt werden kann. Hierzu wurden zwei TCRs ausgewählt, die unterschiedliche Peptidsequenzen aus dem Differenzierungsantigen Myeloperoxidase (MPO) mit gleicher MHC-Restriktion erkennen und zusammen mit deren Peptid-MHC Komplexe (p-MHC) sowohl in-vitro, in-vivo als auch in-silico untersucht. Besonderes Augenmerk lag dabei auf der Oberflächenexpression, funktioneller Avidität, Zytokinsekretion, Zytotoxizität und Dissoziierungsgeschwindigkeiten der TCR-Peptid-

MHC-Komplexe. Die MPO-p-MHC Komplexe wurden mittels verschiedener Stabilitätsexperimente wie UV-vermitteltem Peptid-Austausch und differenzieller Fluorometrie oder mit Hilfe der Massenspektrometrie experimentell untersucht. Abrundend wurden beide MPO-p-MHC Komplexe sowohl mit Sequenz- als auch mit Struktur-basierten in-silico Analysen charakterisiert. Zusammenfassend zeigt diese Arbeit, dass beide TCRs in Mausversuchen sehr beträchtliche Unterschiede in ihrer anti-Tumor-Effizienz zeigen und dies auf Basis nahezu identischer funktioneller Avidität, TCR-p-MHC Dissoziationsgeschwindigkeit und Zytotoxizität in-vitro nicht vorhersagbar gewesen wäre. Deutliche Unterschiede ergaben sich jedoch auf TCR-Seite in der Oberflächenexpression zwischen beiden TCRs, der Zytokinsekretion und Kreuzreaktivitätsprofil TCR-transgener T-Zellen, während sich bei den Untersuchungen der p-MHC Komplexe geringe Peptidflexibilität in der MHC-Bindungstasche bei gleichzeitiger hoher Affinität als aussagekräftige Kriterien für die Auswahl präklinisch geeigneter TCR-p-MHC Kombinationen herausstellten.

Table of Content

List of Abbreviations

APC	Allophycocyanin
BSA	Bovine serum albumin
CAR	Chimeric antigen receptor
CD	Cluster of Differentiation
CDR3	Complementary-determining region 3
CML	Chronic myeloid leukemia
DC	Dendritic cell
DEPC	Diethyl pyrocarbonate
DMEM	Dulbecco's Modified Eagle Medium
DMF	Dimethylformamide
DMSO	Dimethyl sulfoxide
DNA	Deoxyribonucleic acid
dNTP	Deoxynucleotide triphosphates
DsRed	Discosoma sp. red fluorescent protein
EBV	Epstein-Barr virus
EC_{50}	Half maximal effective concentration
EDTA	Ethylenediaminetetraacetic acid
EF	Endotoxin-free
ELISA	Enzyme-linked immunosorbent assay
FACS	Fluorescence-activated cell sorting
FCS	Fetal calf serum
FITC	Fluorescein isothiocyanate
GaLV	Gibbon Ape Leukemia Virus
GFP	Green fluorescent protein
GM-CSF	Granulocyte-macrophage colony-stimulating factor
GVHD	Graft-versus-Host disease
h	Hour
HEPES	2-[4-(2-hydroxyethyl)piperazin-1-yl]ethanesulfonic acid
HLA	Human leukocyte antigen
HRP	Horseradish peroxidase
HS	Human serum
IFN	Interferon
IL	Interleukin
LCL	Lymphoblastoid cell line
MHC	Major histocompatibility complex
min	Minute
ml	Milliliter
mM	Millimolar
MS	Mass spectrometry
nM	Nanomolar
P2A	Peptide 2A
PBMC	Peripheral blood mononuclear cells
PBS	Phosphate-Buffered Saline
PCR	Polymerase chain reaction
PE	Phycoerythrin
PFA	Paraformaldehyde
PI	Propidium Iodide
RNA	Ribonucleic acid
RPMI 1640	Roswell Park Memorial Institute 1640
RT	Room temperature
s	Second
TAA	Tumor-associated antigen
TAE	Tris-acetate-EDTA
TCR	T-cell receptor
TIL	Tumor-infiltrating lymphocytes
TNF	Tumor-necrosis factor

TRAC	T cell receptor alpha constant
TRBC	T cell receptor beta constant
Treg	Regulatory T cell
UV	Ultraviolet
V_{50}	Half-maximal temperature
7-AAD	7-Aminoactinomycin
µl	Microliter
µM	Micromolar

List of Tables

List of Figures

1 Introduction

1.1 Introduction

Within the last decades, adoptive cell therapies (ACT) using T cells evolved into a specific and potent treatment modality for a variety of patients. Since the beginning of treatment with tumor infiltrating lymphocytes [1], isolated from tumor material and expanded in-vitro, a well-defined and specific T-cell product can be administered in adoptive T-cell therapies today [2]. ACT mainly refer to treatments with lymphocytes, either modified [3-5] or unmodified [6-8] and to the treatment using antigen-presenting cells to fight various diseases either directly or to stimulate the recipient immune response, respectively. Thereby, ACT is often used in the background of stem cell transplantation to treat opportunistic viral [9, 10] and fungal infections [11], or to treat relapses [4].

T-cells, intended for the use in ACT modality, can be equipped with different kind of immune receptors to enhance specificity and to engage target cells presenting well-defined antigens. Regarding this, mainly two types of genetically engineered immune receptors are used to redirect T cells to their selected target antigen. The first type of immune receptors comprises chimeric antigen receptors (CAR) composed of different extracellular, antigen binding domains as e.g. single-chain variable-fragments from antibodies [12], membrane-tethered ligands [13] or camelid single-domain antibodies [14] fused to various intracellular domains that evolved over the last years [3, 15]. CARs are designed to recognize extracellular epitopes expressed on the surface of the cells. So far, CARs are mainly used for B-cell malignancies and with promising outcomes [3, 16-20].

In contrast, the second type of immune receptor used for T-cell engineering, the alpha-beta T-cell receptor, targets intracellular processed antigens derived from whole proteins presented as peptides (p) in an MHC (major histocompatibility complexes)-dependent

manner [21-23]. This antigen processing and presentation is one significant advantage of TCRs, since the whole pool of translated proteins with subsequent processing and surface presentation may serve as immunogenic target. The number of possible TCR-p-MHC combinations suitable for clinical application is a lot higher compared to potential CAR-antigen combinations [24]. A second major difference is the principle of target cell recognition. Whereas a CAR directly binds the epitope that is presented on the surface of the target cells, the TCR-based recognition relies on three components. These comprise the peptide, the peptide-presenting MHC molecule and the TCR itself, forming a tri-molecular complex to initiate the TCR-dependent immune response of T cells [25, 26]. Another advantage that becomes increasingly apparent as a critical point is the possibility to target also the tumor-promoting microenvironment via cross-presented and tumor-derived peptides on stroma cells by T cells [27, 28]. As a proof of clinical efficacy, TCR-engineered T cells were applied successfully in a number of clinical settings [29-33].

Concurrently, the countless number of possible TCR-p-MHC combinations and the proteasomal processing of proteins with p-MHC presentation in nearly all eukaryotic cells holds the risk of possible crossreactivity. Target or unrelated peptides can be presented on healthy tissues and may be recognized by TCRs leading to severe crossreactivity [34-36]. One possibility to minimize the risk of on- or off-target toxicities might be the usage of TCRs directed against peptides presented on MHCs derived from tumor-specific neoantigens [37-39].

However, the major challenge seems to be the choice of a target peptide with favorable characteristics which are proposed to be of fundamental importance for effective T-cell responses. Previous studies emphasize the importance of high peptide-MHC affinity [27], optimal peptide length [40], superior peptide-mediated MHC-stability [41] or simply a confirmed cell surface presentation [39, 42-45]. Optimal combinations thereof may have

synergistic effects for enhanced presentation levels of targeted p-MHC epitopes and therefore may lead to more potent T-cell responses.

1.2 T cells equipped with engineered immune receptors

Both types of immune receptors mentioned above are mainly introduced into T-lymphocytes by either retro- or lentiviral transfer [5, 46], or applying transposon technology [47]. However, new methodologies for site-directed gene transfer using the CRISPR/Cas technique are available to insert the CAR- or TCR-coding sequence directly into the endogenous TCR-gene locus [48, 49] to disrupt endogenous TCR expression and thereby potentially preventing TCR mispairing and related crossreactivity. Besides safety aspects regarding side-directed CAR- and TCR-sequence integration via CRISPR/Cas versus random genome integration using viral vectors [50], the engineered TCR expression levels also seems to be influenced by the endogenous TCR because of competition for free available CD3 complexes between both TCR [51]. In some cases, the expression quality is also determined by the respective dominance potential of the introduced TCR [52].

1.3 Identification of suitable TCR for engineered T-cell therapy

1.3.1 Where antigen-specific T cells can be found

One approach, on which this work is based, uses mature dendritic cells from healthy donors electroporated with in-vitro transcribed RNA encoding for a desired allogeneic MHC. Together with external pulsing of the peptide of interest, T cells with matching TCRs are primed and stimulated for clonal expansion [43, 53]. Although this approach can be a source for the identification of high affinity and tumor-antigen specific TCRs, it is often difficult to separate specific T-cell candidates from T cells that are bearing TCRs

with unspecific recognition of allogeneic MHC irrespective of the peptide of interest. Searching for TCR in the autologous background can eliminate this MHC alloreactivity but often lead to only low or intermediate affinity TCRs because of intra-thymic T-cell elimination of high-affinity αβ-TCRs to avoid self-reactive T cells [54]. In general, gene therapies using autologous TCRs are very often hindered because of missing expression of common tumor-derived self-antigens [55] spread over patient cohorts. Additionally, promising TCRs including neoepitope specific TCRs have been directly identified within cancer patients [39, 56]. Murine TCRs, discovered on T cells in HLA-A2-transgenic mice that have been immunized with potential target peptides derived from p53 and tumor-associated antigen gp100, have also been used for T-cell engineering [57]. However, TCRs of murine background are potentially prone to elicit antibody- or T-cell related responses against the murine variable chains of the transgenic TCR in some patients [58]. To avoid the recognition of murine transgenic TCR by the host immune system, an improved murine approach leading to fully human variable TCR chains was established in HLA-A*02:01-transgenic mice carrying the human T-cell repertoire [59].

1.3.2 Immunopeptidomic approach to find peptide candidates

Although in-silico tools are available to predict potential T-cell epitopes from proteins [60, 61], the risk remains that the predicted peptide of interest is not presented on the surface of the target cells [62] because the proteasome composition or the protein sequence itself may not allow processing that will result in the desired peptide sequence. Immunopeptidomics, however, directly identifies HLA-bound peptides by mass spectrometry after elution of peptides from HLA complexes that have been precipitated out of target cell lysates [63]. Since first approaches for immune proteome characterization were available, the field was extensively improved and is nowadays even proficient to

directly detect neoepitopes on patients' tumor material [39, 64]. However, direct quantification of peptide presentation levels on target cells remains challenging because of individual side chain characteristics of amino acids. The quantification of peptide presentation would be beneficial for instance to determine minimal peptide presentation levels on tumor cells necessary for efficient T-cell responses. Unfortunately, methods for peptide and protein quantifications lacks behind the quantification of small molecules using mass spectrometry [65].

1.3.3 How suitable peptide candidates can be estimated

Even if immunopeptidomics is applied to ensure that peptides are indeed presented on the surface of the target cell, the list of identified peptide candidates might be very long. Therefore, a proper filter strategy is needed to consolidate the list to the most promising peptide candidates. The reduction of peptide candidates is often achieved by focusing on the most frequent HLA alleles present in the population and the length of the peptides, typically comprising eight to eleven amino acids. Following this, very often sequence-based peptide-MHC binding affinity predictions based on artificial neural networks is performed to select for peptides with the best binding characteristics [66-68] or the highest scores calculated by specific sequence motifs [69]. Historically, even complex scoring matrices were used to predict sequence-based binding affinities [70]. However, the most sophisticated algorithms using statistic- and sequence-based algorithms [71-73] might have limitations because the quality often depends on available experimental results used to train underlying algorithms. Therefore, the prediction results might be biased by the available data set [74]. To be independent of extensive experimental data sets for algorithm training that are only available for those MHC-alleles that have a higher prevalence in the population, and to get more insight in peptide-MHC binding, structure-based predictions are increasingly being used. Currently used approaches for p-MHC modeling and

structure-based binding affinity [75] are promising tools to get insights into the molecular basis of peptide binding to MHC molecules and, if combined with experimental in-vitro results in interdisciplinary approaches, to estimate immunogenicity of TCR-mediated T-cell responses.

1.3.4 How suitable TCR candidates can be selected

A lot of criteria and qualities have been proposed to be crucial for TCRs to be suitable for concurrent effective and safe T-cell responses. Functional T-cell avidity and TCR affinity, mainly tested in co-incubation assays with titrated amounts of peptides pulsed on target cells [76, 77] and sophisticated k_{on} and k_{off} analyses of TCR-p-MHC complexes [78-81], respectively, are described to be of utmost importance [82-85]. Thereby, the balance between too high or too low avidity seems to be important to induce adequate TCR-mediated T-cell responses. It was discovered that T cells with high-affinity TCRs need less peptide-MHC complexes for stimulation or proliferation [82, 86]. However, if TCR affinity exceeds a tolerable level and displays superior binding characteristics, there might be a high risk for off-target toxicity [34, 36]. In contrast, low avidity TCRs may proliferate well and exert cytotoxicity in-vitro but seem to be inferior in reactivity as shown for viral infections in-vivo [82, 87].

1.3.5 How TCR mediated crossreactivity can be assessed

Crossreactivity is an important aspect of TCR characterization. Even if a superior target peptide with sufficient expression was found, and its presentation is limited to tumor cells, a risk of TCR-related crossreactivity can remain because of slight flexibility within the CDR-domains of the TCR [88] also known as TCR degeneracy for peptides [89] that might lead to off-target toxicity. Very often a screening of randomly chosen peptides with

144 known MHC restriction is performed to estimate the recognition of the p-MHC com-
145 plexes by the TCR [43]. Another screening approach for highly similar peptides uses
146 amino acid exchanges within the target peptide sequence [90]. This approach is concur-
147 rent able to identify the TCR binding motif [43, 91] and to reveal possible crossreactivity
148 [34-36, 92]. Evaluating whether the TCR candidate also recognizes further MHC-alleles,
149 a library of immortalized lymphoblastoid B-cell lines with various MHC expression is
150 frequently applied [43, 93, 94].

151

1.3 Aim of this study

There is a considerable gap between the promise of immunotherapies using TCR-transgenic T cells in adoptive T-cell transfer and the time necessary to identify concurrent safe and effective TCR as well as target epitopes suitable for clinical translation. The personalization of this therapeutic approach is high since TCR are restricted to a high diversity of human leukocyte antigens and may only target antigens relevant for one specific cancer type or even a single tumor. Many assays for epitope- and TCR-characterization have been proposed in the autologous self-restricted setting. The selection process for MHC-mismatched TCR, however, is less well defined and specific features of TCR-MHC-peptide interaction need to be considered. Nevertheless, especially this approach provides access to non-selected TCR repertoires with highly tumor reactive TCR. Therefore, within this work, the selection criteria for both epitope candidates and respective allorestricted TCR are questioned and a timely workflow for the process of development is proposed.

2 Materials and Methods

2.1 Materials

2.1.1 Technical equipment

Table 1: Technical equipment

Device or Unit	Manufacturer
Electrophoresis chamber	G&P Kunststofftechnik, Kassel, Germany
Electrophoresis power supply	VWR, Darmstadt, Germany
Centrifuge 5810R	Eppendorf AG, Hamburg, Germany
Centrifuge J2-HS	Beckman Coulter, Brea, USA
Centrifuge 5417R	Eppendorf AG, Hamburg, Germany
Axiovert 40C microscope	Carl Zeiss Microscopy, Oberkochen, Germany
Analytical balance SI-64	Denver Instrument, Göttingen, Germany
Analytical balance 440-35N	Denver Instrument, Göttingen, Germany
Cytometer LSRII	BD Bioscience, Franklin Lakes, USA
Laminar Flow HERAsafe	Heraeus Holding, Hanau, Germany
Irradiation Cabinet	Gulmay, Byfleet, UK
Incubator BBD6220	Heraeus Holding, Hanau, Germany
-80°C Freezer	Buchner Labortechnik, Pfaffenhofen, Germany
-20°C Freezer	Liebherr-International AG, Bulle, Switzerland
Megafuge 1.0R	DJB Labcare Ltd, Buckinghamshire, UK
Magnet stirrer	Janke & Kunkel, Staufen, Germany
Tube rotator MACSmix	Miltenyi Biotec, Bergisch Gladbach, Germany
Vortex-Genie 2	Scientific Industries, Inc., Bohemia, New York, USA
Thermomixer comfort for 1.5-2.0 ml tubes	Eppendorf AG, Hamburg, Germany
Biometra T professional gradient Thermocycler	Biometra, Göttingen, Germany
StepOnePlus Real-Time PCR System	Applied Biosystems, life technologies, Carlsbad, USA
Pipetboy/Pipetgirl INTEGRA	Biosciences, Fernwald, Germany
Neubauer Counting Chamber	Karl Hecht, Sondheim/Röhn, Germany
Acura® manual 855, multichannel micropipettes (20µl-200µl)	Socorex Isba S.A., Switzerland
NanoDrop ND-100	Peqlab Biotechnologie, Erlangen, Germany
Pipettes (0,5µl-1000µl), multichannel micropipettes (20µl-200µl)	Eppendorf AG, Hamburg, Germany
High-performance cell sorter MoFlo	Dako, Agilent Technologies, Glostrup, Denmark

Separator MidiMACS TM	Miltenyi Biotec, Bergisch Gladbach, Germany
Sunrise 96-well Microplate Reader	Tecan, Männedorf, Switzerland
Peptide synthesizer ResPepMicroScale	Intavis AG Bioanalytical instruments, Cologne, Germany
Nano-flow UHPLC EASY-nLC 1200 system	Thermo Fisher Scientific, Waltham, Massachusetts, USA
Nanoelectrospray unit	Thermo Fisher Scientific, Waltham, Massachusetts, USA
Mass spectrometer Q Exactive HF-X	Thermo Fisher Scientific, Waltham, Massachusetts, USA
UV hand lamp	Köhler Technische Produkte, Neulußheim, Germany
Digital incubators, INCU-Line®	VWR, Darmstadt, Germany
Innova 4000 Benchtop Incubator Shaker	New Brunswick Scientific, Enfield, CT, USA
Electroporation Systems Gene Pulser Xcell™ + CE module	Bio-Rad Laboratories GmbH, Munich, Germany
Cryogenic storage systems BIOSAFE®-MD	Cryotherm GmbH & Co. KG, Kirchen/Sieg, Germany
Centrifuge Avanti J-E	Beckman Coulter GmbH, Krefeld, Germany
Waterbath WNB	Memmert GmbH & Co. KG, Schwabach, Germany
Plate shaker Titramax 1000	Heidolph Instruments GmbH & CO. KG, Schwabach, Germany
Micro scales Balance summit	Denver Instrument, Göttingen, Germany

171

172 2.1.2 Consumables

173 **Table 2: Consumables**

Consumables	**Company**
Pipet tips: 10µl, 100ml, 200µl, 1000µl	Sarstedt, Nümbrecht, Germany
Parafilm	Pechiney Plastic Packaging, Inc., Chicago, USA
Freezing Container, Mr. Frosty™	Nunc, Roskilde, Denmark
Gloves nitrile	KCL, Eichenzell, Germany
Gloves Latex	Sempermed, Wien, Austria
Tubes 15 ml, 50 ml	BD Bioscience, Franklin Lakes, USA
Cell culture flask	Greiner Bio-One, Frickenhausen, Germany
Inoculating loops, PS	VWR, Darmstadt, Germany
Serological pipets (2,5,10,25,50ml)	Sarstedt, Nümbrecht, Germany
Nunc-Immuno™ MicroWell™ MaxiSorp™ flat bottom plate 96 well solid plates	Nunc, Roskilde, Denmark
Filter tips: 10µl, 100µl, 200µl, 1000µl	Sarstedt, Nümbrecht, Germany
Cell separation Columns MACS LD, LS	Miltenyi Biotec, Bergisch Gladbach, Germany
Cell scraper PE 300 mm	TPP Techno Plastic Products, Trasadingen, Switzerland
Nunclon® Δ surface treatment flasks	Nunc, Roskilde, Denmark
MicroAmp™ Fast Optical 96-Well Reaction Plate with Bar-code, 0,1 mL	Thermo Fisher Scientific, Waltham, MA, USA

CryoPure tube: 1,6 ml	Sarstedt, Nümbrecht, Germany
Syringe filter: 0,22µm, 0.45µm	TPP Techno Plastic Products, Trasadingen, Switzerland
Stericup Vacuum Filter Units 0,22µm	Merck Millipore, Darmstadt, Germany
Not Treated Multiple Well Plates: 6, 24 well	BD Bioscience, Franklin Lakes, USA
Reaction tubes: 1.5µl, 2ml	Sarstedt, Nümbrecht, Germany
PCR Reaction tubes: 0.5µl	Peqlab Biotechnologie, Erlangen, Germany
Tissue culture plates, 96, 48, 24, 12, 6 well, round/flat bottom	TPP Techno Plastic products, Trasadingen, Switzerland
Cell strainer 40µm, 100µm	BD Bioscience, Franklin Lakes, USA
Syringe: 5ml, 10ml, 50ml	BD Bioscience, Franklin Lakes, USA
MaxiSorp™ flat-bottom 96 well plate	Nunc, Roskilde, Denmark
Sub_Q syringe 1 ml	BD Bioscience, Franklin Lakes, USA
Sealing Foil	Alpha laboratories, Hampshire, UK
Tubes for flow cytometry, round bottom	BD Bioscience, Franklin Lakes, USA
Petri dishes	Greiner Bio-One, Frickenhausen, Germany

2.1.3 Reagents

Table 3: Reagents

Reagents	**Company**
DNA ladder: 100bp, 1 kb	New England Biolabs, Ipswich, UK
7-Aminoactinomycine D	Merck, Darmstadt, Germany
Gel loading dye 6x	Fermentas, St.Leon-Rot, Germany
Agarose standard	Roth, Karlsruhe, Germany
AIM-V medium	Invitrogen, Carlsbad, USA
Ampicillin	Merck, Darmstadt, Germany
Bovine serum albumine (BSA)	Merck, Darmstadt, Germany
ACK lysis buffer	ThermoFisher Scientific, Waltham, USA
DEPC-H2O	Invitrogen, Carlsbad, USA
1,4 Dithiothreitol	Merck, Darmstadt, Germany
DMEM medium	Invitrogen, Carlsbad, USA
VLE-RPMI	Merck, Darmstadt, Germany
DMSO (Dimethylsulfoxide)	Merck, Darmstadt, Germany
PBS (Phosphate buffered saline)	Invitrogen, Carlsbad, USA
EDTA (Ethylenediaminetetraacetic acid)	Invitrogen, Carlsbad, USA
Ethanol	Merck, Darmstadt, Germany
Ethidium bromide	Roth, Karlsruhe, Germany

Fetal bovine serum, heat inactivated (FCS)	Invitrogen, Carlsbad, USA
Ficoll	Biochrom, Berlin, Germany
DNA ladder Gene Ruler 1 kb	PeqLab, Erlangen, Germany
Gentamicin	Merck, Darmstadt, Germany
RNase out	Invitrogen, Carlsbad, USA
Sulfuric acid (H2SO4)	Roth, Karlsruhe, Germany
HBSS (Hank's Balanced Salt Solution)	Invitrogen, Carlsbad, USA
HEPES (Hydroxyethylpiperazine ethane sulfonic acid)	Invitrogen, Carlsbad, USA
Human serum, heat inactivated (HS)	TU Munich, München, Germany
Isoflurane	CP-Pharma, Burgdorf, Germany
Penicillin	Invitrogen, Carlsbad, USA
Streptomycin	Invitrogen, Carlsbad, USA
OneShot TOP10 bacteria	Invitrogen, Carlsbad, USA
Streptavidin	Sigma Aldrich, St. Louis, USA
NEB5α bacteria	New England Biolabs, Ipswich, UK
Non-essential amino-acids	Invitrogen, Carlsbad, USA
Sodium azide	Merck, Darmstadt, Germany
Sodium chloride	Merck, Darmstadt, Germany
Mycophenolic acid	Merck, Darmstadt, Germany
L-Glutamine	Invitrogen, Carlsbad, USA
LB Broth Base	Invitrogen, Carlsbad, USA
LB Agar	Invitrogen, Carlsbad, USA
Kanamycin	Merck, Darmstadt, Germany
2-propanol	Merck, Darmstadt, Germany
Trypan blue solution 0.4%	Merck, Darmstadt, Germany
Tween® 20	Merck, Darmstadt, Germany
Trypsine EDTA: 0.5%	PAA laboratories, Pasching, Austria
Transfection Reagent TransIT	Mirus, Madison, USA
Sodium pyruvate	Invitrogen, Carlsbad, USA
SOC outgrowth medium	New England Biolabs, Ipswich, UK
RPMI medium	Invitrogen, Carlsbad, USA
RNase Out	Invitrogen, Carlsbad, USA
Retronectin	Takara, Kusatsu, Japan
Restriction enzymes	New England Biolabs, Ipswich, UK
Proteinase K	GeneAll Biotechnology, Seoul, Korea
Protamine sulfate	MP Biomedicals, Illkirch, France
Paraformaldehyde (PFA)	Merck, Darmstadt, Germany
Skim milk powder	Merck, Darmstadt, Germany
SYPRO® Orange	Merck, Darmstadt, Germany

Restriction enzymes	New England Biolabs, Ipswich, UK

2.1.4 Antibodies and HLA-Multimers

Table 4: Antibody and HLA-multimers

Antibody	Clone and Isotype	Company/Manufacturer
anti-hCD3	UCHT-1 mIgG1 κ	BD Bioscience, Franklin Lakes, USA
anti-hCD137	4B4-1 mIgG1, κ	BD Bioscience, Franklin Lakes, USA
anti-hCD4	RPA-T4 mIgG1 κ	BD Bioscience, Franklin Lakes, USA
anti-hCD45	J.33 mIgG1	Beckman Coulter, Krefeld, Germany
anti-hCD45RA	HI100 mIgG2b κ	BD Bioscience, Franklin Lakes, USA
anti-mTCR β	H57-597 Armenian Hamster IgG2, λ1	BD Bioscience, Franklin Lakes, USA
anti-human β Mark TCR Vβ Repertoire		Beckman Coulter, Krefeld, Germany
anti-hCD45RO	UCHL1 mIgG2 κ	BD Bioscience, Franklin Lakes, USA
anti-hCD5	BL1a mIgG2a	Beckman Coulter, Krefeld, Germany
anti-hCD62L	DREG-56 mIgG1 κ	BD Bioscience, Franklin Lakes, USA
anti-hCD8	RPA-T8 mIgG1 κ	BD Bioscience, Franklin Lakes, USA
anti-mTCRb	H57-597 hamster IgG2 λ1	BD Bioscience, Franklin Lakes, USA
anti-HLA-B*07	BB7.1 mIgG1, κ	BioLegend, San Diego, USA
anti-HLA-ABC	W6/32 IgG2a, κ	BioLegend, San Diego, USA
anti-hCD80	L307.4 C3H/Bi IgG1, κ	BD Bioscience, Franklin Lakes, USA
anti-hCD86	2331 mIgG1, κ	BD Bioscience, Franklin Lakes, USA
anti-mouse CD16/32	clone 93	BioLegend, San Diego, USA
anti-beta two microglobulin HRP	polyclonal	Thermo Fisher Scientific, Rockford, USA
Isotypes for mIgG1 κ Abs.		BD Bioscience, Franklin Lakes, USA
Isotype for mIgG2b κ Abs.		BD Bioscience, Franklin Lakes, USA
Isotype for IgG2, λ1		BD Bioscience, Franklin Lakes, USA
Isotype for mIgG2 κ		BD Bioscience, Franklin Lakes, USA
Isotype for mIgG2a		Beckman Coulter, Krefeld, Germany
MPO_{145}-TPAQLNVL-HLA Multimer-PE	HLA-allele B*07:02	D.H. Busch, MRI Munich, Germany
Myb272-VPQPAAAAI-HLA Multimer-PE	HLA-allele B*07:02	D.H. Busch, MRI Munich, Germany

2.1.5 Cytokines, TLR ligands, Prostaglandins, Growth Factors for Cell Culture

Table 5: Cytokines, TLR ligands, prostaglandins, growth factors

Cytokine	Company
human TNF-α	Peprotech, Hamburg, Germany
human IL1-β	Peprotech, Hamburg, Germany
human IFN-γ	Peprotech, Hamburg, Germany
human IL-4	Peprotech, Hamburg, Germany
human GM-CSF	Peprotech, Hamburg, Germany
human IL-7	Peprotech, Hamburg, Germany
human IL-15	Peprotech, Hamburg, Germany
CL075	InvivoGen, San Diego, USA
FLT3LG	Peprotech, Hamburg, Germany
SCF (Stem cell factor)	Peprotech, Hamburg, Germany
PGE2 (Prostaglandine E2)	Merck, Darmstadt, Germany

181 2.1.6 Biochemical Assay Kits

182 **Table 6: Biochemical kits**

Kit	Company
Dynabeads UntouchedTM CD8+	Invitrogen, Carlsbad, USA
HotstarTaq MasterMix Kit Plus	Qiagen, Hilden, Germany
KOD Hot Start Polymerase Kit	Merck, Darmstadt, Germany
Human CD45RO Micro Beads	Miltenyi Biotech, Bergisch Gladbach, Germany
Human CD57 MicroBeads	Miltenyi Biotech, Bergisch Gladbach, Germany
JETSTAR 2.0 Plasmid Purification Kit	Genomed, Löhne, Germany
NucleoSpin Gel and PCR Clean-up	Macherey-Nagel, Düren, Germany
mMESSAGE mMACHINE T7	Invitrogen, Carlsbad, Germany
Poly(A) Tailing Kit	Invitrogen, Carlsbad, Germany
RNeasy Mini Kit	Qiagen, Hilden, Germany
Wizard Genomic DNA Purification Kit	Promega, Madison, USA
Human IFN-γ ELISA Set	BD Bioscience, Franklin Lakes, USA
Human TNF ELISA Set	BD Bioscience, Franklin Lakes, USA
Human IL-2 ELISA Set	BD Bioscience, Franklin Lakes, USA
Human MACSPlex Cytokine 12 Kit	Miltenyi Biotech, Bergisch Gladbach, Germany
TMB Substrate Reagent Set	BD Bioscience, Franklin Lakes, USA
PerfeCTa SYBR Green FastMix ROX	QuantaBio, Beverly, MA, USA
PerfeCTa FastMix II ROX	QuantaBio, Beverly, MA, USA
AffinityScript Multiple Temperature cDNA Synthesis Kit	Agilent Technologies, Santa Clara, USA
DNA blood and tissue kit	QIAGEN GmbH, Hilden, Germany

Intracellular Fixation & Permeabilization Buffer Set	Thermo Fisher Scientific, Waltham, USA
Human total RNA Master Panel II	Clontech Laboratories, Inc., Mountain View, USA
NEB® 5-alpha Competent E. coli	New England BioLabs Inc., Frankfurt am Main, Germany
NucleoBond® Xtra Maxi EF	MACHEREY-NAGEL GmbH & Co. KG, Düren, Germany
Nucleospin Gel and PCR Cleanup kit	MACHEREY-NAGEL GmbH & Co. KG, Düren, Germany
RNeasy Mini Kit	QIAGEN GmbH, Hilden, Germany

2.1.7 Buffer and Solutions

Table 7: Buffer and solutions

Buffer	Additives
FACS buffer for flow cytometry	PBS, 1% FCS
Fixation buffer	2% Paraformaldehyde
ELISA Coating buffer	100 mM NaHCO3, 30 mM Na2CO3 in H2O, pH 9.5
ELISA washing buffer	PBS, 0.02% v/v Tween®20
ELISA blocking solution	PBS, 1 % v/v Skim milk powder
ACK Lysis buffer for lysis of erythrocytes	150 mM NH4Cl, 10 mM KHCO3, 0.1 mM EDTA in H2O
10xTAE buffer for DNA gel electrophoresis	0.4 mM Tris-HCl, pH 7.8
heat inactivated FCS and human serum	20'min, 58°C
Central memory T-cell isolation buffer	PBS, 2% BSA, 2 mM EDTA
Retronectin buffer for transduction	PBS, 12 µg/ml RetroNectin

2.1.8 Cell Culture Media

Table 8: Cell culture media

Medium	Composition
cRPMI	RPMI supplemented with Penicillin/Streptomycin (100 IU/ml), Sodium pyruvate (1 mM), L-Glutamine (2 mM), non-essential amino-acids (10 mM) and 10% (v/v) Fetal bovine serum
cDMEM	DMEM supplemented with Penicillin/Streptomycin (100 IU/ml), Sodium pyruvate (1 mM), L-Glutamine (2 mM), non-essential amino-acids (10 mM) and 10% (v/v) Fetal bovine serum
T-cell medium (0,22 µm filtered)	RPMI supplemented with Penicillin/Streptomycin (100 IU/ml), Gentamicin (16 µg/ml), Sodium pyruvate (1 mM), L-Glutamine (2 mM), non-essential amino-acids (10 mM), 5% (v/v) Fetal bovine serum and 5% (v/v) Human serum
Dendritic cell medium (DCM) (primary)	VLE-RPMI supplemented with 1,5% human serum
DC-medium I	VLE-RPMI supplemented with 1,5% human serum, IL-4 20 ng/ml, GM-CSF 100ng/ml

DC-medium II	VLE-RPMI supplemented with 1,5% human serum, TNF-alpha 10 ng/ml, IL1-beta 10 ng/ml, IFN-gamma 5000 IU/ml PGE2 250 ng/ml, CL075 1 µg/ml, IL-4 20 ng/ml, GM-CSF 100 ng/ml
Freezing medium	Fetal bovine serum with 10% DMSO

2.1.9 Cell Lines and Primary Cells

Table 9: Cell lines

Cell line	Culture medium	Disease / transformed	Origin
HL60	cRPMI	APL	CLS, Eppelheim, Germany
NB4	cRPMI	APL	CLS, Eppelheim, Germany
ML2	cRPMI	AML	The Cabri consortium
MV4-11	cRPMI	AML	CLS, Eppelheim, Germany
SiG-M5	cRPMI	AML	DMSZ, Braunschweig, Germany
UT7	cRPMI	AML	DMSZ, Braunschweig, Germany
LAMA84	cRPMI	CML	DMSZ, Braunschweig, Germany
K562	cRPMI	CML	ATCC, Manassas, USA
BJAB	cRPMI	Burkitt lymphoma	J. Mautner, München, Germany
C1R	cRPMI	EBV-transformed	S. Stevanović, Tübingen, Germany
Molt4	cRPMI	T-ALL	CLS, Eppelheim, Germany
NSO-IL-15	cRPMI	Mouse myeloma	S. Riddell, Seattle, USA
KG-1a	cRPMI	AML	CLS, Eppelheim, Germany
SET2	cRPMI	AML	DMSZ, Braunschweig, Germany
293Vec-RD114	cDMEM	Human embryonic kidney cells	Biovec pharma, Québec, Canada
T2	cRPMI	T-B-Lymphoblast (hybrid)	ATCC, Manassas, USA
MV4-11	cRPMI	AML	CLS, Eppelheim, Germany
Jurkat, clone E6-1	cRPMI	Acute T-cell leukemia	AG Ruland, MRI, München, Germany

Table 10: HLA-typing of Lymphoblastoid cell lines (LCL)

LCL cell line	HLA-A*	HLA-B*
AMALA	02:17/ --	15:01/ --
BM21	01:01/ --	41:01/ --
DKB	24:02/ --	40:01 / --
DUCAF	30:02 / --	18:01 / --
HOM2	03:01/ --	27:05/ --
JNB3	01/02:01	07/40:01
KLO	02:08/ --	50:01/08:01
LSKB1	01/02	07/08
LWAGS	33:01/ --	14:02/ --
MaOe	02:01/ --	07:02/15:01

OZB	02:09/03:01	35:01/38:01
RML	02:04/ --	51:01/ --
RSH	68:02/30:01	42:01/ --
SWEIG007	29:02/ --	40:02/ --
XLIND	02:10 /30	13/61

Table 11: Primary cell lines

Cells	Culture medium	Origin
PBMC	TCM	Healthy donors
Dendritic cells	DCM (basic, day 0, day 2)	Healthy donors
T lymphocytes	TCM	Healthy donors
PBMC from CML patients	TCM	CML patients

2.1.11 Primers

All primers were synthesized and delivered lyophilized by Sigma-Aldrich (Merck), Germany and dissolved in DEPC water to a final concentration of 100 µM. Table 12 lists all primer sequences in 5'→ 3' direction.

Table 12: TCRVA and TCRVB primer

T-cell receptor variable alpha (TCRVA) primer		T-cell receptor variable beta (TCRVB) primer	
Primer	**Sequence**	**Primer**	**Sequence**
P-5'aST	CTGTGCTAGACATGAGGTCT	**5bST**	AAGCAGAGATCTCCCACAC
P-3'aST	CTTGCCTCTGCCGTGAATGT	**P-3bST**	GAGGTGAAGCCACAGTCTG
3'T-Ca	GGTGAATAGGCAGACAGACTTGTCACTGGA	**P-3CbII**	GATGGCTCAAACACAGCGACCTC
Va1	AGAGCCCAGTCTGTGASCCAG S=C/G	**Vb1**	GCACAACAGTTCCCTGACTTGGCAC
Va1.1	AGAGCCCAGTCRGTGACCCAG R=A/G	**Vb2**	TCATCAACCATGCAAGCCTGACCT
Va2	GTTTGGAGCCAACRGAAGGAG	**Vb3**	GTCTCTAGAGAGAAGAAGGAGCGC
Va3	GGTGAACAGTCAACAGGGAGA	**Vb4**	ACATATGAGAGTGGATTTGTCATT
Va4	TGATGCTAAGACCACMCAGC	**Vb5.1**	ATACTTCAGTGAGACACAGAGAAAC
Va5	GGCCCTGAACATTCAGGA	**Vb5.2**	TTCCCTAACTATAGCTCTGAGCTG
Va6	GGTCACAGCTTCACTGTGGCTA	**Vb6.1**	GCCCAGAGTTTCTGACTTACTTC
Va7	ATGTTTCCATGAAGATGGGAG	**Vb7**	CCTGAATGCCCCAACAGCTCTC
Va8	TGTGGCTGCAGGTGGACT	**Vb8**	ATTTACTTTAACAACAACGTTCCG
Va9	ATCTCAGTGCTTGTGATAATA	**Vb9**	CCTAAATCTCCAGACAAAGCT
Va10	ACCCAGCTGCTGGAGCAGAGCCCT	**Vb10**	CTCCAAAAACTCATCCTGTACCTT
Va11	AGAAAGCAAGGACCAAGTGTT	**Vb11**	TCAACAGTCTCCAGAATAAGGACG

Va12	CAGAAGGTAACTCAAGCGCAGACT	**Vb12**	AAAGGAGAAGTCTCAGAT
Va13	GAGCCAATTCCACGCTGCG	**Vb13.1**	CAAGGAGAAGTCCCCAAT
Va14	CAGTCTCAACCAGAGATGTC	**Vb13.2**	GGTGAGGGTACAACTGCC
Va14.1	CAGTCCCAGCCAGAGATGTC	**Vb14**	GTCTCTCGAAAAGAGAAGAGGAAT
Va15	GATGTGGAGCAGAGTCTTTTC	**Vb15**	AGTGTCTCTCGACAGGCACAGGCT
Va16	TCAGCGGAAGATCAGGTCAAC	**Vb16**	AAAGAGTCTAAACAGGATGAGTCC
Va17	GCTTATGAGAACACTGCGT	**Vb17**	CAGATAGTAAATGACTTTCAG
Va18	GCAGCTTCCCTTCCAGCAAT	**Vb18**	GATGAGTCAGGAATGCCAAAGGAA
Va19	AGAACCTGACTGCCCAGGAA	**Vb19**	CAATGCCCCAAGAACGCACCCTGC
Va20	CATCTCCATGGACTCATATGA	**Vb20**	AGCTCTGAGGTGCCCCAGAATCTC
Va21	GTGACTATACTAACAGCATGT	**Vb21**	AAAGGAGTAGACTCCACTCTC
Va22	TACACAGCCACAGGATACCCTTCC	**Vb22.1**	CATCTCTAATCACTTATACT
Va23	TGACACAGATTCCTGCAGCTC	**Vb23**	GCAGGGTCCAGGTCAGGACCCCCA
Va24	GAACTGCACTCTTCAATGC	**Vb24**	ATCCAGGAGGCCGAACACTTCT
Va25	ATCAGAGTCCTCAATCTATGTTTA		
Va26	AGAGGGAAAGAATCTCACCATAA		
Va27	ACCCTCTGTTCCTGAGCATG		
Va28	CAAAGCCCTCTATCTCTGGTT		
Va29	AGGGGAAGATGCTGTCACCA		
Va30	GAGGGAGAGAGTAGCAGT		
Va31	TCGGAGGGAGCATCTGTGACTA		
Va32	CAAATTCCTCAGTACCAGCA		

198 **Table 13: Primer for cloning, sequencing and real-time PCR**

Primer	Sequence	Application
MP71 fwd	TGAAAATTAGCTCGACAAAG	Sequencing of inserts in MP71
MP71 rev	GTAAATGATTGCCCCACCA	Sequencing of inserts in MP71
cloning Va2 F5.4 fwd	TAGCGGCCGCCACCATGATGAAATCCTTGAGAGT	Cloning of TCRF5.4 alpha domain
cloning Va2 F5.4 rev	TAGAATTCTCAGCTGGACCACAGCCGCA	Cloning of TCRF5.4 alpha domain
cloning Vb1 F5.4 fwd	TAGCGGCCGCCACCATGGGCTTCAGGCTCCTCTG	Cloning of TCRF5.4 beta domain
cloning Vb1 F5.4 rev	TAGAATTCCTAGCCTCTGGAATCCTTTC	Cloning of TCRF5.4 beta domain
F5.4om fwd	TAGCGGCCGCCACCATGGGATTTCGCCTGCTGTG	Codon optimized, murinized TCRF5.4
F5.4om rev	TAGAATTCTTAGGAGGACCACAGCCGCA	Codon optimized, murinized TCRF5.4
PSMB8 fwd	GATCTCCAGAGCTCGCTTTA	real-time PCR
PSMB8 rev	GTTCACCCGTAAGGCACTAA	real-time PCR
PSMB9 fwd	CTTGTCTGCACATCTCATGG	real-time PCR
PSMB9 rev	AATAGCGTCTGTGGTGAAGC	real-time PCR

PSMB10 fwd	CGAGAACTGCCAAAGAAATG	real-time PCR
PSMB10 rev	ATCTTCTCGCAGCTCTTGTC	real-time PCR
GAPDH fwd	GGAGCCAAAAGGGTCATCATCTC	real-time PCR
GAPDH rev	GGCCATCACGCCACAGTTTC	real-time PCR
HMBS fwd	AGGATGGGCAACTGTACCTG	real-time PCR
HMBS rev	TCGTGGAATGTTAACGAGCAG	real-time PCR
HPRT1 fwd	AAGCTTGCTGGTGAAAAGGAA	real-time PCR
HPRT1 rev	AAGCAGATGGCCACAGAACT	real-time PCR
NotI Kozak MPO_{145} Mini gene start	TACAGGCGGCCGCCACCATGACGGCGGTGAGGGCCGC	Cloning MPO-minigenes
MPO_{145} Mini gene_w/o Stop SalI reverse	TAGTCGACGGGGCTGCGTCTGTTGTTGC	Cloning MPO-minigenes
NotI Kozak MPO_{466} Mini gene start	TACAGGCGGCCGCCACCATGCTGGCAGGGGACACCCG	Cloning MPO-minigenes
MPO466 Mini gene_w/o Stop SalI reverse	TAGTCGACGTACTTCCTCATGGCCGTTG	Cloning MPO-minigenes
MPO Fwd RT	GACGTTCATTTGTGTGCTCA	real-time PCR
MPO Rev RT	CTGCCTTCCACATACTCAGT	real-time PCR
MPO internal oligo	[6FAM]TGGCTTTTCATGCGTGTGTGTTGTCT[TAM]	real-time PCR
GAPDH Taq. Probe	[6FAM]TTCCATGGCACCGTCAAGGC[TAM]	real-time PCR
HMBS Taq. Probe	[6FAM]CCTGAGGCACCTGGAAGGAGGCTG[TAM]	real-time PCR
HPRT1 Taq. Probe	[6FAM]CATTATGCTGAGGATTTGGAAAGGGTG[TAM]	real-time PCR
GAPDH Taq. fwd	TTCCAATATGATTCCACCCA	real-time PCR
GAPDH Taq. rev	GATCTCGCTCCTGGAAGATG	real-time PCR
HMBS Taq. fwd	ACGATCCCGAGACTCTGCTTC	real-time PCR
HMBS Taq. rev	GCACGGCTACTGGCACACT	real-time PCR
HPRT1 Taq. fwd	CTGGCGTCGTGATTAGTGAT	real-time PCR
HPRT1 Taq. rev	CTCGAGCAAGACGTTCAGTC	real-time PCR

199 2.1.12 Vectors

200 **Table 14: DNA Vector**

Vector	Origin
pMP71GPRE-eGFP MPSV-LTR promotor retroviral vector coding for eGFP	W. Uckert, Berlin, Germany, [95]
pMP71GPRE-P2A-eGFP MPSV-LTR promotor retroviral vector coding for eGFP	Cloned by M. Rami and R. Klar, former group members
pMP71GPRE-P2A-DsRed MPSV-LTR promotor retroviral vector coding for DsRed	Cloned by R. Klar, the former group member

pMP71GPRE-TCR2.5D6 MPSV-LTR promotor retroviral vector coding for 2.5D6	Cloned by R. Klar, former group member, 2.5D6-sequence synthesis and delivery in pUC57 cloning vector: Invitrogen, Carlsbad, USA
pMP71GPRE-TCRF5.4 MPSV-LTR promotor retroviral vector coding for F5.4	F5.4-sequence synthesis and delivery in pUC57 cloning vector: Genscript, Piscataway, USA
pUC57-TCRF5.4om	Cloning vector, Genscript, Piscataway, USA

2.1.12 Peptides

Table 15: Peptides synthesized by Genscript, Piscataway, USA

Peptide	Sequence	Peptide	Sequence
MPO2 wt	TPAQLNVL	**MPO2-L1_1A**	ATPAQLNVL
MPO2_1A	APAQLNVL	**MPO2-L1_2A**	LAPAQLNVL
MPO2_2A	TAAQLNVL	**MPO2-L1_3A**	LTAAQLNVL
MPO2_3A_wt	TPAQLNVL	**MPO2-L1_4A_wt**	LTPAQLNVL
MPO2_4A	TPAALNVL	**MPO2-L1_5A**	LTPAALNVL
MPO2_5A	TPAQANVL	**MPO2-L1_6A**	LTPAQANVL
MPO2_6A	TPAQLAVL	**MPO2-L1_7A**	LTPAQLAVL
MPO2_7A	TPAQLNAL	**MPO2-L1_8A**	LTPAQLNAL
MPO2_8A	TPAQLNVA	**MPO2-L1_9A**	LTPAQLNVA
MPO2_1T_wt	TPAQLNVL	**MPO2-L1_T1**	TTPAQLNVL
MPO2_2T	TTAQLNVL	**MPO2-L1_T2_wt**	LTPAQLNVL
MPO2_3T	TPTQLNVL	**MPO2-L1_T3**	LTTAQLNVL
MPO2_4T	TPATLNVL	**MPO2-L1_T4**	LTPTQLNVL
MPO2_5T	TPAQTNVL	**MPO2-L1_T5**	LTPATLNVL
MPO2_6T	TPAQLTVL	**MPO2-L1_T6**	LTPAQTNVL
MPO2_7T	TPAQLNTL	**MPO2-L1_T7**	LTPAQLTVL
MPO2_8T	TPAQLNVT	**MPO2-L1_T8**	LTPAQLNTL
MPO2_1P	PPAQLNVL	**MPO2-L1_T9**	LTPAQLNVT
MPO2_2P_wt	TPAQLNVL	**MPO2+R9**	TPAQLNVLS
MPO2_3P	TPPQLNVL	**pp65417-426**	TPRVTGGGAM
MPO2_4P	TPAPLNVL		
MPO2_5P	TPAQPNVL		
MPO2_6P	TPAQLPVL		
MPO2_7P	TPAQLNPL	Peptides synthesized by Genscript,	
MPO2_8P	TPAQLNVP	Piscataway, USA	

2.1.13 Mouse Model

NOD.Cg-Prkdc^{scid}Il2rg^{tm1Wjl}/SzJ (NSG), The Jackson Laboratory, Bar Harbor, Maine, US

2.1.14 Software

Table 16: Software and Software packages

Software	Application	Origin
GraphPad Prism 8	Graph, present and analyze of data	GraphPad Software, La Jolla, USA
FlowJo	Single-cell flow cytometry analysis	FlowJo, LLC, Ashland, USA
IMGT	TCR sequence analysis	http://www.imgt.org/
BLAST (Basic Local Alignment Search Tool)	TCR reconstruction	https://blast.ncbi.nlm.nih.gov/Blast.cgi
Ensembl	TCR reconstruction	https://www.ensembl.org/index.html
StepOnePlus Software v2.3	Real-time PCR processing	Applied Biosystems, Foster City, CA, USA
Microsoft Excel and Powerpoint	Spreadsheet used to graph, present and analyze of data	Microsoft, Redmond, USA
Sequencer v5.0	DNA data analysis	Gene codes Corp., Ann Arbor, USA
NetMHC3.4, NetMHC4.0	Binding of peptides to MHC class I alleles	http://www.cbs.dtu.dk/services/
NetMHCstab	Stability prediction of peptide-MHC-I complexes	http://www.cbs.dtu.dk/services/
SYFPEITHI	Binding prediction for MHC-I ligands	http://www.syfpeithi.de/
MaxQuant	Quantitative proteomics software	MPI of Biochemistry, Martinsried, Germany
Clone Manager 7	cloning simulation, graphics vector-map drawing, sequence analysis	Scientific & Educational Software, Denver, USA
Primer3	Primer and probe design	http://bioinfo.ut.ee/primer3/
SIM - Alignment Tool	Protein alignment	https://web.expasy.org/sim/
DSF Analysis v3.0.2	Thermal shift analysis	ftp://ftp.sgc.ox.ac.uk/pub/biophysics
Magellan	ELISA-plate reader software for determination of OD values	Tecan Group Ltd., Männedorf, Switzerland
DSF Analysis v3.0.2	Thermal shift analysis	ftp://ftp.sgc.ox.ac.uk/pub/biophysics
PyMOL 2.1	Molecular visualization system	https://pymol.org/2/
PDB	Protein data bank	http://www.rcsb.org/
MAFFT v7.395	Multiple sequence alignment program	https://mafft.cbrc.jp/alignment/server/
AmberTools 16 and Amber 16 software	Molecular simulation package	http://ambermd.org/
PDB2PQR v2.0.0	Preparing structures for solvation calculations, modeling, simulation, analysis	http://www.poissonboltzmann.org/
APBS v1.3	Electrostatics calculation program	PyMOL Plugin
VMD v1.9.2	Molecular visualization program	http://www.ks.uiuc.edu/Research/vmd/
Endnote	Reference manager	Clarivate Analytics, Philadelphia, USA

2.2 Methods

2.2.1 Cell Culture

Cell culturing was done under sterile condition in a safety workbench. Human blood, patient material, cell lines with biosafety level S2 and retroviral transductions were performed according to S2 safety guidelines. All tumor cell lines were periodically tested for the absence of mycoplasma infections. Usually, cell lines grown in suspension or adherent cell lines were split according to their proliferation kinetics to maintain optimal cell line stability. Suspension cell lines were split by replacing the used medium or adding it to expand the cells. In the case of adherent cell lines, except the 293Vec-RD114, the cells were treated with 1x trypsin/EDTA/PBS solution. After detachment of the cells, the reaction stopped by adding cDMEM supplemented with 20% FCS followed by a washing step at 500 g for 5'min and resuspension in fresh cDMEM.

2.2.1.1 Cell counting

The cell count was assessed by using a Neubauer chamber. To discriminate living cells from dead cells, trypan blue [1%] solution was used. The cell concentration of living cells was calculated using the following formula:

$$\frac{cell\ concentration}{ml} = \frac{\text{cells counted in all 4 areas x dilution factor}}{4}\ x\ 10^4$$

2.2.1.2 Freezing and thawing of eukaryotic cells

Cells which have chosen for cryopreservation in liquid nitrogen were centrifuged at 500 g for 5'min and resuspended in DMSO supplemented with 10% FCS. Transferred to 1.8 ml cryotubes (Merck) the aliquots were stored in freezing container to ensure 1°C/min cooling rate in a -80°C freezer. Subsequently, the cryotubes were transferred to a liquid nitro-

gen cryopreservation tank. For cell thawing, the samples were removed from liquid nitrogen and placed into a water bath at 37°C. Immediately after thawing, the cells were transferred to a 15 ml or 50 ml falcon and washed with RPMI at 500 g for 5'min. Afterwards, the cells were ready to use for downstream applications.

2.2.1.3 Isolation and activation of PBMC from EDTA-blood samples

Biocoll density gradient centrifugation was used to isolate PBMC out of whole blood withdrawals dosed with EDTA. The whole blood was diluted 1:1 with RPMI and 35 ml of the dilution was carefully covered on 15 ml Biocoll reagent (Merck) in a 50 ml falcon. After 20'min of centrifugation at 880 g with disabled breaks at RT, the buffy coat was collected into a new 50 ml falcon and washed twice with RPMI at 500 g for 5'min. Finally, the PBMC were resuspended in TCM to a final concentration of $2x10^6$ cell/ml. For activation, 2 ml of the PBMC were transferred to a cell culture treated 12-well plate and incubated with 50 U/ml hIL-2 and 30 ng/ml OKT3 for 48 h at 37°C.

2.2.1.4 Purification of $CD4^-/CD45RA^-/CD62L^+$ T_{CM}

Purification of $CD8^+$ T_{CM} was done using 250 ml blood from healthy donors. First, the PBMCs were isolated using the Biocoll (Merck) separation protocol (chapter 2.2.1.3). Second, $1x10^8$ PBMCs were incubated rotating with 40 µl of an anti-human CD4-APC-(BD) and 40 µl of an anti-human CD45RA-APC antibody (BD) for 20' min in a final volume of 800 µl isolation buffer at 4°C. After a washing step with isolation buffer, the antibody stained PBMCs were adjusted to $1x10^8$ cells per 1 ml containing 800 µl isolation buffer and 200 µl anti-APC magnetic beads (Miltenyi Biotec). Following a rotary incubation step at 4°C for 20' min and an additional washing step, the $CD4^+$ and $CD45RA^+$ cells were depleted using LD columns (Miltenyi Biotec) for magnetic cell separation in 500 µl isolation buffer per $1x10^8$ cells according to the manufacturer protocol. Third, the remaining cells were incubated with 20 µl anti-human CD62L-PE antibody in a final volume of 100 µl isolation buffer per $1x10^7$ cells rotating at 4°C for 20'min. After incubation,

the cells were washed and stained for 20'min rotary at 4°C with 20 µl anti-PE beads in a final volume of 100 µl per 1x10*7 cells. Followed by an additional washing step, the cells were resuspended in 500 µl isolation buffer and separated via a LS-column according to the manufacturer's instruction (Miltenyi Biotec). The phenotype of remaining $CD4^-$ $CD45RA^-CD62L^+$ cells was analyzed by flow cytometry and activated using anti-human CD3 and CD28 beads (chapter 2.2.1.5).

2.2.1.5 Activation of PBMCs and $CD4^-/CD45RA^-/CD62L^+$ T_{CM}

The activation of PBMCs or CD4-/CD45RA-/CD62L+ T_{CM} was done using anti-CD3 and CD28 labeled beads (Merck) according to the manufacturer's instructions. 50 µl bead was used per $2x10^6$ cells in a final volume of 2 ml TCM supplemented with 30 U/ml hIL-2. The cells were activated for two days in a 12-well tissue culture plate (TPP).

2.2.1.6 Transfection of 293Vec-RD114 using pMP71

The transduction of T-Lymphocytes and tumor cell lines follows a six days protocol starting with plating of the packaging cell line 293Vec-RD114 (biovec pharma) with $2.5x10^5$ cells per well in a 6-well cell culture plate in 3 ml cDMEM. The confluence of the cells should be around 60% after 24 h of culture. For the transfection of the 293Vec-RD114 200 µl, serum-free DMEM was supplemented with 3 µl TransIT reagent (Mirus Bio LLC) and was incubated after thoroughly mixing for 20' min at RT. Following this, 1 µg of pMP71 containing the gene of interest was added to the reaction, gently mixed and incubated for an additional 30' min at RT. Finally, the transfection mix was added to the plated 293Vec-RD114 cells and incubated for 48 h at 37°C. Subsequently, half of the supernatant was harvested and filtered through a 0.45 µm syringe filter and used for the transduction of target cells. The remaining supernatant was harvested 24 h later, also filtered and used for an additional round of transduction.

2.2.1.7 Retroviral transduction of activated PBMC and T_{CM}

Activated PBMC and T_{CM} were transduced twice on two consecutive days in non-cell culture treated 24-well plates coated with 12.5 mg/ml RetroNectin (Takara) in PBS. The solution was plated to each well and incubated for 24 h followed by removal of the solution and subsequently blocking with 500 µl of a 2% BSA/PBS solution for 30' min at 37°C. After blocking, the wells were washed twice with 2 ml PBS supplemented with 2.5% (v/v) HEPES and were ready to use for retroviral transduction. $1x10^6$ activated PBMC or T_{CM} in a final volume of 1 ml in TCM were supplemented with 200 U/ml hIL-2, 2% HEPES and 8 µg/ml protamine sulfate and seeded in one well of the RetroNectin-coated 12-well plates. Subsequently, 1 ml of viral supernatant harvested from the transfection of 293Vec-RD114 cells (see chapter 2.2.1.6) was pipetted to the activated PBMC or T_{CM} and centrifuged for 90' min at 933 g and 32°C. After that, the cells incubated for 24 h at 37°C, and the transduction was repeated a second time accordingly after resuspension and washing of the cells. Finally, the cells were resuspended in TCM supplemented with hIL-7 and hIL15 at a final concentration of 5 ng/ml. Five days after the second transduction the transduction efficiency was analyzed by flow cytometry (see chapter 2.2.5.1).

2.2.1.8 Retroviral transduction of tumor cell lines

The retroviral transduction of tumor cell lines with pMP71 containing the HLA-restriction elements, the MPO-protein sequences or the MPO-minigenes was analog to the retroviral transduction of activated PBMC and T_{CM} except for the following variations. Instead of TCM, cRPMI was used and no hIL-2 was added to the tumor cell lines during the transduction protocol (see chapter 2.2.1.7).

2.2.1.9 Isolation of $CD8^+$ naïve T cells

PBMC were isolated according to chapter 2.2.1.3 but not activated. $CD8^+$ T cells were negatively sorted using the CD8 untouched isolation kit (Thermo Fisher Scientific) according to the procedure of the manufacturer. $CD8^+$ enriched T cells subsequently were used for the depletion of $CD45RO^+$ and $CD57^+$ cells with magnetic microbeads (Miltenyi Biotec) according to the manufacturer instructions. The phenotype of the obtained $CD8^+CD45RO^-CD57^-$ naïve T cells was verified by flow cytometry.

2.2.1.10 Expansion of peptide specific CD8+ naïve T cells

The generation of dendritic cells (DC) used for the single HLA-mismatch (sHLAm) stimulation was done as previously described [43]. After Isolation of PBMCs (see chapter 2.2.1.3) 150 million PBMCs were used to adhere monocytes to the bottom of an 80 cm^2 Nunclon-surface flask via plate adherence in 12 ml pre-warmed (37°C) DC-medium for 1.5 h at 37°C. Afterward, the cells which have not been attached to the bottom of the flask were carefully removed by gentle rinsing the cells with DC-medium for three times. The remaining adherent cells were cultivated with 15 ml DC-medium II for 48 h. Finally, the maturation was induced by adding 500 µl DC-medium III to the cell culture. After 24 h of cultivation, the DC were detached by washing the flask three times with 12 ml PBS + 0.5% HS and additional use of a cell scraper. The result of DC maturation was verified by flow cytometry. Mature DC were washed twice in OptiMEM. Three million DC were resuspended in 200 µl cold (4°C) OptiMEM and transferred to a 4 mm electroporation cuvette to chill for 3’ min on ice before electroporation. Immediately before the electroporation in a *Gene Pulser Xcell* Electroporation System (Bio-Rad) 40 µg of in-vitro transcribed HLA-eGFP-RNA (see chapter 2.2.2.11) was added to the DC and resuspended with a 200 µl tip. The protocol of the electroporator was as follows: exponential protocol, 300 µF, and 300 V. Directly after the electroporation the DC were transferred to a well containing 3 ml pre-warmed DC-medium of a 6-well cell culture plate (TPP) and cultured

overnight at 37°C. The DC with transient HLA-eGFP expression were washed twice with AIM-V medium and pulsed with MPO-peptides in 100 µl AIM-V at a final concentration of 0.1 µM for 2h at 37°C. Finally, the DC were washed twice with RPMI and co-cultured with CD8+ naïve T cells (see chapter 2.2.1.10) of the same donor in 500 µl TCM supplemented with 30 ng/ml hIL-21 at an effector to target ratio of 10:1 for three days in a well of a 48-well cell culture plate. During the expansion of peptide-specific CD8+ naïve T cells, every 2-3 days hIL-7 and hIL-15 was added to the culture to a final concentration of 5 ng/ml, and if required, the cells were split with fresh TCM. At day 10 of co-culture, the cells were re-stimulated with γ-irradiated (30 Gy) C1R cells transgenic for the desired HLA-allele pulsed with 0.1 µM MPO-peptide. The ratio between effector and target cells was 10:1 for the re-stimulation in a final volume of 2 ml TCM supplemented with 30 ng/ml hIL-21 (2 million expanded T cells: 0.2 million C1R cells) in a well of a 12-well cell culture plate. Again, every 2-3 days hIL-7 and hIL-15 was added to the culture to a final concentration of 5 ng/ml, and if necessary, the cells were split. At day 16 after the start of co-culture the frequency of peptide-specific T-cells was measured by multimer staining (see chapter 2.2.5.3).

2.2.1.11 CD137 allo-depletion and sort of MPO-HLA-tetramer positive T cells

Before the sort of peptide-specific T cells by MPO-HLA-tetramers the cells derived from the sHLAm approach were allo-depleted using γ-irradiated (30 Gy) C1R cells, transgenic for the HLA-allele used in the sHLAm approach. The HLA-transgenic C1R cells without any peptide pulsing were co-cultured overnight with the stimulated T cells to elicit MPO-peptide independent HLA-alloreactivity and CD137 upregulation on the surface of allo-reactive T cells. $CD137^+$ T cells were depleted by MACS separation using the CD137 MicroBead Kit (Miltenyi Biotec) according to the manufacturer instructions. The remaining T cell population was FACS-sorted by MPO-HLA-tetramers to get peptide-specific T cells (see chapter 2.2.5.3).

2.2.1.12 Limited dilution cloning of T-cell lines

Peptide-specific T cells sorted by MPO-HLA-tetramers were cloned by limited dilution to a final concentration of 0.5 to 1.0 sorted T cells per well in a 96-well cell culture plate (TPP). These cells were co-cultured with 50.000 cells of γ-irradiated (30 Gy) PBMCs from three different donors (feeder cells) in TCM supplemented with 30 ng/ml OKT-3 and 50 U/ml hIL-2. Continuing, hIL-2 was added twice per week at the same concentration. After two weeks, the cloned T cells were analyzed for peptide specificity using 50 µl of T cell suspension. Another 50 µl were used for RNA isolation using the TRIzol reagent protocol (see chapter 2.2.2.2). Remaining T cells were chosen for another round of expansion with feeder cells as described before.

2.2.2 Molecular biology methods

2.2.2.1 Restriction digest, Ligation, and Transformation

Vector DNA and PCR-products were digested for 2 h at 37°C using different restriction enzymes (New England Biolabs) in a digestion mix indicated in Table 17. After digestion, the enzymes were heat-inactivated at 65°C for 20’min followed by gel purification after separation using agarose gel electrophoresis in case of vector DNA or direct purification using the *Nucleospin Gel and PCR Cleanup Kit* (Macherey-Nagel) in case of PCR-products (inserts).

Table 17: Digestion mix for the restriction enzymes NotI, EcoRI or SalI

Reagent	Concentration	Vector	Insert
Vector DNA or PCR-product	variable	15 µl	23.5 µl
Buffer “O”	10x	10 µl	10 µl
NotI	10.000 U/ml	2 µl	2 µl
EcoRI or SalI	20.000 U/ml	2 µl	2 µl
DEPC water		ad 100 µl	ad 100 µl

Ligation of digested and purified vector DNA and inserts was done using the T4 ligase according to the following equation:

$$Volume\ of\ insert = n * 1\ \mu l\ Vector * \frac{C\ Vector}{C\ Insert} * \frac{length\ of\ Insert\ [bp]}{length\ of\ Vector\ [bp]}$$

n = molar ratio of insert to vector; C = concentration; bp = base pair

The ligation mix and the incubation time is shown in Table 18:

Table 18: Reagent mix for insert ligation

Reagent	Volume	Incubation
Digested vector	1 µl	1. 16 h, 16°C 2. 20’ min, 65°C
Digested insert	variable	
10x T4 buffer	1 µl	
T4 ligase	1 µl	
DEPC water	ad 10 µl	

After the ligation of vector and insert the completed vector construct was clonal amplified by NEB5α competent E. coli (New England Biolabs). The transformation was performed according to the manufacturer's instructions with the following modifications. Competent *E. coli* were thawed on ice for 10’ min 1 µl containing 100 ng vector construct was pipetted to the bacteria and carefully flicked five times. After incubation on ice for an additional 30’ min, a heat-shock of 42°C for exact 30 s was performed, and the tube was replaced on ice for another 5’min. The bacteria were gently mixed with 400 µl SOC medium (RT) and incubated for 1 h at 37°C and 250 rpm. Afterward, several dilutions of the bacteria mix were plated on ampicillin (100 µg/ml) supplemented LB-agar plates and incubated overnight at 37°C. Finally, grown colonies of bacteria were picked with pipette tips and incubated for expansion in 3 ml LB-medium supplemented with ampicillin (100 µg/ml) for at least 6 h on a shaker at 250 rpm at 37°C.

The amplified vector constructs were purified using the *JETSTAR™ 2.0 Plasmid Purification Kit* and protocol (Genomed). 2 ml of the bacteria mix was used for the purification, and the isolated vector constructs were verified after a control digest by gel electrophoresis (see chapter 2.2.2.6 and digest protocol above) and vector sequencing (MWG Eurofins). Correct vector construct was chosen for an additional round of transformation, expansion, and purification, as described above with the following modifications: 0.5 ml of the heat-shock transformed bacteria mix after 6 h of incubation, were used to inoculate 250 ml of LB-medium supplemented with ampicillin (100 µg/ml). The bacteria were expanded overnight at 37°C and 250 rpm. For the purification of vector constructs, the endotoxin-free *NucleoBond® Xtra Maxi EF* kit and protocol (Macherey Nagel) was used according to the manufacturer's instructions and stored until use at -20°C. The vector sequence was confirmed again by Sanger sequencing (MWG Eurofins).

2.2.2.2 RNA isolation

RNA was isolated out of different AML cell lines and T-cell clones. Whenever enough cell material was available (more than $1x10^6$ cells), the cell pellets were firmly resuspended in 4°C cold 1 ml TRIzol reagent. Cell pellets not exceeding $1x10^6$ cells were resuspended in only 200 µl TRIzol reagent, and in case of T-cell clones, 10 µg yeast RNA was added. The samples were incubated for 5'min at RT followed by addition of 200 µl (40 microliter for T-cell clones in 200 microliter TRIzol) chloroform and subsequent incubation for 10' min at RT. Afterward, the samples were centrifuged for 15' min at 15.000 g and 4°C. For RNA precipitation the RNA phases were transferred to new tubes containing 500 µl 2-propanol followed by incubation for 1 h at -20°C and centrifugation for 20' min at 15.000 g and 4°C. After removal of the supernatants, the pellets were washed with 1 ml 75% ethanol and centrifuged again for 5'min at 15.000 g at 4°C. Finally, the dried

pellets were resuspended in 21.5 µl DEPC water, and 1.5 µl were used for the determination of RNA concentration using a *NanoDrop ND-1000* (PeqLab). Until the use in downstream applications the RNA was stored at -80°C.

2.2.2.3 cDNA synthesis from RNA templates

Isolated RNA samples (see chapter 2.2.2.2) were reverse transcribed into cDNA (complementary DNA) with the *Affinity Script cDNA Synthesis Kit* (Agilent Technologies) according to the manufactures' protocol except for the following variations: see Table 19. Until the use in downstream applications the cDNA was stored at -20°C.

Table 19: cDNA synthesis using the *Affinity Script cDNA Synthesis Kit*

Steps	Reagent	Volume	Incubation
1.	RNA (1 µg/µl)	1 µl	1. 65°C, 5'min
2.	oligo(dT) Sigma (500 ng/µl)	1 µl	2. RT, 10'min
3.	DEPC water	11.5 µl	3. 4°C, ∞

Steps	Reagent	Volume	Incubation
4.	Affinity Script Puffer	2 µl	
5.	dNTPs Fermentas (10 mM)	2 µl	1. 47,5°C, 1 h
6.	RNase out (Invitrogen)	0.5 µl	2. 70°C, 15' min
7.	Affinity Script	1 µl	

2.2.2.4 PCR using KOD polymerase

For the amplification of genes of interest, RNA out of cell lines and T-cell clones were reverse transcribed to cDNA (see chapter 2.2.2.3) and used as a template in a PCR reaction. The different primers used for the PCR cycling are listed in Table 12 and Table 13. For the amplification, the *KOD Hot Start Polymerase* kit (Merck) was used, and the reaction mixture (Table 20) was set up in a 0.5 ml PCR reaction tube. The PCR (Table 21) was performed on a Biometra *TGradient Thermocycler* (Analytik Jena).

Table 20: PCR reaction mix using KOD polymerase

Volume	Reagent
10 µl	10x KOD buffer
10 µl	dNTPs (2 mmol/l)
6 µl	$MgSO_4$ (25 mmol/l)
3 µl	forward Primer (15 mmol/L)
3 µl	Reverse Primer (15 mmol/L)
2 µl	cDNA
2 µl	KOD polymerase
ad 100 µl	DEPC water

Table 21: PCR program using KOD polymerase

Temperature	Time	Cycles	Reaction
95°C	2'min	1x	Pre-denaturation
95°C	30 s		Denaturation
55°C	30 s	35x	Annealing
70°C	1' min		Extension
70°C	10' min	1x	Final extension
4°C	∞	1x	Infinite hold

2.2.2.5 TCR alpha and beta repertoire PCR

For the analysis of the TCR alpha and beta repertoire, RNA of T-cell clones was isolated and reverse transcribed into cDNA (see chapter 2.2.2.2 and 2.2.2.3). Various primers were used to cover the different regions of the variable alpha and variable beta domain in order to analyze the TCR repertoire (Table 12). The PCR was performed using the *HotStar MasterMix Plus* reagents (Qiagen) in V-alpha, or V-beta PCR reaction mixes shown in Table 22 and Table 23 using a Biometra *TGradient Thermocycler* with the setup shown in Table 24. Specific PCR products were extracted from an agarose gel and the DNA sequenced after purification with the respective V-alpha and V-beta primer by Eurofins MWG.

Table 22: PCR reaction mix for TCR V-alpha repertoire

Reagent	Volume
cDNA	0.55 µl
P-5'aST (5 µmol/l)	1.5 µl
P-3' aST (5 µmol/l)	1.5 µl
3'-Ca (5 µmol/l)	2 µl
Va-Primer (5 µmol/l)	3 µl
Coral load	2.5 µl
DEPC water	1.4 µl
HotStar MasterMix	12.5 µl

Table 23: PCR reaction ingredients for TCR V-beta repertoire

Reagent	Volume
cDNA	0.55 µl
P-5'βST (5 µmol/l)	1.5 µl
P-3'βST (5 µmol/l)	1.5 µl
3'CβII (5 µmol/l)	2.0 µl
Vβ-Primer (5 µmol/l)	3 µl
Coral load	2.5 µl
DEPC water	0.29 µl
HotStar MasterMix	12.5 µl

Table 24: PCR program TCR alpha and beta repertoire

Temperature	Time	Cycles	Reaction
95°C	15'min	1x	Pre-denaturation
94°C	1'min		Denaturation
54°C	1' min	35x	Annealing
72°C	1' min		Extension
72°C	10' min	1x	Final extension
4°C	∞	1x	Infinite hold

2.2.2.6 Agarose gel electrophoresis

Agarose gel electrophoresis was performed to verify the correct length of PCR constructs or vector constructs. The gel was prepared using 1.0-1.5% agarose in 1x TAE (TRIS-Acetate-EDTA-Puffer) buffer followed by heating of the suspension till the complete dissolution of agarose. Before transfer into a gel chamber, ethidium bromide was added to a final concentration of 0.25 µg/ml. If necessary, the samples were prepared by adding loading dye to a 1x dilution. As references 100 bp or 1 kb DNA ladders were used. The run of the gel electrophoresis was performed on a *Compact M Horizontal Gel Electrophoresis Apparatus* (Biometra) with 100 V for 45'min in 1x TAE buffer. For the visualization of bands within the gel, the *BioDocAnalyze Gel documentation system* (Biometra) was used.

2.2.2.7 PCR product purification out of agarose gels

For the purification of PCR products out of agarose gels, the *Nucleospin Gel and PCR Cleanup kit* and protocol (Macherey-Nagel) was used. In the final step of the protocol, the PCR product was eluted in 20 µl DEPC water. The concentration was analyzed using the NanoDrop ND-1000 spectrophotometer.

2.2.2.8 In-silico TCR reconstruction using IMGT vQuest and BLAST

After performing the TCR repertoire (see chapter 2.2.2.5), purification (see chapter 2.2.2.7) and Sanger sequencing of PCR products (MWG Eurofins), the sequences were used for reconstruction of TCR domains. To identify the complementarity determining region 3 (CDR3) and the VDJ-segments (variable (V), diversity (D), joining (J)), a database search was performed using the IMGT vQuest platform. Missing sequence parts not covered by the TCR repertoire were reconstructed using reference TCR sequences available at the NCBI server using the Basic Local Alignment Search Tool (BLAST) and the Ensembl browser. To verify the sequences of the alpha and the beta domain, primers were designed (Sigma-Aldrich) to amplify both chains from cDNA, reverse transcribed from isolated RNA (see chapter 2.2.2.3) of peptide-specific T-cell clones.

2.2.2.9 Optimization and murinization of TCR sequences

For the enhanced surface presentation and reduced miss-pairing of exogenous TCR alpha and beta domains with endogenous TCR of recipient T cells after retroviral transduction (see chapter 2.2.1.7), a bicistronic vector element was designed containing both TCR domains linked with a P2A element [96]. Also, the constant human domains (TRAC and TRBC) were substituted by murine constant domains as previously described [97]. Besides a new cysteine disulfide bond between position S211C and T543C, the whole construct was codon optimized (Genscript) to improve the expression in human transgenic T cells [98] and finally synthesized by Genscript. The complete sequence (see appendix) was cloned into the vector pMP71 for retroviral transduction into recipient T cells.

2.2.2.10 qPCR using SYBR Green for PSMB subunits

Total RNA was isolated from either not treated or IFN-γ pretreated (24 h, 250 U/ml) AML/APL cell lines using the TRIzol reagent (see chapter 2.2.2.2). 1 µg of isolated RNA was used for reverse transcription into cDNA (see chapter 2.2.2.3) and the QuantaBio PerfeCTa® SYBR® Green FastMix®, ROX™ reagent (Quantabio) was used to set up the master mix for PCR reactions (Table 25). Semi-quantitative real-time PCR (qPCR) was performed using the StepOnePlus system (Thermo Fisher Scientific) (Table 26). Primers specific for the proteasomal subunit sequences PSMB8, PSMB9 and PSMB10 (Table 13) were used for the qPCR. The PSMB expression was relatively quantified by normalization to the geometric mean of the housekeeping genes HPRT1, GAPDH and HMBS using the delta/delta CT method [99]. As a reference, total RNA from bone marrow cells of healthy donors was used.

Table 25: qPCR reaction using SYBR Green

Reagent	Volume
PerfeCTa SYBR Green FastMix, ROX	10 µl
Primer forward (250 nM)	0,5 µl
Primer reverse (250 nM)	0,5 µl
cDNA	2 µl
DEPC water	7 µl

Table 26: qPCR program StepOnePlus using SYBR Green for PSMB

Step	Temp.	Ramp rate	Time	Cycles	Stage	Signal Acquisition
1	50°C		2’ min	1x	Holding	
2	95°C		3’ min	1x		
3	95°C		3 s		Cycling	
4	65°C		30 s	40x		
5	95°C		15 s		Melt curve	step and hold
6	65°C	+ 0.3°C	15 s	1x		
7	95°C		15 s			

2.2.2.11 In-vitro transcription of HLA-RNA for DC electroporation

Tumor cell lines and DC were electroporated (see chapter 2.2.1.10) with mRNA coding for HLA-P2A-eGFP. The mRNA was in-vitro transcribed (ivt) according to the mMESSAGE mMACHINE® T7 Transcription Kit protocol (Thermo Fisher Scientific) using linearized pcDNA3.1–HLA-P2A-eGFP vector constructs. In the next step, ivt-RNA was polyadenylated using the Ambion™ Poly(A) Tailing Kit protocol (Thermo Fisher Scientific). A NanoDrop ND-1000 spectrophotometer was used to measure the yield of ivt-RNA at the end. Efficiency was tested using 10 µg of ivt-RNA for electroporation of the Jurkat cell line following the protocol in chapter 2.2.1.10. Each batch of ivt-RNA was stored at -80°C.

2.2.3 Analyses of T-cell lines, T-cell clones, and TCR-transgenic T cells

2.2.3.1 Co-incubation of effector and target cell lines

Co-incubation assays of effector and target cells were performed using 10.000 – 100.000 T cells per well in a 96-well cell culture plate (TPP) by adding target cells in different ratios according to the requirements of the assay in a final volume of 200 µl TCM. The cells were co-incubated for 4 – 20 h at 37°C. Wherever necessary the target cells were pulsed with peptides in AIM-V medium at different concentrations for 2 h at 37°C followed by two washing steps with RPMI and final resuspension in TCM before the use in the co-incubation assay.

2.2.3.2 IFN-γ and hIL-2 ELISA

IFN-γ and hIL-2 ELISA were performed using the supernatants of co-incubation assays according to the manufacturer instructions using the BD *OptEIA™* human ELISA sets with modifications for the different cytokines:

IFN-γ and hIL-2: Capture antibody dilutions used for the coating of 96-well ELISA plates were 1:250 and incubation was done overnight at 4°C. The standards of both cytokines

were prepared in TCM by serial dilution to meet concentrations ranging from 1000 pg/ml (for IFN-γ) or 500 pg/ml (for hIL-2) to 31.25 or 15.63 pg/ml, respectively, and blank controls. If not stated otherwise, 50 µl of supernatant from the co-culture and standard was used per well. For detection, 100 µl blocking solution containing a 1:250 dilution of anti-IFN-γ- or a 1:500 dilution of anti-hIL-2-enzyme conjugate was used. The final development was done using 100 µl per well of the BD *OptEIA*^{TM} TMB substrate reagent set. The reaction was stopped after the standard was obvious by adding 50 µl of sulfuric acid. The ELISA was measured with a Tecan Sunrise photometer using the Magellan software, setting the absorbance to 450 nm and the reference channel to 570 nm. Whenever the measured OD-values for the samples exceeded the OD-values of the highest standard condition, the ELISA was repeated using dilutions of the remaining supernatants of co-cultures.

2.2.3.3 Functional avidity of TCR

For the measurement of the functional avidity, supernatants of co-cultures (see chapter 2.2.3.1) of TCR-transgenic T cells and the target cell line KG-1a-B7 or C1R-B7, pulsed with graded amounts of MPO-peptides ranging from 20 µM to 1 pM, were analyzed by IFN-γ ELISA (see chapter 2.2.3.2). The effector to target ratio was set to 1:1 comprising 20.000 cells per party.

2.2.3.4 K_{off}-measurements of TCR

The k_{off}-measurements and the calculations of dissociation half-lives of the MPO-TCRs were performed by Manuel Effenberger (Institut für Medizinische Mikrobiologie, Immunologie und Hygiene, Munich, Germany). A detailed description of the measurement protocol was reported previously [81].

2.2.3.5 Effector to target ratio titration

Effector to target ratio titrations followed the underlying protocol for co-incubation assays (see chapter 2.2.3.1). MPO-TCR-transgenic T cells were serially diluted fifteen

559 times 1:1 to meet effector to target ratios ranging from 5:1 to calculated 0.00031:1. Here,
560 the actual T-cell number started from 100.000 T cells per well of a 96-well cell culture
561 plate down to six T cells per well pipetted to the number of 20.000 NB4-B7 target cells
562 in a final volume of 200 µl TCM. The controls comprised either only T cells (20.000 cells
563 per well) or only target cells (20.000 NB4-B7 cells per well). Supernatants were harvested
564 either after 4 h or 20 h of co-culture and were analyzed by IFN-γ ELISA (see chapter
565 2.2.3.2). Also, cytotoxicity using the remaining cells after co-culture were analyzed by
566 flow cytometry for both time points (see chapter 2.2.3.6).

567 2.2.3.6 Cytotoxicity measured by flow cytometry
568 The cytotoxicity of TCR-transgenic T cells against target cells was analyzed after co-
569 incubation (see chapter 2.2.3.1 and 2.2.3.5). Remaining cells after co-culture were stained
570 with 7-AAD and analyzed by flow cytometry (see chapter 2.2.5). For the calculation of
571 percentages of cytotoxicity, the following procedure was used: First, the absolute number
572 of remaining HLA-B7eGFP target cells was quantified using the AccuCheck counting
573 beads (Thermo Fisher Scientific) according to the manufacturer recommendations:

574

575 $$Absolute\ count\ (cells/\mu l) = \frac{number\ of\ remaining\ target\ cells\ counted}{\text{total number of beads counted}} * beads\ per\ \mu l$$

576

577 Subsequently, the absolute target cell count per µl was used to calculate the cytotoxicity:

578

579 $$Cytotoxicity\ (\%) = \left(1 - \left(\frac{\text{absolute count of remaining target cells}}{mean\ of\ remaining\ target\ cell\ count\ of\ controls}\right)\right) * 100$$

2.2.4 Analyses of p-MHC characteristics

2.2.4.1 UV-mediated peptide exchange assays

Biotinylated HLA-B*07:02 monomers in complex with the UV-sensitive AARG(J)TLAM peptide were kindly provided by Stefan Stevanović (Tübingen, Germany). The UV-mediated peptide exchange was done as previously described [100] with slight modifications: The peptide exchange was performed using a concentration of 0.025 µg/µl UV-sensitive monomers in a final volume of 125 µl PBS per well of a polypropylene *MicroAmp™ Optical* 96-well reaction plate (Thermo Fisher Scientific). Graded amounts of the peptide of interest were added to the reaction wells with a final concentration ranging from 0.1 µM up to 200 µM in triplicates. As controls, conditions without peptide of interest (0 µM) and UV-irradiation were used. The 96-well reaction plate was stored on ice under a UV hand lamp (Köhler Technische Produkte) for 60’ min with a distance between the plate and the UV hand lamp of approximately 5 cm. The UV wavelength was set to 365 nm. After irradiation, the plate was centrifuged for 5’min at 3000 x g at 4°C and 100 µl supernatant of each well transferred to a new 96-well reaction plate and if necessary, stored covered with a sealing foil at -80°C.

2.2.4.2 Beta-2-microglobulin ELISA for Determination of HLA-stability

Nunc-Immuno™ MicroWell™ Max-iSorp™ flat bottom 96-well plates were coated with Streptavidin at a final concentration of 3 µg/ml in PBS and incubated for 2 h at 37°C. After four washing steps with PBS supplemented with 0.05% *Tween20* the plates were blocked for 30’ min at RT with 300 µl 1% BSA/PBS. The blocking solution was discarded by flicking the plates, and without an additional washing step, 100 µl of a 1:10 (PBS) dilution of the supernatant of UV-peptide exchanged HLA-B*07:02 complexes (see chapter 2.2.4.1) was transferred to each well. The plates were incubated for 1 h at 37°C covered with a sealing foil followed by four washing steps. Subsequently, the wells were incubated with 100 µl anti-beta-2-microglobuline antibody conjugated to HRP

(horseradish peroxidase) at a final concentration of 4 µg/ml in 1% BSA/PBS for 1 h at 37°C in the dark and covered with sealing foil. After the final four washing steps 100 µl of *OptEIA™ TMB substrate reagent* (BD) was added to the wells and incubated for 10'min. The reaction was stopped by pipetting 50 µl of sulfuric acid. The plates were measured with a Tecan Sunrise photometer using the Magellan software, setting the absorbance to 450 nm and the reference channel to 570 nm.

2.2.4.3 Differential Scanning Fluorimetry (Thermal shift assay)

For further determination of MPO-peptide-MHC stability, the Differential Scanning Fluorimetry was performed for UV-exchanged MPO_2- MPO_2+L1-, MPO_5- and as a control for pp65(417-426)-HLA-B7 complexes (see chapter 2.2.4.1). This technique was either used to measure the thermal stability with increasing temperature or the dissociation half-life of the peptides at constant physiological temperature (37°C). The p-MHC complexes were pipetted in MicroAmpR Fast Optical 96-well reaction plates (Applied Biosystems) in a final volume of 20 µl containing 10 mM HEPES (pH 7.4), 150 mM NaCl, 3 mM EDTA, 2 µM of UV-exchanged p-MHC-complexes and 10x SYPRO orange dye (Thermo Fisher Scientific). Afterward, the reaction plate was sealed with a film, and the samples were analyzed using a StepOnePlus RT-PCR instrument (Applied Biosystems, Foster City, USA). For thermal stability, a two-step melt curve analysis was selected, and a scan rate for the temperature of 1°C/min ranging from 20°C to 95°C was chosen. Step one: percentage ramp rate, start temperature = 20°C and time = 2`min. Step two: Endpoint temperature = 95°C, time = 2'min, melt curve = 1.0 and data were collected as well as on ramp and hold. For dissociation measurements, the setup was as follows: Melt curve stage: 100% ramp rate, 37°C, time = 00:15 data collection on the ramp and hold. Cycling stage: 160 cycles, 37°C, time = 05:00 and again data collection on the ramp and hold. The thermal stability analysis was performed as described elsewhere [101]. In brief, the recorded multicomponent data were exported to the Microsoft Excel-based *DSF Analysis*

tool (v3.0.2) available under the following link: (ftp://ftp.sgc.ox.ac.uk/pub/biophysics). The tool provided processed data that where exported to GraphPad Prism (version 7.04, San Diego, USA) to fit them against Boltzmann equations to calculate the half-maximal temperature where p-MHC-complexes are denaturized (V_{50}). For the calculating of the slowest dissociation rate of each p-MHC complex at 37°C, the multicomponent data set was used to plot the curves followed by a fit using a two-phase decay algorithm of GraphPad Prism (version 7.04, San Diego, USA).

2.2.4.4 Molecular modeling of p-MHC complexes

The in-silico modeling of MPO-HLA-B7 complexes was kindly done by Manuel Glaser and Iris Antes from the Center for Integrated Protein Science at the Technical University Munich in Freising, Germany. A detailed description of experimental procedure and results can be found in the PhD-thesis related publication [102].

2.2.4.5 Immunopeptidomics

The purification and identification of HLA-I MPO-peptides were performed using LC-MS/MS analysis and was kindly done by Matteo Pecoraro at the Max Planck Institute of Biochemistry in Munich. For quantification of MPO-peptides using mass spectrometry, heavy labeled versions of the peptides were synthesized and spiked into the samples for coinstantaneous detection and ratio-based calculation of wildtype peptide levels. A detailed description of the method and the immunopeptidomics workflow was published previously [39].

2.2.5 FACS (Fluorescence-Activated Cell Sorting)

2.2.5.1 Surface staining

Cells were washed with FACS buffer and blocked with ΔHS for 20’ min at 4°C followed by an additional washing step. In case of ex vivo isolated cells from mouse models, the cells were simultaneously blocked with anti-mouse CD16/32 antibody (1 µg per million

cells in 100 µl) and if necessary, before the blocking treated with ACK lysis buffer (ThermoFisher Scientific) according to the manufacturer's instructions. Following this, the cells were re-suspended in FACS buffer and stained for surface markers and 7-AAD for live/dead discrimination for 30' min at 4°C in the dark. If not otherwise stated, the final concentrations of antibodies and 7-AAD was chosen according to the manufacturer's recommendations. Afterward, the cells were washed with FACS-buffer, re-suspended in 2% fixation buffer and stored at 4°C in the dark until measurement.

2.2.5.2 Intracellular staining

The intracellular staining was used to characterize the expression quality of different T-cell receptors. Therefore, the T cells were blocked with human serum added with ethidium monoazide bromide (EMA) at a final concentration of 1:500 for 10' min on ice in the dark. Following this, the samples were exposed to glaring light on ice for additional 10' min to bind the EMA label during the photolysis reaction covalently to the DNA of cells with compromised cell- and core membranes. After EMA-staining, the cells were washed in FACS-buffer followed by surface antibody staining (see chapter 2.2.5.1), and after an additional washing step with FACS-buffer, the cells were fixed with IC fixation buffer (eBioscience) for 20' min on ice in the dark. After fixation, the cells were washed twice with 1x permeabilization (eBioscience) buffer. Subsequently, the cells were stained for intracellular targets according to the manufacturer's recommendations for 20' min on ice protected from light. Finally, the cells were washed with 1x permeabilization buffer and once more with FACS-buffer containing 0.1% sodium azide before the cells were suspended in the same buffer for analysis by flow cytometry.

2.2.5.3 Tetramer staining

For tetramer staining, the cells were blocked with human serum for 20' min on ice followed by a washing step with FACS-buffer. The tetramers were prepared for staining by centrifugation of the aliquot at 14.000g for 5'min to pellet possible aggregations. The

required amount of tetramer-supernatant was pipetted to PBS supplemented with 2mM EDTA and 50% FCS to meet a final concentration of tetramers in the sample of 30 µg/ml. The staining protocol follows the basic surface staining protocol described above (see chapter 2.2.5.1) with one exception. If the samples are co-stained with an antibody, the antibodies were pipetted 20’ min later to the samples to ensure the correct binding of tetramers.

2.2.5.4 Multi-cytokine analyses

For analyzation of human cytokines released by TCR-transduced T-Lymphocytes, the MACSPlex human Cytokine 12 Kit from Miltenyi Biotec (Bergisch Gladbach, Germany) was used. Sample preparation and data acquisition were performed according to manufacturer guidelines. In brief, The MPx Cytokine 12 standard was gently mixed with 200 µl TCM to obtain a concentration of 10 ng/ml. This stock solution was used to produce a standard of six levels by serial 1:5 dilutions comprising 2.000 pg/mL, 400 pg/mL, 80 pg/mL, 16 pg/mL, 3.2 pg/mL and 0 pg/ml in TCM. The samples were prepared at room temperature and protected from light by centrifugation for 10’ min at 10.000xg. In the meantime, the filter of the MACSPlex filter plate was pre-wetted with 200 µl MACSPlex buffer followed by centrifugation on top of a 96-flat-bottom plate for 3’ min at 300xg and room temperature. Subsequently, 50 µl of standard and samples were transferred to the plate and mixed with 20µl of thoroughly vortexed capture beads for 2 h protected from the light on an orbital shaker at 450 rpm. The incubation was stopped by centrifugation for 3’ min at 300xg followed by two washing steps with 200 µl MACSPlex buffer per well using the same centrifugation protocol. The filter bound beads were resuspended with 80 µl MACSPlex buffer and 20 µl detection reagent followed by another 1 h incubation protected from the light on an orbital shaker at 450 rpm. After the incubation, the samples were again centrifuged and washed as described above. Finally, the samples were resuspended in 200 µl MACSPlex buffer supplemented with 2% PFA and stored at 4°C

until FACS-based data acquisition. The data acquisition followed exactly the general instructions for MACSPlex Cytokine Kits data acquisition and analysis without the MACSQuant® Analyzer from Miltenyi Biotec.

3 Results

3.1 Selection of tumor-associated antigens

The Myeloperoxidase (MPO)-derived peptides MPO_{67}, MPO_{145}, MPO_{360}, MPO_{368}, and MPO_{466} were identified by immunopeptidomics as previously described [43]. All examined MPO peptides within this work are restricted to HLA class I and described as potential therapeutic targets for cell-based immunotherapies [43]. Thereby, the MPO protein is highly overexpressed in several patients' derived MPN and AML samples compared to PBMC reference material [43]. The MPO-peptides MPO_{266}, MPO_{357}, and MPO_{603} were identified elsewhere [44]. Another fourteen MPO-peptides (Table 27) have been identified by immunopeptidomics within this work either on the APL or AML-derived tumor cell lines NB4, HL60 and ML2 with transgenic HLA-B7 expression or on the SiG-M5 cell line with endogenous HLA-B7 expression. The immunopeptidomics approach was kindly performed by Matteo Pecoraro at the Max Planck Institute of Biochemistry in Martinsried, Germany.

Table 27: NetMHC predicted affinities and Syfpeithi scores of MPO-derived peptides

Peptide numbering derived from Isoform H7 (UniProtKB - P05164-3 (PERM_HUMAN))					NetMHC 4.0 [67, 103]	Syfpeithi [104]
Peptide	**Source**	**Sequence**	**Restriction**	**Sample Type**	**Affinity (nM)**	**Score**
MPO049		AAPAVLGEVDT (11mer)	possible HLA restriction: A*24:02, A*01:01, B*07:02, B*51:01	SiG-M5	for all HLAs very high	-
MPO067	[43], [44]	EEAKQLVDKAY (11mer)	B*44:02	AML, CML	2663.60	26
MPO100		SYFKQPVAAT (10mer)	possible HLA restriction: A*02:01, B*07:02, B*44:02, B*51:01	ML2-B7	for all HLAs very high	14 (A*02:01)
MPO104		QPVAATRTA (9mer)	possible HLA restriction: A*02:01, B*07:02, B*44:02, B*51:01	ML2-B7	binder for A*02:01 (329.23)	18 (B*07:02)
MPO104		QPVAATRTAV (10mer)	presumably B*07:02	ML2-B7, NB4-B7, SiG-M5	29.54	20
MPO136		RPFNVTDVL (9mer)	B*07:02	HL60-B7	34.06	23
MPO144		LTPAQLNVL (9mer)	B*07:02	-	15292.21	12
MPO145	[43]	TPAQLNVL (8mer)	B*07:02	CML	305.31	n.a.
MPO164		GVTCPEQDKY (10mer)	possible HLA restriction: A*01:01, A*24:02, B*07:02, B*51:01	SiG-M5	binder for A*01:01 (743.06)	16 (A*01)
MPO266	[44]	IVRFPTDQL (9mer)	published A*02 (rather B*07:02)	AML, HL60-B7, ML2-B7, NB4-B7, SiG-M5	20906.66 / (270.40)	18
MPO275		TPDQERSLM (9mer)	presumably B*07:02	HL60-B7, ML2-B7, NB4-B7, SiG-M5	743.14	18
MPO275		TPDQERSLMFM (11mer)	possible HLA restriction: A*01:01, B*07:02, B*57:01	HL60-B7	for all HLAs very high	12 (A*01)
MPO357	[44]	TIRNQINAL (9mer)	presumably B*07:02	HL60-B7, ML2-B7, NB4-B7, SiG-M5	540.61	13
MPO360	[43]	NQINALTSF (9mer)	B*15:01	CML	9.25	21

MPO365		LTSFVDASMVY (11mer)	possible HLA Restriction: A*01:01, B*07:02, B*57:01	HL60-B7	binder for A*01:01 (151.35)	22
MPO368	[43]	FVDASMVY (8mer)	A*01:01	CML	211.35	n.a.
MPO438		SSEMPELTSM (10mer)	possible HLA Restriction: A*11:01, B*07:02, B*35:01, B*40:01	NB4-B7	binder for B*40:01 (958.96)	13 (A*11:01)
MPO439		SEMPELTSM (9mer)	possible HLA Restriction: A*11:01, B*07:02, B*35:01, B*40:01	NB4-B7	binder for B*40:01 (109.61)	13 (B*40:01)
MPO466	[43]	NPRWDGERL (9mer)	B*07:02	CML, HL60-B7, ML2-B7, NB4-B7, SiG-M5	36.75	23
MPO549		QPMEPNPRVPL (11mer)	possible HLA Restriction: A*11:01, B*07:02, B*35:01, B*40:01	NB4-B7	binder for B*07:02 (36.03)	-
MPO603	[44]	RLFEQVMRI (9mer)	A*02:02	AML	12.33	n.a.
MPO678		GVSEPLKRK (9mer)	presumably A*11	NB4-B7	binder for A*11:01 (173.59)	23 (A*11:01)
MPO718		FSMQQRQAL (9mer)	presumably B*07:02	HL60-B7, ML2-B7	148.45	13

n.a. = not available. Peptides without reference are identified within this work.

3.1.1 Immunogenicity evaluation of possible target peptides using single HLA-mismatched stimulations

The MPO-peptides identified by immunopeptidomics were restricted to different HLA class I molecules (Table 27) and were used to prime naïve $CD8^+$ T cells negative for the respective HLA-allele in a sHLAm setting. For that, autologous dendritic cells (DC) were electroporated with in-vitro transcribed (ivt)-RNA coding for the restriction element coupled to eGFP by a P2A element and pulsed with a peptide candidate before co-stimulation with the $CD8^+$ naïve T cells. Figure 1A exemplarily shows the phenotyping of mature DC and the electroporation efficiency of HLA-B*07:02eGFP ivt-RNA assessed by flow cytometry using anti-CD83, -CD86 and -CD209 antibodies as well as eGFP, respectively. The DC data set shows a very high maturation phenotype with 98% of CD83 and CD86 double positive DC with ~89% of CD209 expression. Compared to the non-electroporated control, ~82% of the ivt-RNA electroporated DC express HLA-B7eGFP. Afterwards, these DC were pulsed with respective peptides of interest and subsequently used to expand autologous HLA-$B7^-$ naïve $CD8^+$ T cells that were stimulated by the respective HLA-B7-peptide complex presented on the surface of the DC. Figure 1B graphically summarizes the sHLAm stimulation approach for the expansion of target antigen-responsive T cells with mature DCs.

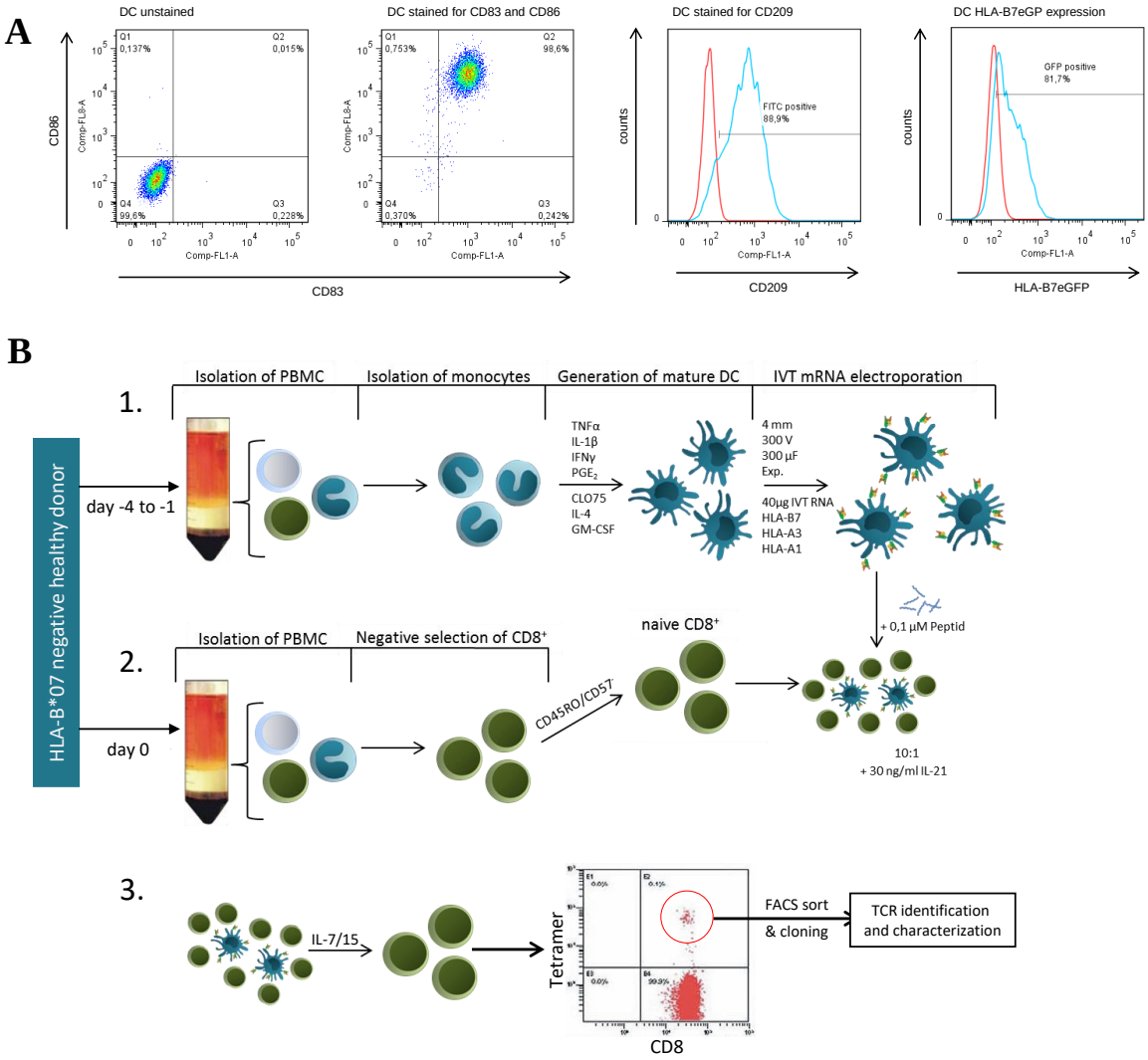

Figure 1: Phenotyping of maturated Dendritic Cells (DC) and single HLA-mismatched stimulation. (A) DC phenotyping using the marker CD83, CD86 and CD209 and eGFP for HLA-B7 expression. (B) Expansion of peptide-specific CD8$^+$ T cells using sHLAm DC followed by T-cell enrichment and cloning after fluorescence-activated cell sorting (FACS).

3.2 Isolation of MPO-specific TCRs

For the identification of MPO-peptide specific T cells, HLA-multimer$^+$ CD8$^+$ T cells stimulated in the sHLAm setting were sorted by flow cytometry. Subsequent clonal expansion followed by evaluation of their reactivity against either T2, K562 or C1R tumor cell lines with transgenic-HLA expression was applied to select T-cell lines with reactivity against these target cell lines.

3.2.1 Identification of MPO_{145}-, MPO_{368}- and MPO_{603}-specific T-cells

In the case of MPO_{145}-stimulated T-cells a $CD137^+$ depletion step before HLA-multimer sort was performed to reduce the proportion of T cells with an HLA-B7 reactivity that is independent of the MPO_{145} peptide. Therefore, the $CD8^+$ T cells, that had been stimulated with the HLA-B7 restricted MPO_{145}-peptide in the sHLAm approach were stimulated with the lethally irradiated C1R-B7 tumor cell line. As those cells do not express MPO, cells with a reactivity against HLA-B7 that is independent of MPO_{145} were activated and upregulated CD137. Those cells were depleted and the population of unspecific HLA-B7 alloreactive T cells was reduced from ~22% to ~3% (Figure 2).

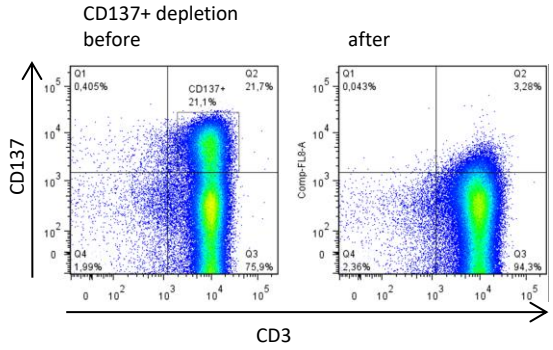

Figure 2: Depletion of $CD137^+$ alloreactive T cells. Co-cultivation of T cells with lethally irradiated HLA-B7-transgenic C1R cells in order to stimulate transient expression of the activation marker CD137 used for flow cytometry-based depletion of $CD137^+$ T cells. Proportions of 7-AAD^- /$CD137^+$/$CD3^+$ T cells are shown before and after depletion of $CD137^+$ T cells.

After the reduction of potential alloreactive T cells, the remaining MPO_{145}-stimulated T cells were sorted by MPO_{145}-HLA-multimer. The MPO_{368}- and MPO_{603}-stimulated T cells were sorted accordingly. A proportion of 0.1% of all T cells used for sorting was positive for the MPO_{145}-HLA-multimer, 0.4% for the MPO_{368}-HLA-multimer, and 0.03% for the MPO_{603}-HLA-multimer (Figure 3). The results of initially evaluated peptide-specificity of the MPO_{368}- and MPO_{603}-peptide-stimulated T-cell lines were promising (Figure 4) and sorted populations were additionally cloned by limiting dilutions. The cultured

T-cell line of the MPO_{145} approach did not expand sufficiently and was lost. Therefore, no results for the peptide specificity of the MPO_{145}-T-cell line are available.

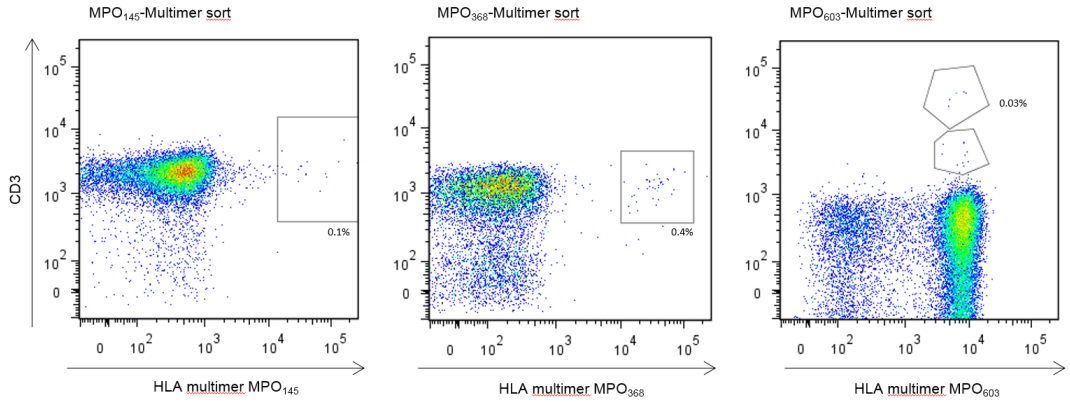

Figure 3: MPO-HLA-multimer sort of T cells. Staining and multimer sort of MPO_{145}-, MPO_{368}- and MPO_{603}-stimulated T cells were done using the HLA-multimer technology. Cells were pre-selected on propidium iodide negative events.

For MPO_{368} (HLA-A1) and MPO_{603} (HLA-A2), however, T-cell line expansion was successful and T cells displayed both reactivity and peptide specificity against K562/C1R-A1 or C1R-A2 target cells pulsed with the respective MPO-peptide or transduced with a vector coding for the whole MPO protein (Figure 4).

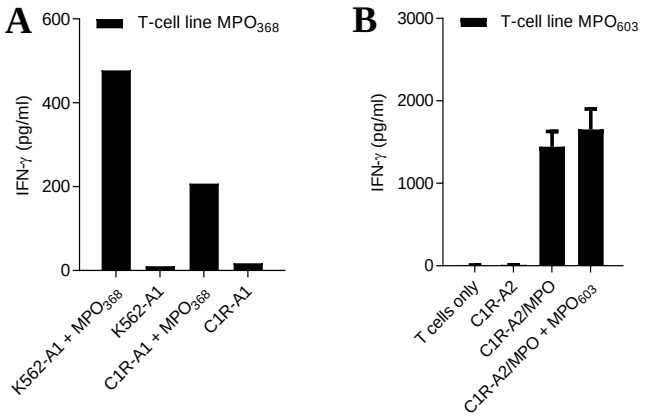

Figure 4: IFN-γ release of T-cell lines against peptide-pulsed or antigen-transduced target cell lines. (A): T-cell line MPO_{368} stimulated with K562-A1 or C1R-A1 target cells either pulsed with MPO_{368} or not. (B): T-cell line MPO_{603} stimulated with C1R-A2 target cells either pulsed with MPO_{603}, transduced with the whole MPO-antigen (/MPO) or without expression of the antigen. T-cell responses were analyzed by IFN-γ ELISA.

Figure 5 shows the results of MPO_{368}-, MPO_{603}- and MPO_{145}-peptide-specific T-cell clones evaluated by either IFN-γ production after stimulation with and/or cytotoxicity against the HLA-B7-transgenic tumor cell lines K562-A1, K562-B7, C1R-A1, C1R-A2 or NB4-A2. For MPO_{145} all tested T-cell clones showed peptide-specific reactivity against the MPO_{145}-pulsed K562-B7 cell line (Figure 5A). Three examined T-cells clones of the MPO_{368}-condition showed peptide specificity against the MPO_{368}-pulsed tumor cell lines C1R-A1 and K562-A1 (Figure 5B). For the MPO_{603}-condition, a clear peptide-specific T-cell response could be observed against the tested C1R-A2 cell line pulsed with the MPO_{603}-peptide. NB4-A2 cells express MPO endogenously and were recognized without pulsing with the MPO603 peptide. The reactivity against the NB4-A2 cell line after MPO_{603}-peptide pulsing showed no beneficial effect on the T-cell response (Figure 5C). This might be related to the already sufficient endogenous presentation of MPO_{603} on HLA-A2 complexes.

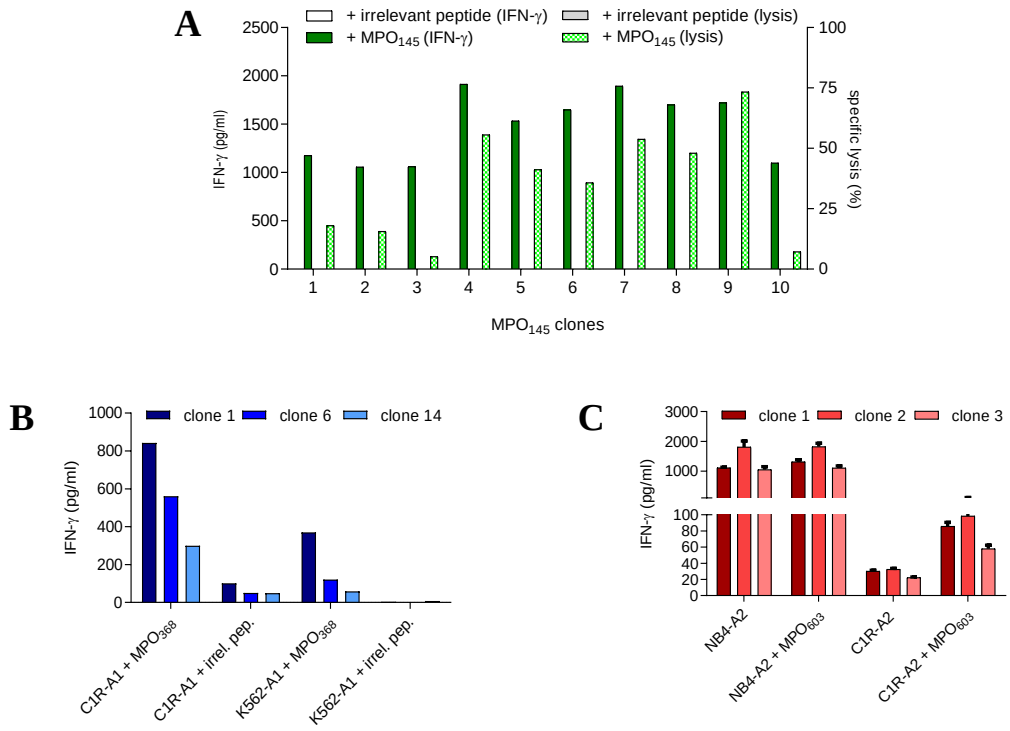

Figure 5: MPO-peptide specificity of T-cell clones. T-cell clones were assessed for peptide specificity against peptide-pulsed target cells. (A) MPO_{145} T-cell clones directed against K562-A1 target cells either pulsed with MPO_{145} or an irrelevant peptide. (B) MPO_{368} T-cell clones directed against C1R-A1 or K562-A1 target cells either pulsed with MPO_{368} or an irrelevant peptide. (C) MPO_{603} T-cell clones directed against NB4-A2 or C1R-A2 target cells either pulsed with MPO_{603} or without peptide pulsing. (A-C): IFN-γ release was analyzed by IFN-γ ELISA and peptide-specific lysis of target cells by flow cytometry at an effector to target ratio of approximately 20:1.

3.2.2 Isolation of MPO_{145}-, MPO_{368}- and MPO_{603}-specific TCRs

For the identification of the TCR sequences of MPO_{145}-, MPO_{368}- and MPO_{603}-specific T cells, T-cell repertoires were analyzed by PCR and gel electrophoresis using cDNA extracted from specific T-cell clones as starting material. Specific PCR products besides the amplified controls were extracted from the gel, and the sequences including the CDR3 regions were identified by sequencing (Table 28). As a representative result for all three TCRs, the TCR-α and TCR-ß repertoire of the MPO_{145}-TCR is shown in Figure 6.

Table 28: Variable α- and ß-chains of MPO_{145}-, MPO_{368}- and MPO_{603}-TCR

TCR	variable α-chain + CDR3	variable ß-chain + CDR3
MPO_{145}-TCR	Va2 - CAVVSGGYQKVTF	Vb1 - CASSVVRSTDTQYF
MPO_{368}-TCR	Va1 - CAVTGGGNKLTF	Vb21 - CASSWDNSYEQYF
MPO_{603}-TCR	Va23 - CAVTKDSNYQLIW	Vb7 - CASSQDWTGTFSEKLFF

824
825

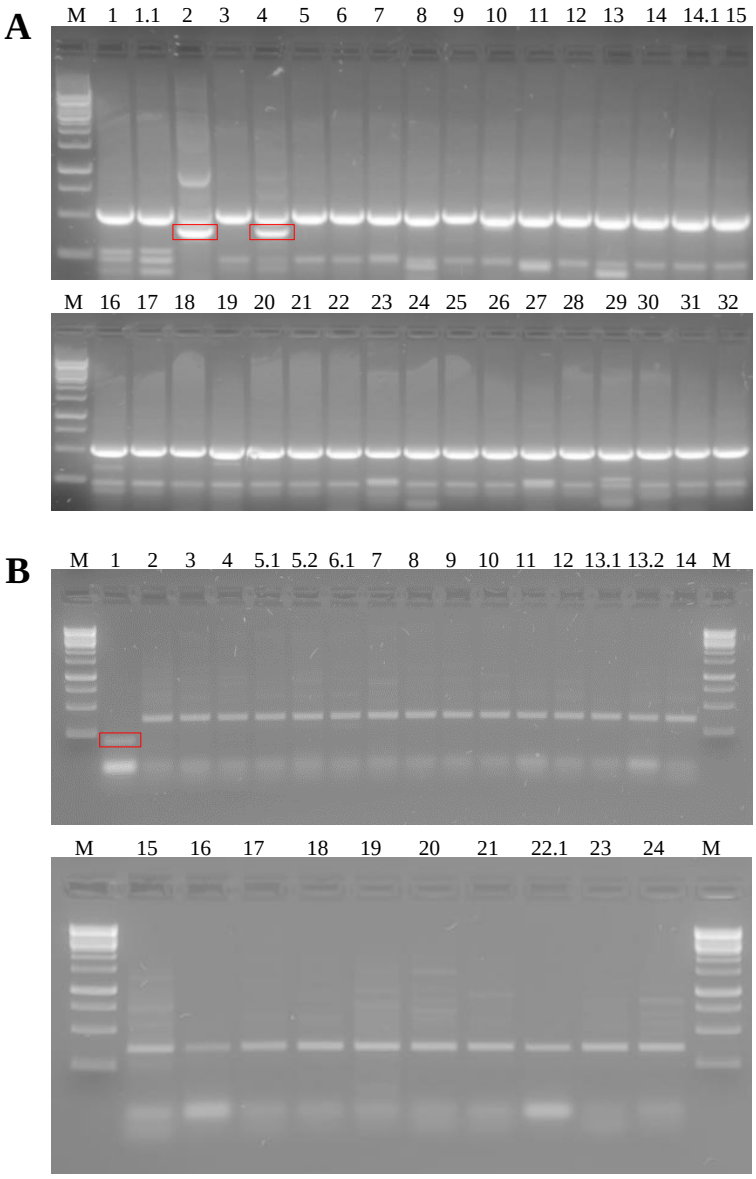

Figure 6: TCR-α and TCR-ß repertoire of MPO_{145}-TCR. The MPO_{145}-TCR revealed prominent PCR products for the Primer Va2 and Va4 (A) as well as for Vb1(B). The PCR product for Va4 was identified as an unproductive TCR rearranged sequence. M = marker, Number = either variable α- or ß-Primer used for amplification.

3.2.3 Transfer of TCR specific for MPO_{145}, MPO_{368}, and MPO_{603} to recipient T cells

To be able to use TCRs in adoptive T-cell therapies using TCR-transgenic T cells, it is necessary to transfer the TCRs to recipient T-lymphocytes. To additionally enhance TCR expression and reduce mispairing of transgenic with endogenous TCR chains in recipient cells, codon optimized and murinized versions of the α- and β-chains of the MPO_{145}-, MPO_{368}- and the MPO_{603}-TCR were synthesized, cloned into the retroviral vector MP71

and retrovirally transduced into healthy donor T-lymphocytes. The results in Figure 7 show representatively, that all three TCRs differ in their transduction efficiencies as determined by FACS-based measurements using an anti-mouse TCR-β chain antibody (TCRm) specific for the murinized constant ß-chain of all three TCRs. While the MPO_{145}- and the MPO_{368}-TCR could be efficiently transferred, exemplarily shown for PBMCs (Figure 7A, B, ~ 42%/63%), the MPO_{603}-TCR displayed only minimal amounts of the murinized TCR-β chains after transduction (Figure 7C, ~ 5%). Intracellular staining for the murinized TCR-β chains in MPO_{603}-TCR-transduced T cells revealed that the TCR was almost completely trapped intracellularly (Figure 8). Because of this insufficient surface expression, the characterization of the MPO_{603}-TCR had to be discontinued.

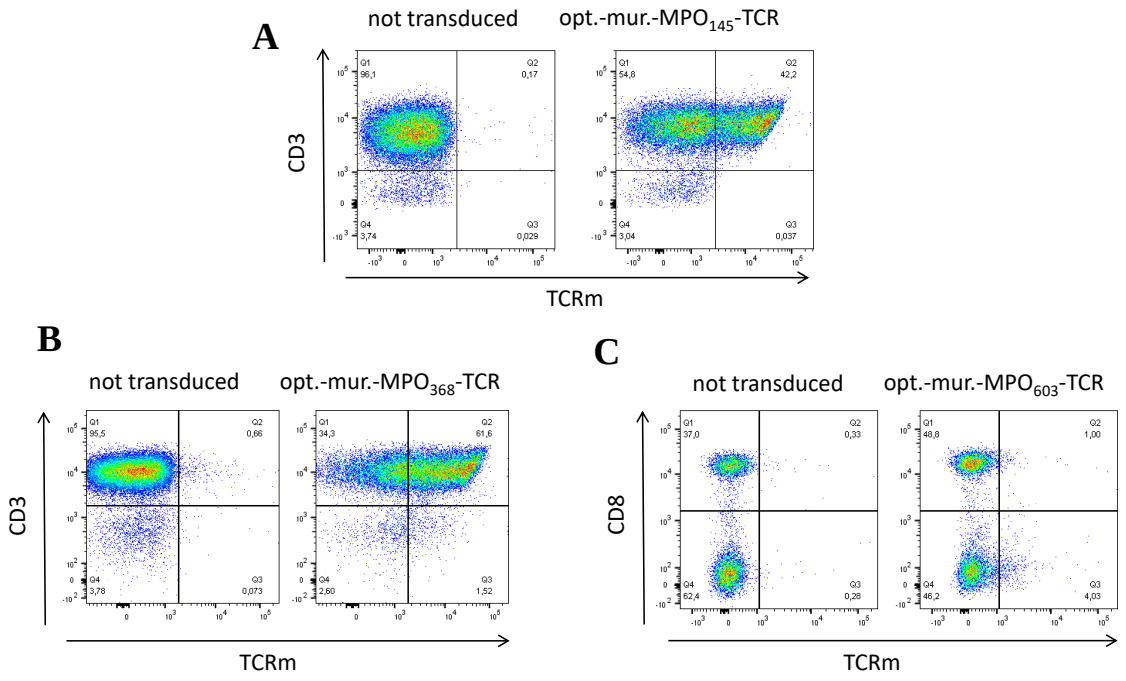

Figure 7: Transduction efficacies of the MPO145-, MPO368- and MPO603-TCR. Flow cytometry analysis of 7-AAD⁻ TCR-transduced healthy donor lymphocytes. (A): MPO_{145}-TCR. (B): MPO_{368}-TCR. (C): MPO_{603}-TCR.

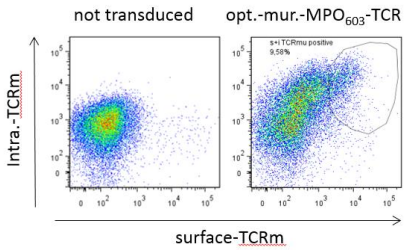

Figure 8: Intracellular TCRm staining of the MPO_{603}-TCR. Flow cytometry analysis of EMA^- TCR-transduced healthy donor lymphocytes.

After successful transduction of the MPO_{145}- and MPO_{368}-TCR in T cells, peptide specificity and cytotoxic potential of the TCR-transgenic T-cell lines were tested. Surprisingly, the MPO_{368}-TCR with HLA-A1 restriction recognized the HLA-B7 transgenic and MPO^+ tumor cell line NB4 that does not express HLA-A1 (Figure 9). The recognition of the MPO^+ HL60-B7 cell line, however, was expected because of endogenous expression of HLA-A1 that is absent in the tested NB4 cell line. As the MPO_{368}-independent recognition of HLA-B7-transgenic NB4 cells has been observed in several experiments, the characterization of the MPO_{368}-TCR was discontinued.

The MPO_{145}-TCR-transduced T cells specifically recognized MPO_{145}-pulsed or MPO_{145}-minigene transduced KG-1a (Figure 10A) as well as C1R transgenic for the MPO protein (Figure 10B) with the correct restriction element HLA-B7. Furthermore, MPO_{145}-TCR-transduced T cells efficiently killed the NB4-B7 cell line with endogenous MPO-protein expression (Figure 10C).

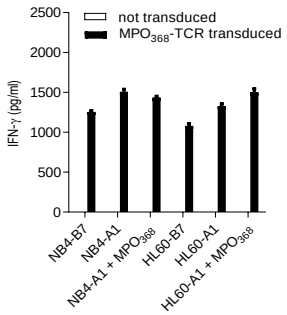

Figure 9: Missing MPO_{368}-specificity of MPO_{368}-TCR-transduced T cells. The T-cell response of MPO_{368}-TCR-transduced T cells was analyzed by IFN-γ ELISA after co-cultivation with either the MPO_{368}-pulsed target cell lines NB4-B7, NB4-A1, HL60-A1 or HL60-B7 or without peptide pulsing.

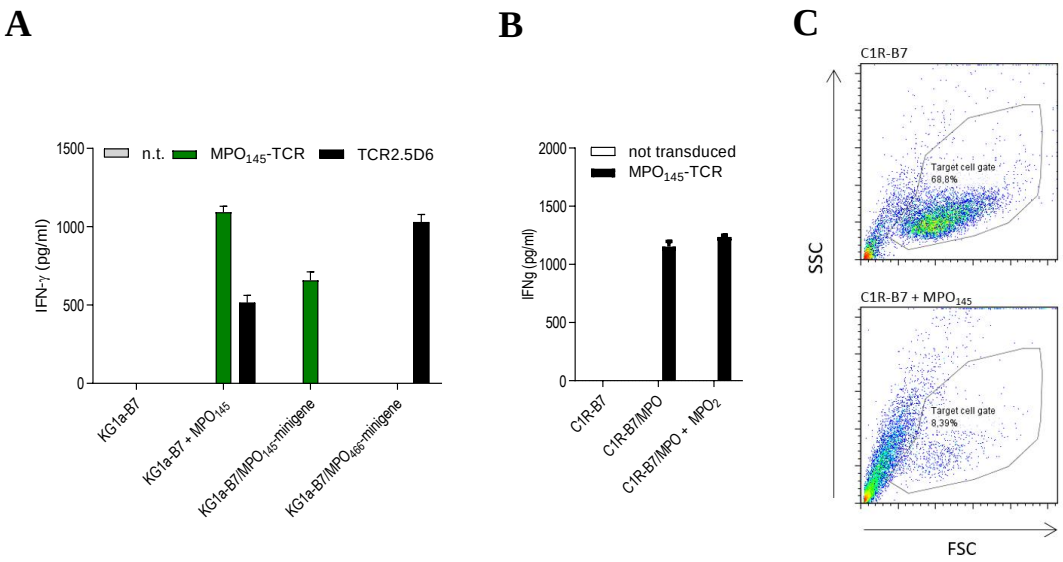

Figure 10: Peptide specificity of MPO_{145}-TCR-transduced T cells. (A, B): T-cell response of MPO_{145}-TCR-transduced T cells directed against the target cell lines KG-1a-B7 or C1R-B7 either pulsed with the relevant MPO-peptide or transduced with the MPO-minigene (/MPO_{xxx}-minigene) or the MPO-protein sequence (/MPO). (C): Cytotoxicity of MPO_{145}-TCR-transduced T cells against the C1R-B7 target cell line pulsed with MPO_{145}. IFN-γ release was assessed by IFN-γ ELISA; Cytotoxicity was assessed by measuring the number/percentage? of 7-AAD^-GFP^+ C1R-B7 target cells using flow cytometry. TCR2.5D6 served as control for epitope-specific target recognition.

Taken together, the peptide-specific TCR reactivity of all three TCRs, observed at the clonal T-cell level, could be successfully transferred to recipient-donor T cells for the MPO_{145}-TCR. This TCR is from now on named TCRF5.4.

3.2.4 Peptide-dependent and -independent cross-reactivity of TCRF5.4 against various HLA molecules

For further cross-reactivity analysis of the MPO_{145}-TCR, the peptide-dependent and independent cross-reactivity against a set of lymphoblastoid cell lines (LCL) were tested covering a broad variety of different HLA-alleles (Table 29). The LCLs were either pulsed with the MPO_{145}-peptide or not and co-cultured with MPO_{145}-TCR-transgenic T cells. The results (Figure 11) revealed MPO_{145}-independent cross-reactivities against the RML- and LWAGS-LCLs expressing HLA-A02 and HLA-B51 or HLA-A33 and HLA-B14, respectively. The LCL cell lines MaOe, JNB3 and LSK1 served as positive controls after MPO_{145}-peptide pulsing.

Table 29: HLA-A* and HLA-B* phenotype of lymphoblastoid cell lines

LCL cell line	HLA-A*	HLA-B*	LCL cell line	HLA-A*	HLA-B*
AMALA	02:17/ --	15:01/ --	LWAGS	33:01/ --	14:02/ --
BM21	01:01/ --	41:01/ --	MaOe	02:01/ --	07:02/15:01
DKB	24:02/ --	40:01 / --	OZB	02:09/03:01	35:01/38:01
DUCAF	30:02 / --	18:01 / --	RML	02:04/ --	51:01/ --
HOM2	03:01/ --	27:05/ --	RSH	68:02/30:01	42:01/ --
JNB3	01/02:01	07/40:01	SWEIG007	29:02/ --	40:02/ --
KLO	02:08/ --	50:01/08:01	XLIND	02:10 /30	13/61
LSKB1	01/02	07/08			

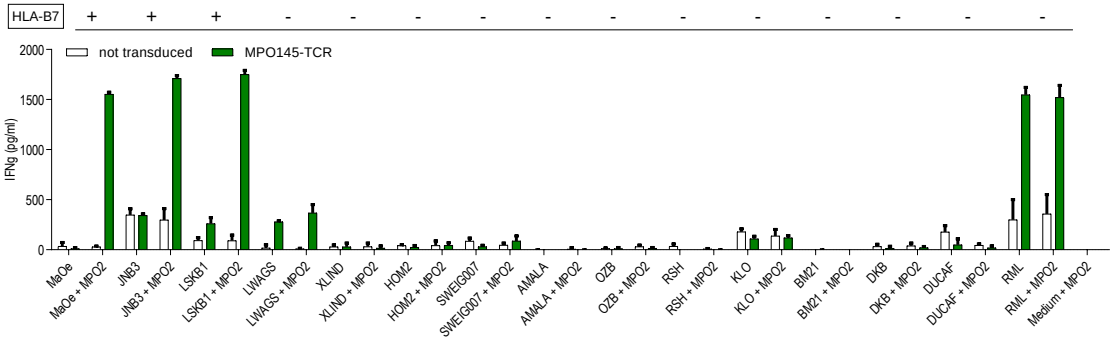

Figure 11: MPO_{145}-dependent and -independent reactivity against a panel of lymphoblastoid cell lines. The T-cell response of MPO_{145}-TCR-transduced T cells directed against various LCL target cell lines either pulsed with the MPO_{145}-peptide or without peptide pulsing. IFN-γ release was assessed by IFN-γ ELISA. HLA-expression of the LCL cell lines is shown in Table 29.

In other experiments, the reactivity against a set of HLA-B7 restricted peptides pulsed in pools on C1R-B7 cells was tested. Here, no recognition of the tested peptides (list of peptide sequences and composition of pools is shown Table 30) by MPO_{145}-TCR-transgenic T cells could be observed (Figure 12). As controls, the C1R-B7 cell line pulsed with the MPO_{145}-peptide (positive control) and not transduced T cells or target cells not pulsed with the MPO_{145}-peptide (negative controls) were used.

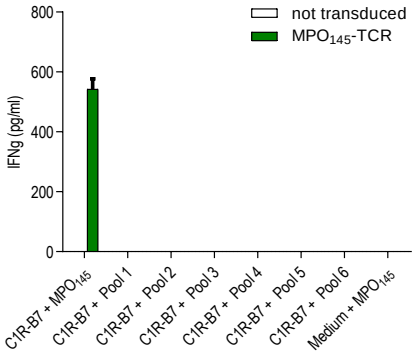

Figure 12: Stimulation of MPO_{145}-TCR-transgenic T cells with pools of HLA-B*07:02 restricted peptides. The T-cell response of MPO_{145}-TCR-transduced T cells directed against the C1R-B7 cell lines pulsed with peptide pools containing known HLA-B7 binding peptides was investigated. The IFN-γ release was analyzed by IFN-γ ELISA.

909 **Table 30: Pools of HLA-B*07:02 restricted peptides.**

Peptide pool	Sequence	Peptide pool	Sequence
1	APRGPHGAASGL	**4**	APRGKSGAAL
	EPRPVFAV		IPQRLVNVVL
	FPESLMVGLAV		LPDAQRLY
	FPNIPGKSL		LPNGTRVPM
	GPALGRSFL		QPMEPNPRVPL
	IARNLTQQL		QPVPHGTQCL
	IPQIRNPSL		RPHERNGFTVL
	KPGKFVTTL		RPHERNGFTVL
	NPRTQTHATL		RPILTIITL
	RPELVRPAL		TPRVTGGGAM
2	APAPIHNQF	**5**	GPHYSTQRGV
	APRAPRVPR		GPRTAALGLL
	KPNANRIAL		GPRYSTQRGV
	LPHAPGVQM		IPRAALLPLL
	RPPIFIRRL		KPNANRIAL
	RPQGGSRPEF		KPSKDGVTV
	RPQGGSRPEFV		SPSSILSTL
	RPQGGSRPEFVKL		SPYQNIKIL
	RPTLWAAAL		TPHQTFVRL
	WPMGYRTAT		YPDRIMNTF
3	FPKGFSVEL	**6**	APYSRPKQL
	HPEYNRPLL		EPAKTSSVSL
	RPKSSLPPVL		HPTSVISGY
	RPPPIGAEV		LPDDKVTAL
	RPRAATVVA		LPNVGKSTLF
	SPIKVTLATL		QPAKTSSVSL
	SPQQVDFRSVL		RPMSLRSTII
	TPKEKAQAL		RPRALPGHL
	VPLIQSRI		
	VPTRGSLEL		

910

911 3.2.5 Reactivity of TCRF5.4 against hematopoietic tumor cell lines

912 As the MPO_{145}-TCR revealed a promising safety pattern, reproducible high transgenic
913 expression in transduced T cells and peptide specificity, this TCR was characterized in
914 more detail.

First, the reactivity against tumor cells of hematopoietic origin was tested using a set of HLA-B7-transgenic tumor cell lines with or without endogenous MPO expression. As controls MPO-negative target cell lines, not transduced T cells or PMA/IONO-stimulated T cells were used. Only the target cell lines with the MPO_{145}-restriction element, namely HLA-B7, and endogenous MPO expression or pulsed with the MPO_{145}-peptide were recognized by TCRF5.4-transgenic T cells (Figure 13). While all cell lines with exact requirements were recognized reliable by TCRF5.4-transgenic T cells, substantial differences in quantitative responses could be observed between the different target cell lines. However, except for target cell lines SET2-B7 and MOLT4-B7, the IFN-γ response levels towards all MPO_{145}-pulsed target cell lines were similar. The observed differences in IFN-γ release upon stimulation with the target cell lines with endogenous MPO expression in comparison to their additionally MPO_{145}-pulsed pendants, is an indication for limited saturation of HLA-B7 molecules on the cell surface with endogenously processed MPO_{145}-peptides which could be enhanced after additional MPO_{145}-peptide pulsing.

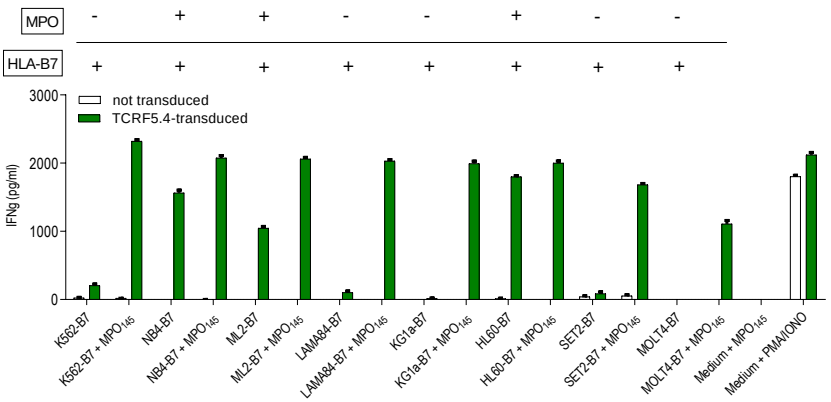

Figure 13: Reactivity of TCRF5.4-transduced T cells against target cell lines of hematopoietic origin. The T-cell response of TCRF5.4-transduced T cells is shown against various cell lines of hematopoietic origin with or without endogenous MPO expression either pulsed with the MPO_{145}-peptide or not. The T-cell response was analyzed by IFN-γ ELISA.

3.2.6 TCRF5.4 reactivity against primary cell material

To evaluate the reactivity of TCRF5.4-transduced T cells against primary tumor cells, a panel of CML cell samples were used. CML 1, 2, 5, 13 and 15 are positive for both MPO and HLA-B7 expression while CML 9 and 10 are negative for both markers and served beside the C1R-B7 cell line as negative controls (Figure 14). The validation of MPO-protein expression was evaluated by Richard Klar by immunopeptidomics, flow cytometry or qPCR [43]. TCRF5.4-transduced T cells showed reactivity against CML 2, 5, 13 and 15 without additional MPO_{145}-peptide pulsing. CML 1 was only recognized after additional MPO_{145}-peptide pulsing indicating insufficient endogenous MPO_{145}-HLA-B7-epitope presentation on the surface of the cells. In general, the IFN-γ release of TCRF5.4-transduced T cells was higher after additional MPO_{145}-peptide pulsing.

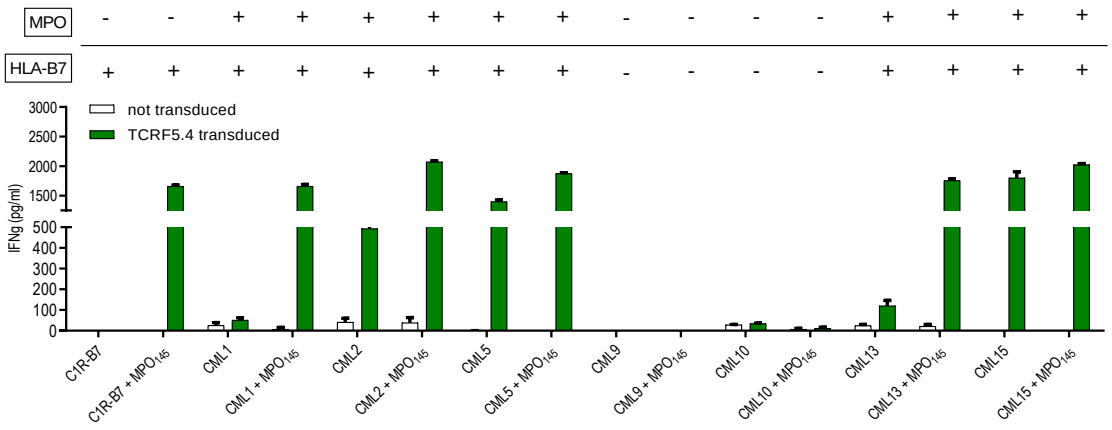

Figure 14: Reactivity of TCRF5.4-transduced T cells against primary CML samples. The T-cell response of TCRF5.4-transduced T cells is shown against primary CML cells either with or without endogenous MPO expression and correct or missing HLA-B7 restriction. As a control, the target cell lines were additionally pulsed with the MPO_{145}-peptide. The T-cell response was analyzed by IFN-γ ELISA.

3.2.7 Amino acid substitution assays of the MPO_{145}-peptide

For the identification of the most critical amino acids of the MPO_{145}-peptide responsible for the peptide specificity of TCRF5.4, amino acid exchange experiments were per-

formed. For that, each amino acid of MPO_{145} was successively substituted by either alanine or threonine (Figure 15 A, B). MPO-peptide variants were pulsed on the LCL cell line MaOe with endogenous HLA-B7 expression. After co-cultivation with TCRF5.4-transgenic T cells, secretion of IFN-γ was analyzed, and the TCR-binding motifs of the recognition patterns were assessed.

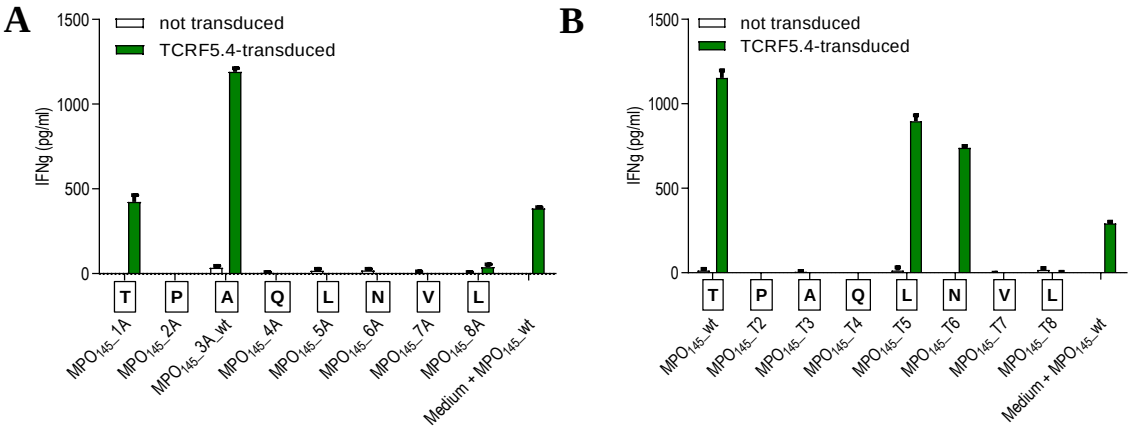

Figure 15: Recognition of Alanine- or Threonine substituted MPO_{145}-peptide variants. The T-cell response of TCRF5.4-transduced T cells is shown against the LCL target cell line (MaOe) pulsed with either Alanine- (A) or Threonine- (B) substituted MPO_{145}-peptide variants. T-cell responses were assessed by IFN-γ ELISA.

Using the ScanProsite tool [92], alanine substitutions resulted in the binding motif *X-P-A-Q-L-N-V-X* with no hit outside the MPO source protein. The threonine variant counterparts led to the motif *T-P-A-Q-X-X-V-L* with one hit in the human proteome outside the MPO source protein. Taken together, the amino acid substitutions using alanine and threonine revealed different TCR recognition motifs. The combination of both patterns resulting in the motif *X-P-A-Q-X-X-V-X* generates numerous hits (297) outside the MPO source protein. This result would indicate highly critical peptide promiscuity.

3.3 Functional characterization of TCRF5.4 compared to TCR2.5D6

The MPO_{466}-peptide-specific TCR named TCR2.5D6 with HLA-B7 restriction was characterized in-depth previously [43]. To broaden the understanding of TCR-mediated recognition and evaluation of characteristics that are essential for TCR's successful clinical translation, TCR2.5D6 was selected for detailed comparison with the novel TCRF5.4. Both TCR share the same restriction element, but target different peptides derived from the same MPO antigen.

3.3.1 Comparison of TCR transduction efficiency and surface expression

The mean transduction efficiency for TCRF5.4 (72.2%) was approximately 10% lower compared to TCR2.5D6 (84.5%) (Figure 16A). Although this holds true for nearly all examined healthy donor T cells, partly substantial differences could be observed between different donors used for transduction. An even stronger effect was observed for the TCR-surface expression (mean fluorescens intensity, MFI) analyzed by flow cytometry using the anti-mouse TCR-ß chain (TCRm) antibody. Here, the TCR2.5D6 showed considerably enhanced TCR surface density compared to TCRF5.4 (Figure 16B). Additional staining for residual intracellular TCRs revealed that a part of the TCRF5.4 is kept inside the T cells while the TCR2.5D6 is completely located on the surface of the T cells (Figure 17). Summarized, the TCRF5.4 could not compete with the TCR2.5D6 regarding transduction efficacy, surface expression as well as surface density.

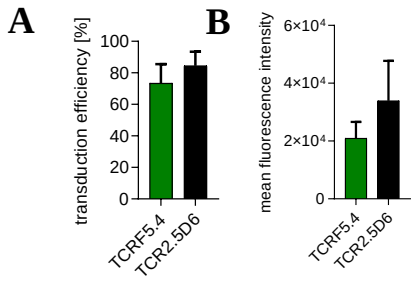

Figure 16: Transduction efficiency and mean fluorescence intensity of TCRF5.4 compared to TCR2.5D6. (A): murine TCR-ß chain transduction efficiency of $CD3^+$7-AAD^- T cells; (B): Mean fluorescence intensity of the murine TCR-ß chain of T cells analyzed in (A).

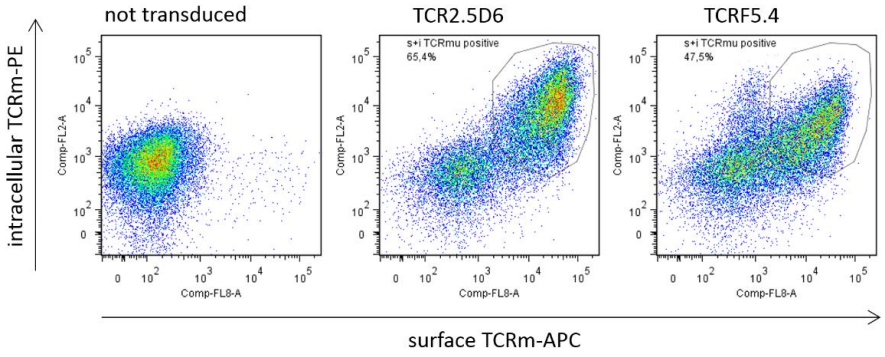

Figure 17: Intracellular staining of PBMCs for TCR2.5D6 and TCRF5.4. Intracellular versus surface presentation of the murine TCR-ß chain (TCRm) of TCR2.5D6- or TCRF5.4-transduced T cells. The cells were pre-gated for EMA^-CD3^+ events.

3.3.2 Comparison of functional avidity

To test the functional avidity, the KG-1a and the C1R target cell lines without endogenous MPO but transgenic HLA-B7 expression were used. The target cells were pulsed with graded amounts of either MPO_{145} or MPO_{466} and co-incubated with TCRF5.4- or TCR2.5D6-transduced T cells, respectively. The calculation of half maximal response (EC_{50}) of the transduced T cells after stimulation was used as a basis to determine the TCR's functional avidity. Of note, for this comparison both TCR-transduced T cells were neither adjusted to TCR-expression nor to TCR-transduction efficiency in order to char-

acterize both TCRs with their limitations. The results revealed highly comparable functional avidity values for both TCRs with a median of 40.89 nM for the TCRF5.4 and 46.15 nM for the TCR2.5D6 (Figure 18).

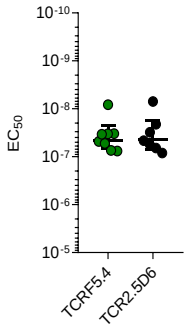

Figure 18: Pooled results of functional avidity for TCRF5.4 and TCR2.56. Comparison of EC_{50} values of functional avidity assessed for both TCR-transduced T cells (n=8). The functional avidity was calculated measuring the IFN-γ release of TCR-transduced T cells stimulated with the KG-1a-B7 target cell line pulsed with graded amounts of the relevant MPO-peptide and consecutive EC_{50} determination using GraphPad Prism (version 8).

3.3.3 Comparison of dissociation rates of TCR-p-MHC-complex (K_{off})

For further characterization of TCR-p-MHC binding kinetics, the dissociation rate of the p-MHC complexes from the TCR-transduced T cells was calculated. These k_{off}-measurements were used to evaluate the half-life ($t_{1/2}$) and subsequently to get an indication for the stability of both complexes (Figure 19). Equivalent to the results of the functional avidity, no significant differences could be observed for both TCRs displaying similar k_{off} values of a median of 70.7 s for TCRF5.4 and 64.6 s for TCR2.5D6.

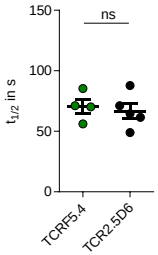

Figure 19: Dissociation rate of the MPO-peptide-MHC complexes from TCRF5.4- or TCR2.5D6-transduced T cells (k_{off}). Comparison of k_{off} of both TCR-transduced T cell populations (TCRF5.4, n=4; TCR2.5D6, n=5). The signal decay of fluorescent labeled MPO-peptide-MHC complexes bound to the T cells was monitored by flow cytometry of pre-gated $CD3^+PI^-$ T cells over time. $T_{1/2}$ was calculated using GraphPad Prism's exponential decay algorithm [102].

3.3.4 Comparison of cytokine secretion patterns

After the assessment of TCR-transduction qualities, TCR functional avidity and dissociation times of both TCR-p-MHC complexes, the quality and quantity of cytokine secretion after stimulation of TCR-transduced donor T cells were analyzed usingthe AML cell lines ML2, NB4, HL60 and SiG-M5. Common to all these cell lines is the endogenous MPO expression. The cell lines ML2, NB4, and HL60 are transgenic for HLA-B7 while the SiG-M5 cell line is endogenously expressing HLA-B7.

Initially, the HLA-B7 expression of all cell lines was analyzed by flow cytometry. The results indicated substantial differences in HLA-B7 expression levels between the different AML-cell lines. The HL60 cell line displayed the highest expression of transgenic

HLA-B7 whereas the SiG-M5 was the cell line with the lowest HLA-B7 expression (Figure 20A). Additionally, the differences in the MPO-mRNA expression of the four AML cell lines were assessed using the SYBR-Green qPCR technique. The results were compared to the expression of MPO-mRNA of human bone marrow samples. Within all AML-cell lines, the SiG-M5 cell line showed the highest level of MPO-mRNA (3.4x) followed by NB4 (2.8x), ML2 (1.8x) and HL60 (1.7x) with the lowest mRNA expression (Figure 20B). Compared to the results of the HLA-B7 expression, the MPO expression is precisely the opposite. The HL60 cell line with the highest HLA-B7 surface density expressed the lowest amounts of MPO-mRNA while the SiG-M5 cell line expressed the highest MPO-mRNA levels displayed the lowest HLA-B7 density on the surface of the cells. Therefore, the chosen set of AML-cell lines for the cytokine release characterization of TCR-transgenic T cells covers a broad range of possible HLA-B7- and MPO-expressions.

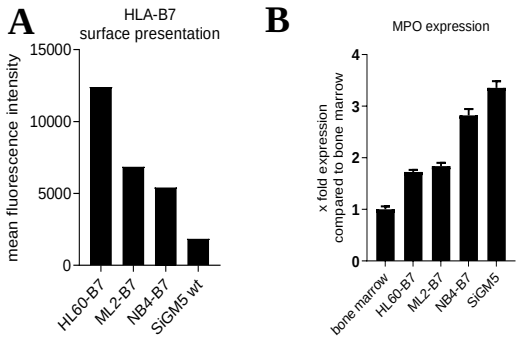

Figure 20: Cell surface expression of HLA-B7 and mRNA expression of the MPO protein in AML cell lines. (A): Mean fluorescence intensity of transgenic HLA-B7 on the AML-cell lines HL60-B7, ML2-B7 and NB4-B7 as well as endogenous expressed HLA-B7 on the SiG-M5 cell line. (B): Semi-quantitative real-time PCR normalized to the genes GAPDH, HPRT1, and HMBS. The MPO expression levels in the AML-cell lines HL60-B7, ML2-B7, NB4-B7, and SiG-M5 were compared to the expression in healthy bone marrow samples [102].

As a next step, the cytokine profile of TCRF5.4 and TCR2.5D6 transduced PBMC was assessed after co-incubation with AML-cell lines HL60-B7, ML2-B7, NB4-B7 and SiG-M5 comprising the following cytokines: GM-CSF, IFNα, IFN-γ, IL-2, IL-4, IL-5, IL-6, IL-9, IL-12, IL-10, IL17A and TNFα (Figure 21 A-D).

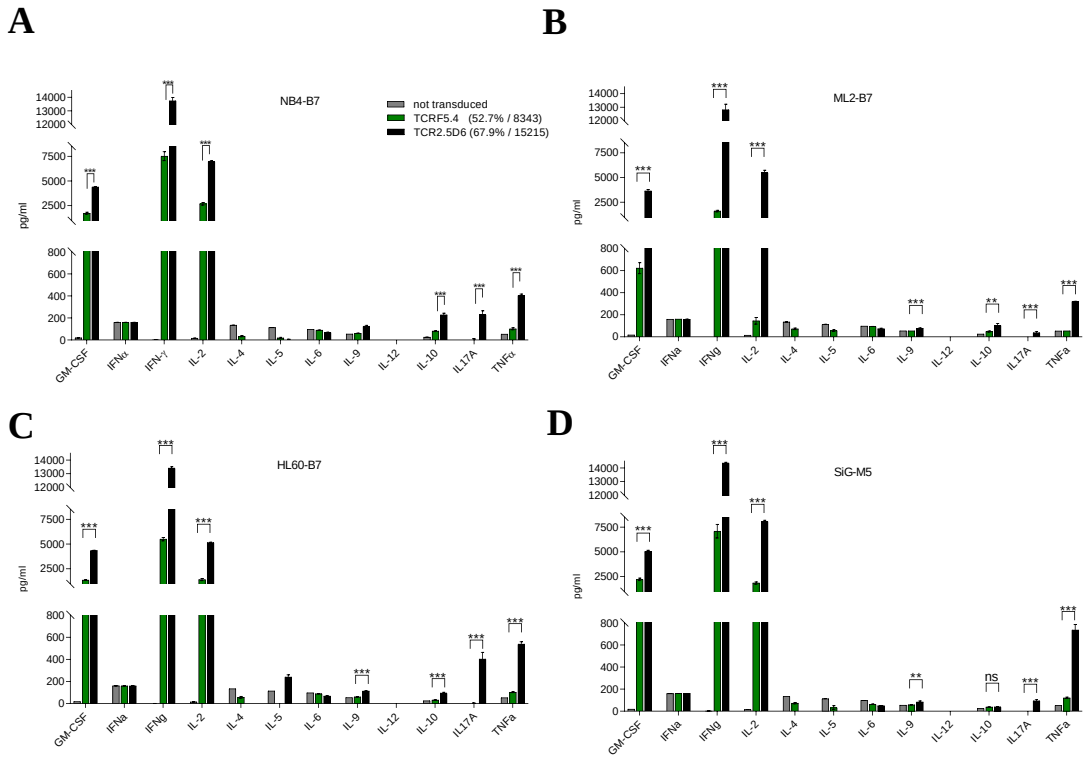

Figure 21: Cytokine release of TCRF5.4- and TCR2.5D6-transduced T cells. Selected cytokines were analyzed by a multiplexed flow cytometry approach. The AML-cell lines NB4-B7 (A), ML2-B7 (B), HL60-B7 (C) and SiG-M5 (D) were co-incubated either with the TCRF5.4- or TCR2.5DD6-transduced T cells for 20h and the supernatants used for the consecutive cytokine staining. The quantity of cytokines was calculated according to standard curves measured for each cytokine. The results were compared to a not transduced T-cell control. The results are shown in triplicates for n=2, **p > 0.05, ***p >0.001.

As shown before in previous co-stimulation experiments for the IFN-γ release, differences were also seen in the quantity of cytokine secretion for GM-CSF, IFN-γ and IL-2 between TCRF5.4 and TCR2.5D6. TCR2.5D6-transduced PBMCs significantly secreted higher amounts of cytokines compared to TCRF5.4-transduced PBMCs. Additionally, TCR2.5D6-transduced PBMCs secreted detectable amounts of IL-10, IL-17A and TNFα

compared to TCRF5.4-transduced PBMC with very low or even undetectable cytokine levels. Thus, besides quantitative differences in cytokine secretion, there is also a qualitative difference between both TCR-transduced T cells.

However, in repetition experiments using the same four AML-cell lines with additional exogenous peptide pulsing of 1 µM MPO_{145} or MPO_{466}, the quantitative lower cytokine secretion observed for TCRF5.4-transduced T cells was compensated and similar to TCR2.5D6-transduced T cells (Figure 22). Interestingly, additional MPO_{466}-peptide pulsing showed a beneficial effect for SiG-M5 cells whereas the other AML-cell lines remained rather unaffected. This result is in line with the low HLA-B7 expression of the SiG-M5 cell line and indicates an incomplete saturation of endogenous processed and HLA-presented MPO_{466}-peptides. In the case of MPO_{145}, this is true for all tested AML-cell lines.

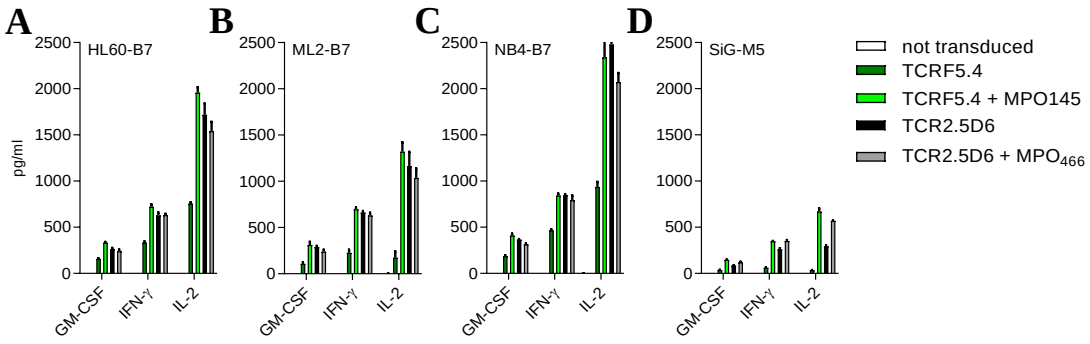

Figure 22: Cytokine release of TCR-transduced T cells after additional MPO-peptide pulsing. TCRF5.4- or TCR2.5D6-transduced T cells were analyzed for secretion of the cytokines GM-CSF, IFN-γ and IL-2 after co-incubation with the AML-cell lines HL60-B7 (A), ML2-B7 (B), NB4-B7 (C) and SiG-M5 (D) with or without additional MPO-peptide pulsing. The secreted cytokines were measured by multiplexed flow cytometry analyses. The results are shown in triplicates for n=2; adapted from [102].

3.3.5 Comparison of IFN-γ release and cytotoxicity in effector to target ratio titrations

In consecutive co-stimulation experiments, the cytotoxic potential was analyzed besides the IFN-γ release for both TCR-transduced T cells. Notably, no substantial differences in

cytotoxicity against the set of AML-target cell lines could be observed between both TCR-transduced T-cell populations (Figure 23A) although the IFN- γ releases were again markedly different (Figure 23B).

Effector to target titrations performed for 4h and 20h co-stimulation confirmed the previous results. Again, the IFN-γ release of TCRF5.4-transduced T cells was inferior for high E/T ratios compared to TCR2.5D6-transduced T cells (Figure 24A, B). However, the cytotoxicity was similar for both TCRs with a trend for TCRF5.4 to be more cytotoxic than TCR2.5D6 over a broad range of E/T ratios (Figure 24 C, D). These finding could be confirmed by calculating the half-maximal (EC_{50}) killing efficacy and IFN-γ release for both TCR-transduced T cells at both time points (4h and 20h, Table 31). The EC_{50} values favor the TCRF5.4-transduced T cells regarding killing efficacy and responsiveness. Furthermore, there is a tendency that approximately ½ of TCRF5.4-transduced T cells are necessary to lyse target cells and to release IFN-γ compared to TCR2.5D6.

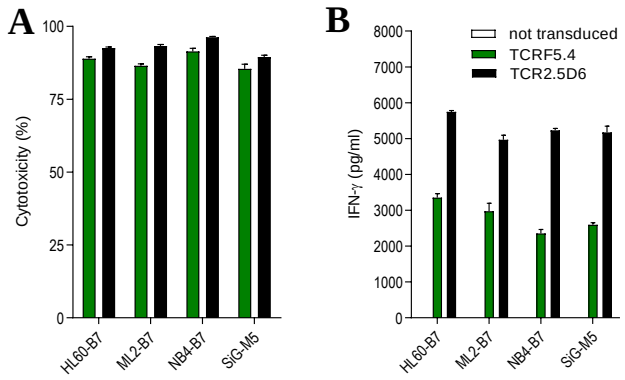

Figure 23: Cytotoxicity and IFN-γ release of TCRF5.4- and TCR2.5D6-transduced T cells. Cytotoxicity (A) and IFN-γ release (B) of selected AML-cell lines were analyzed after 20 h of co-incubation with either TCRF5.4- or TCR2.5D6-transduced T cells. The cytotoxicity was analyzed by flow cytometry and the IFN-γ release was assessed by IFN-γ ELISA.

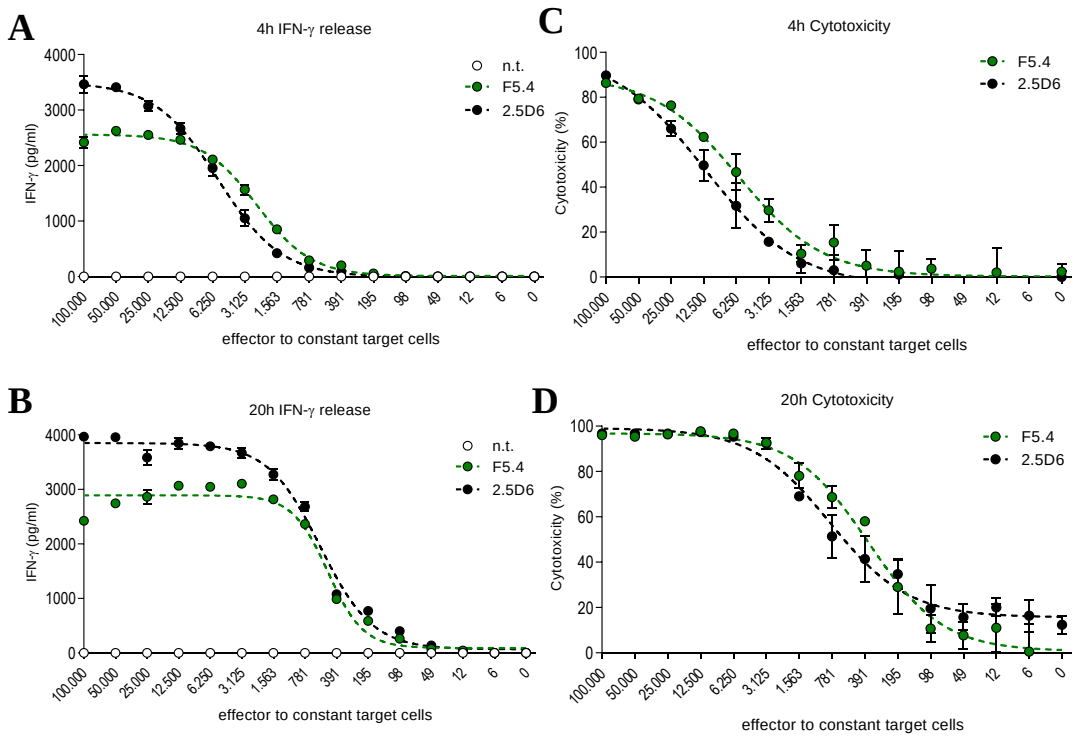

Figure 24: Cytotoxicity and IFN-γ release of TCRF5.4- and TCR2.5D6-transduced T cells at different effector to target ratios. Effector to target titrations ranging from 5:1 to 0.0031:1 were performed for selected quantities of TCR-transduced CD8⁺ TCM co-incubated for either 4h (upper row) or 20h (lower row) with 20.000 NB4-B7 target cells. IFN-γ release was measured by IFN-γ ELISA (A, B). The cytotoxicity was analyzed by flow cytometry (C, D). Adapted from [102].

Table 31: EC_{50}-values of cytotoxicity and IFN-γ release for effector to target titrations

EC_{50}	TCRF5.4 [cells]	TCR2.5D6 [cells]
Cytotoxicity 4h	4542 to 8459, E/T* 0.33	9188 to 19066, E/T 0.71
Cytotoxicity 20h	299 to 441, E/T 0.02	654 to 1007, E/T 0.04
IFN-γ 4h	2263 to 2541, E/T 0.12	5207 to 5887, E/T 0.28
IFN-γ 20h	417 to 532, E/T 0.02	510 to 615, E/T .0.03

*E/T = mean of T-cell range necessary to reach EC_{50} at constant number of 20.000 engaged target cells.

3.4 In-vivo characterization of TCRF5.4 compared to TCR2.5D6

The in-vivo characterization of promising TCR-candidates using tumor mouse models is essential for preclinical testing. In the following in-vivo experiments, the NOD.Cg-Prk-dcscidIl2rgtm1Wjl/SzJ (NSG) immunocompromised tumor mouse model was used

[105]. In a first experiment, the HLA-B7-transgenic tumor cell line ML2 with endogenous MPO expression was used for subcutaneous solid tumor inoculation. As this cell line turned out to be positive for the HLA-B*51:01 allele and the TCRF5.4 showed HLA-B51-related cross-reactivity, the AML-cell lines HL60 and NB4 were initially tested in ex vivo co-stimulation experiments for immunogenicity as an alternative tumor model. Finally, the NB4 cell line was chosen for short- and long-term in-vivo experiments to compare the tumor growth kinetics and overall survival of the mice after adoptive transfer of TCRF5.4- and TCR2.5D6-transduced $CD8^+$ T cells enriched for the central memory phenotype ($CD8^+$ T_{CM}). All in-vivo experiments described below followed a defined workflow. Starting with the T_{CM}-phenotyping of the T-cell product and analysis of the transduction efficacy at the day of (or one day before) adoptive T-cell transfer, the T-cell products were tested in-vitro for their cytotoxicity and the capacity to release IFN-γ upon stimulation with cultured tumor cells used for tumor induction in the mice.

3.4.1 ML2-tumor mouse model

The phenotyping and evaluation of TCR-transduction efficiency of TCRF5.4- or TCR2.5D6-transgenic $CD8^+$ T_{CM} phenotype was done two weeks after in-vitro expansion. A representative phenotyping is shown in Figure 25A and B. Both T-cell products were highly similar regarding CD45RO (~73% of living CD8+ cells) and CD62L (~34% of living CD8+ cells) proportions. The transduction efficiency was ~87% for TCRF5.4 and ~97% for TCR2.5D6 and reflects the often-observed difference of approximately 10% in transduction efficiency between both TCRs.

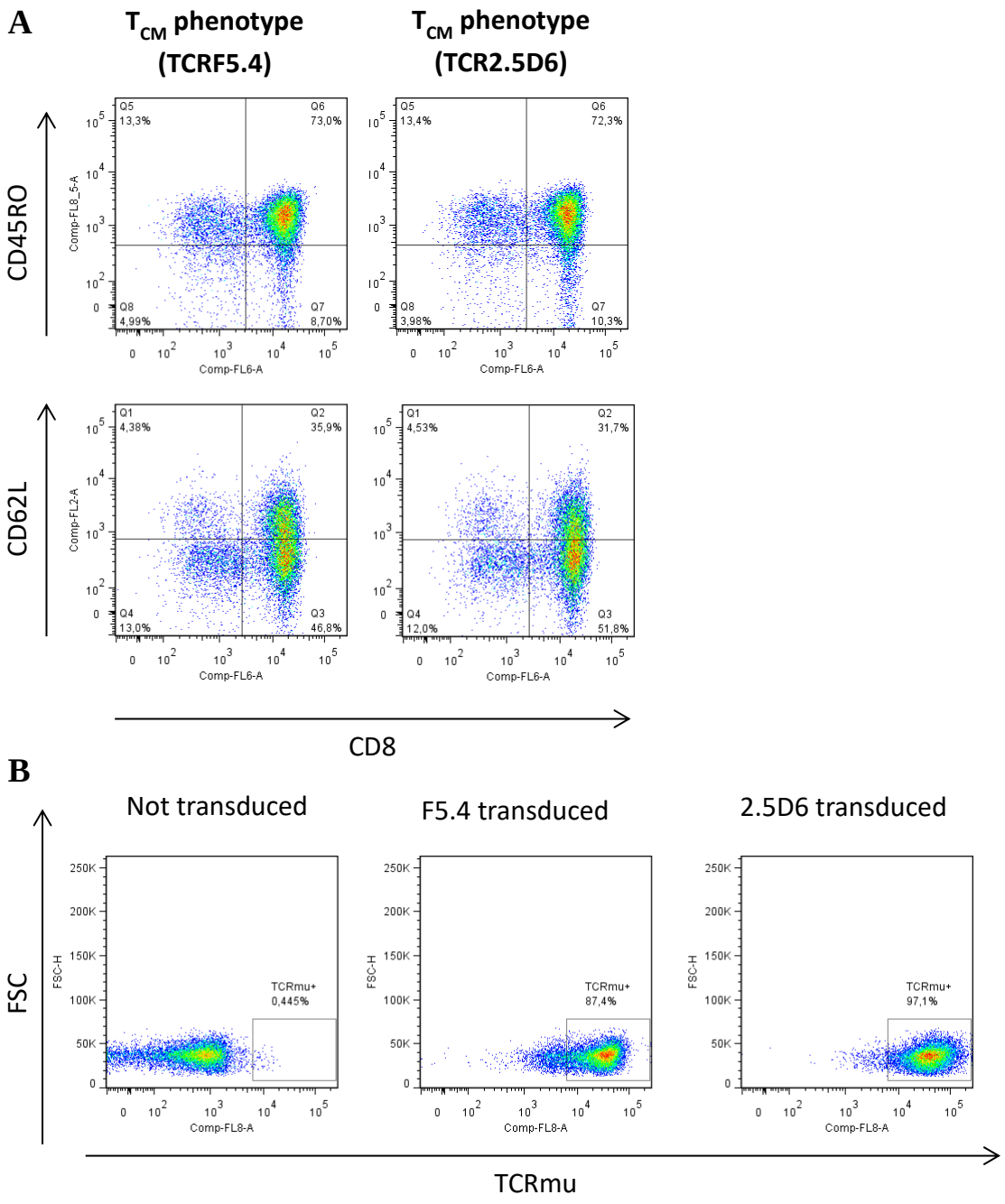

Figure 25: CD62L, CD45RO and TCR-transduction efficiency phenotyping of T-cell products used for the ML2-mice experiment. (A) Characterization of CD8$^+$ T-cells enriched for the T_{CM} phenotype isolated from EDTA blood of healthy donors. PBMCs were depleted for the markers CD45RA$^+$/CD4$^+$ and finally positively selected for CD62L$^+$ using magnetic beads. (B) Analysis of transgenic expression of the constant murine TCR-ß chain (TCRm) of either TCRF5.4- or TCR2.5D6-transduced CD8$^+$ T-cells enriched for the T_{CM} phenotype by flow cytometry.

The in-vitro co-stimulation with HLA-B7-transgenic ML2 cells revealed a slightly enhanced IFN-γ release for TCR2.5D6-transduced T cells compared to TCRF5.4-transduced T cells (Figure 26A) but similar levels of cytotoxicity for both TCRs assessed after

24h of co-stimulation (Figure 26B). Compared to not transduced or TCR2.5D6-transduced T cells, the ML2-B15 cell line with endogenous HLA-B51 expression was partly lysed by TCRF5.4-transduced T cells.

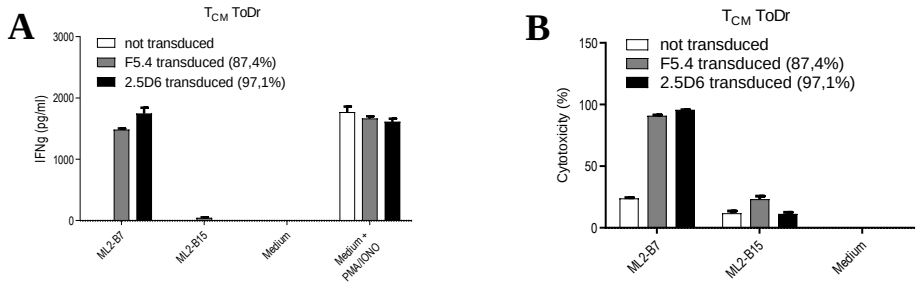

Figure 26: In-vitro reactivity of TCR-transduced T-cell products used for the ML2-NSG mouse model. (A) IFN-γ release of either TCRF5.4- or TCR2.5D6-transduced T cells enriched for the central memory phenotype (T_{CM}) measured by IFN-γ ELISA and (B) cytotoxicity, evaluated by flow cytometry of remaining target cells after 20h of co-incubation with the ML2-B7 target cell line. The ML2-B15, not transduced T_{CM} and PMA/Ionomycin-stimulated T_{CM} served as controls. The mean and standard deviation is shown for triplicates.

The tumor growth kinetics of ML2-B7-derived tumors was nearly identical for both TCR-transduced populations and compared to PBS and not transduced controls. Three days after T-cell injection the ML2-B7-derived tumors were controlled by the injected TCR-transgenic T-cells and tumor shrinkage finally started one day later. Up to day 10 after T-cell injection, the time point where the experiment was stopped, the mean tumor size of all tumors were continuously reduced below palpability (Figure 27A) while the PBS and the not transduced controls showed tumor growth continuously over the entire period. However, the growth kinetics of ML2-B15-derived tumors revealed a cross-reactivity of TCRF5.4-transduced T cells against the control tumors starting at day 3 after T-cell injection (Figure 27B) reflecting the in-vitro observed cytotoxicity results.

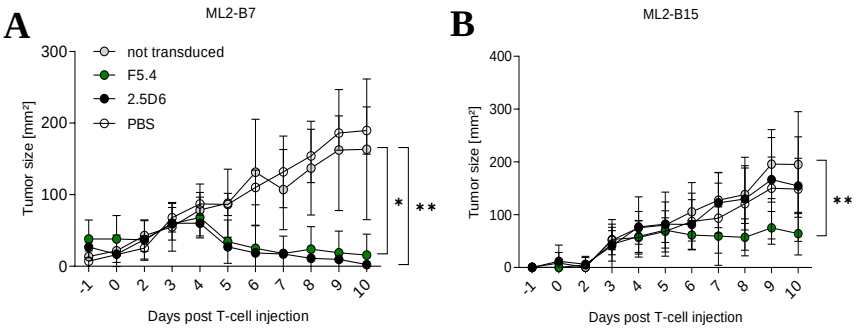

Figure 27: Subcutaneous growth of ML2-derived tumors after adoptive transfer of TCR-transduced T cells. (A) Growth of ML2-B7 and (B) ML2-B15 derived tumors at indicated days is shown for TCRF5.4-and TCR2.5D6-treated mice compared to not transduced, and PBS controls. Mean ± s.d. of tumor size is indicated in mm². ML2-B7 mice: not transduced n=6, PBS n=6, TCRF5.4 n=4 and TCR2.5D6 n=4 animals. ML2-B15 mice: not transduced and PBS n=6, TCRF5.4, and TCR2.5D6 n=7 animals. The Mann-Whitney test was used for statistical analysis: *p<0.05, **p<0.01.

Taken together, the ML2 in-vivo experiment revealed highly similar tumor reduction potential of both TCR-transduced T-cell populations. However, results are not conclusive because of the interfering HLA-B51-related cross-reactivity against the ML2 cell line of the TCRF5.4.

3.4.2 Ex vivo immunogenicity of NB4- and HL60-derived subcutaneous tumors

Because of the HLA-B51-related cross-reactivity of the TCRF5.4 against the ML2 cell line, it was necessary to establish a new tumor model in the NSG mouse model. Therefore, the focus was laid on the two AML cell lines HL60 and NB4 with endogenous MPO expression. As a first step both cell lines were transduced either with HLA-B7 or HLA-B15 and subcutaneously injected into NSG mice after clonal expansion. The tumor growth was assessed for two weeks and the tumors finally removed to test the immunogenicity ex vivo. Both AML-cell lines turned out to be suitable for subcutaneous tumor induction in NSG mice (Figure 28 A, B). The HL60 tumor cell line was more aggressive in tumor growth than the NB4 tumor cell line. The mean of tumor size at day 14 for HL60-B7-derived tumors (320 mm²) was nearly twice as high as for NB4-B7-derived tumors

(180 mm^2). The overall tumor growth of their HLA-B15 counterparts (HL60-B15 and NB4-B15) was even faster compared to the HLA-B7-derived tumors, however, still reflects the superior growth of HL60-derived tumors compared to NB4-derived tumors.

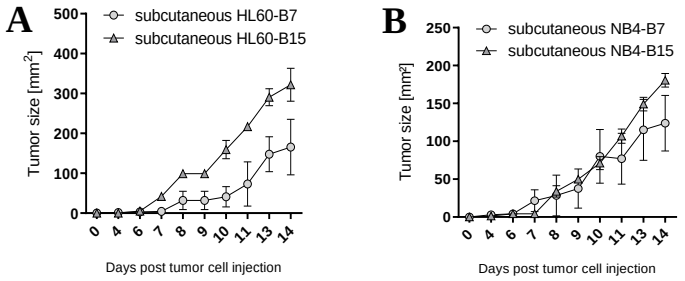

Figure 28: Tumor growth of subcutaneous injected HL60 and NB4 tumor cell lines in NSG mice. Subcutaneous growth of (A) HL60-B7 and HL60-B15 or (B) NB4-B7 and NB4-B15 derived tumors at indicated days. In each mouse, two tumors were induced by subcutaneous injections (left flank HLA-B7$^+$ tumor cells; right flank the HLA-B15$^+$ tumor cells). The mean and standard deviation is shown for triplicates.

After resection of the tumors and single cell preparations, the tumor cells were used in co-stimulation experiments with either not transduced, TCRF5.4- or TCR2.5D6-transduced lymphocytes. Both tumor-derived cell lines elicited robust IFN-γ release of TCR-transduced lymphocytes after co-incubation and were even more immunogenic than cell lines cultured in-vitro. The overall IFN-γ release in HL60 co-stimulation experiments (Figure 29A) was even higher compared to the NB4 co-stimulation (Figure 29B) for two independent TCR-transduced donor T-lymphocytes. The expression of HLA-B7eGFP- or HLA-B15eGFP in both tumor-derived cell lines could be verified by flow cytometry.

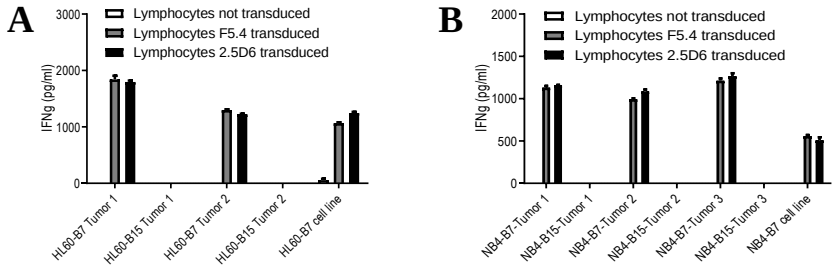

Figure 29: T-cell reactivity of TCRF5.4- and TCR2.5D6-tranduced Lymphocytes against ex vivo processed HL60- and NB4-derived tumors grown in NSG mice. IFN-γ release of either TCRF5.4- or TCR2.5D6-transduced T-lymphocytes measured by IFN-γ ELISA after 20h of co-incubation with single cell suspensions of (A) HL60-B7 or (B) NB4-B7 derived subcutaneous tumors grown in NSG mice. The HLA-B15$^+$ tumors, T cells without TCR-transduction and in-vitro cultured target cell lines were used as controls. The mean and standard deviation is shown for triplicates.

3.4.3 NB4-tumor mouse model

For the following in-vivo experiments, the NB4 tumor cell line was chosen because of its moderate tumor growth kinetics and the reliable in-vitro results (see chapter 3.4.2). In initial mouse trials, the tumor growth of mice that received either a not transduced, a TCRF5.4-transduced or a TCR2.5D6-transduced T-cell product was analyzed. The experiment was stopped after seven days after adoptive T-cell transfer to assess tumor weight and TCR-transduced T-cell infiltration into the tumor, lung, spleen, blood and bone marrow. The initial phenotyping of the $CD8^+T_{CM}$ one day prior to T-cell injection resulted in ~83% $CD8^+CD45RO^+$ and ~23% $CD8^+CD62L^+$ T cells within the TCRF5.4 T-cell product and ~74% $CD8^+CD45RO^+$ and ~10% $CD8^+CD62L^+$ T cells within the TCR2.5D6 T-cell product. The transduction efficiency was ~85% for TCRF5.4-transduced T cells and ~88% for the TCR2.5D6-transduced T cells. The mean fluorescent intensity of the transgenic TCR2.5D6 was higher (23840) compared to TCRF5.4 (14605). To test the in-vitro reactivity of the T-cell product before T-cell injection, IFN-γ release (Figure 30A) and cytotoxicity (Figure 30B) were assessed in effector to target titration assays. Except for the reduced IFN-γ release of TCRF5.4-transduced T cells at the highest

effector to target ratio of 5:1, the TCRF5.4 T-cell product showed very similar responses in cytotoxicity and IFN-γ release compared to the TCR2.5D6 T-cell product in-vitro.

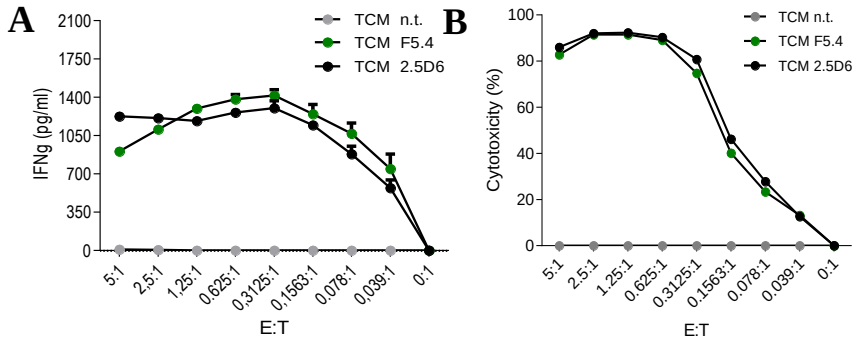

Figure 30: Effector to target titration of TCRF5.4- and TCR2.5D6-tranduced CD8$^+$ T_{CM} against the target cell line NB4-B7. (A) IFN-γ release of either TCRF5.4- or TCR2.5D6-transduced T cells enriched for the central memory phenotype (T_{CM}) measured by IFN-γ ELISA and (B) cytotoxicity evaluated by flow cytometry of remaining target cells after 20h of co-incubation with the NB4-B7 target cell line at indicated effector to target ratios. As a negative control, not transduced T cells were used. The mean and standard deviation is shown for each data point in triplicates.

Interestingly, tumor growth in both mice populations receiving either TCRF5.4- or TCR2.5D6-transduced T-cells was again similar (Figure 31) as seen before in the ML2 mouse model (see chapter 3.4.1). Although the reduction in tumor size was not as effective as for the ML2 tumors, both TCR-transduced T-cells showed a tumor control starting at day 2 to 3 with a continuous tumor reduction starting at day 3 to 4 (Figure 31A). The NB4-B15 control tumors displayed an unaffected tumor growth for all three mice populations that received either not transduced, TCRF5.4-transduced or TCR2.5D6-transduced T cells (Figure 31B).

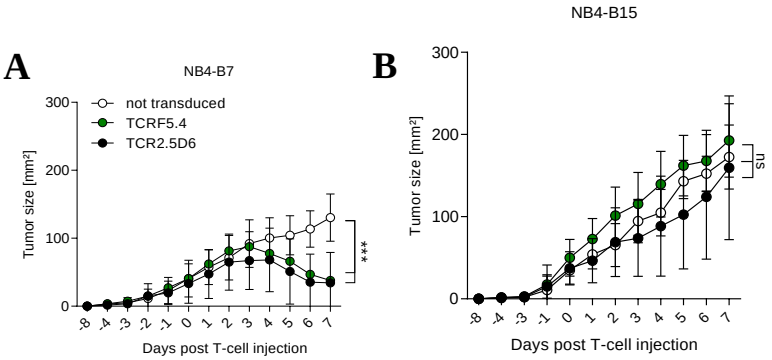

Figure 31: Subcutaneous growth of NB4-derived tumors after adoptive transfer of TCR-transduced T cells. (A) Growth of NB4-B7 and (B) NB4-B15 derived tumors at indicated days is shown for TCRF5.4-and TCR2.5D6-treated mice compared to not transduced controls. Mean ± s.d. of tumor size is indicated in mm². NB4-B7 mice: not transduced n=12, TCRF5.4 n=14, and TCR2.5D6 n=12 animals. NB4-B15 mice: not transduced n=6, TCRF5.4 n=7, and TCR2.5D6 n=7 animals. The Mann-Whitney test was used for statistical analysis: ***p<0.001. Adapted from [102].

To consider the tumor growth regardless of mouse-individual tumor sizes at each measured time point, the first deviation of each growth kinetic was calculated using the non-linear fitting algorithms provides by GraphPad Prism 8. Afterward, the deviation curves were plotted using the smoothing parameters of the software as follows: Numbers of neighbors to average = 5; Orders of the smoothing polynomial = second order (Figure 32). This consideration of tumor growth is not biased by individual tumor size in mice causing high standard deviations and distorted mean calculation in small populations. Instead, only the slopes of tumor growth for each time point is considered and revealed for both TCR-transduced groups an increasing tumor growth rate till the time point of T-cell injection. Closely after T-cell injection, the tumor growth rates slowed down until day 4 for both TCR-transduced groups and turned finally into continuous tumor shrinkage until the end of the experiment at day 7. Both TCR-transduced groups are significantly different from the not transduced T-cell group that served as a negative control and displayed positive tumor growth rates over the entire period.

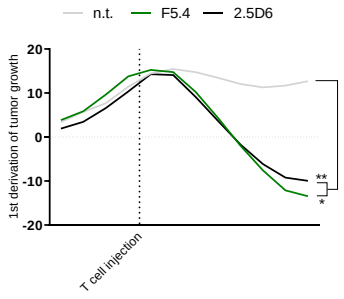

Figure 32: Analysis of tumor growth rates of NB4-derived tumors in NSG mice. The first deviation of tumor growth is shown for TCRF5.4- (green) and TCR2.5D6-treated mice (black) against the control of mice treated with not transduced T cells (gray). The determination of tumor growth equations and their first deviation was calculated using GraphPad Prism 8's smoothing and differentiating analysis tools (smoothing: numbers of neighbors to average = 5 and order of the smoothing polynomial = 2). X-axis: Time in days starting 8 days before T-cell injection to 7 days after T-cell injection, dashed line = time point of T-cell injection; Y-axis: Growth rates/slopes of tumors (1st deviation of tumor growth). The unpaired t-test was used for statistical analysis: TCRF5.4: *p = 0.237; TCR2.5D6: **p = 0.0057.

The ex vivo analysis of tumor weight for all three mouse groups confirmed the results of tumor growth measurements and displayed a significantly reduced tumor weight in TCRF5.4- and TCR2.5D6 –treated mice compared to the not transduced control group. No significant difference between the tumor weights of the TCRF5.4- (median = 0.21) and TCR2.5D6 group (median = 0.15) could be observed (Figure 33). Summarized, the tumor growth rates and the tumor weights of the TCRF5.4- and TCR2.5D6 group are highly similar and indicate comparable tumor killing efficiency of both TCRs in-vivo.

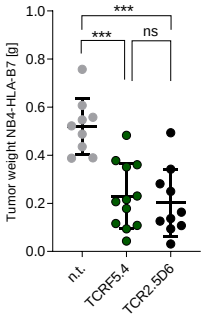

Figure 33: Tumor weight at day 7 of NSG-mice receiving TCR-transduced T-cell product. Not TCR-transduced T cells (n.t.) n = 9, TCRF5.4 n = 12, TCR2.5D6 n = 10. The Mann-Whitney test was used for statistical analysis: ***p<0.001. Adapted from [102].

Looking at the T-cell distribution within the tumors, the levels of $CD45^+CD3^+$ T cells for both TCR-transduced groups were significantly elevated compared to the not transduced control. Both TCR-transduced groups share a median of T-cell infiltration of around 1% compared to the median of 0.3% for the not transduced group. All NB4-B15 control tumors displayed no T-cell infiltration (Figure 34).

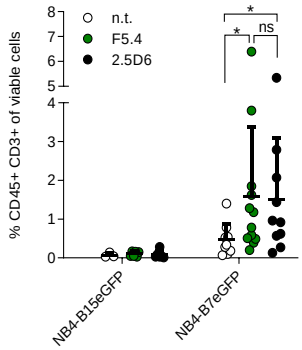

Figure 34: T-cell infiltration in NB4-derived tumors in NSG mice. Percentage of viable $CD45^+CD3^+$ T cells in NB4-B7 or NB4-B15 extracted tumor material of mice treated with not TCR-transduced T cells (n.t.), TCRF5.4- or TCR2.5D6-transduced T cells analyzed by flow cytometry. The Mann-Whitney test was used for statistical analysis: *p<0.05. Adapted from [102].

The results of the T-cell infiltration into the bone marrow, blood, lung, and spleen revealed only significant differences within the lung in TCRF5.4-treated mice. Here, higher levels of $CD3^+TCRmu^+$ TCRF5.4-transduced T cells (median = 24.7) were found compared to TCR2.5D6-transduced T cells (median = 6.9) in the lungs of TCR2.5D6-treated mice (Figure 35).

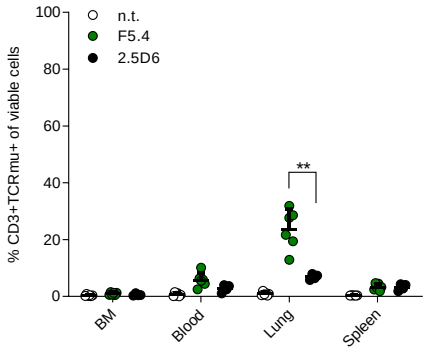

Figure 35: T-cell infiltration in bone marrow, blood, lung, and spleen of NSG mice after T-cell injection. Percentage of viable $CD3^+TCRmu^+$ T cells in indicates samples of mice treated with not TCR-transduced T cells (n.t.), TCRF5.4- or TCR2.5D6-transduced T cells analyzed by flow cytometry. The Mann-Whitney test was used for statistical analysis: **p<0.01. Adapted from [102].

3.4.4 Long-term survival of NB4 tumor mice after adoptive T-cell transfer

Within the short period of 15 days of the previous in-vivo experiments, no clear differences in tumor growth between TCRF5.4- or TCR2.5D6-treated mice could be observed. Therefore, the next mouse trials focused on the overall survival of the mice.

Phenotyping of the $CD8^+T_{CM}$ at the day of T-cell injection showed for TCRF5.4-transduced T cells ~62% of $CD8^+CD45RO^+$ cells, ~26% of $CD8^+CD62L^+$ cells and a TCR-transduction efficiency of ~85%. For the TCR2.5D6-transduced T cells ~61%, ~27%, and 87%, respectively. Within this experiment, the transduction efficiencies as well as the TCR-surface densities were highly comparable (MFI ~ 13,000). The responsiveness of both TCR-transgenic T-cell products was tested by in-vitro co-stimulation experiments and IFN-γ release as well as cytotoxicity were assessed. Again, the IFN-γ release of TCRF5.4-transduced T cells (2600 pg/ml) was inferior compared to the TCR2.5D6-transduced T cells (3400 pg/ml) (Figure 36A). However, both TCR-transgenic T cells showed again highly similar cytotoxicity levels (~97%) against the in-vitro cultured NB4-B7 cell line used for tumor induction in recipient mice (Figure 36B).

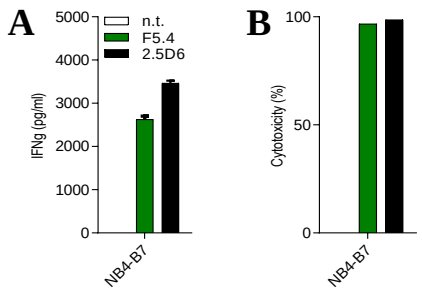

Figure 36: T-cell reactivity of TCRF5.4- and TCR2.5D6-tranduced CD8$^+$T$_{CM}$ against the NB4-B7 tumor cell line used for the long-term mouse experiment. (A) IFN-γ release of either TCRF5.4- or TCR2.5D6-transduced T cells enriched for the central memory phenotype (T$_{CM}$) measured by IFN-γ ELISA and (B) cytotoxicity evaluated by flow cytometry of remaining target cells after 20h of co-incubation with the NB4-B7 target cell line. Not transduced T cells were used as a negative control. The mean and standard deviation is shown for each data point in triplicates for (A). In (B) the triplicates were pooled before the analysis by flow cytometry in order to have enough detectable events for the measurement. Adapted from [102].

The tumor growth for individual mice of the not transduced group, TCRF5.4- and TCR2.5D6-transduced group is shown in Figure 37. In this long-term experiment, substantial differences between TCRF5.4 and TCR2.5D6 became apparent. Similar to previous experiments (see chapter 3.4.3), both groups treated with the TCR-transduced T cells showed at the beginning comparable tumor control and reduction of the tumor's sizes. However, starting at day 6 the tumors in TCRF5.4-treated mice started to progress again. In contrast, in nearly all TCR2.5D6-treated mice the tumor sizes were reduced below palpability at day 12. Interestingly, approximately one week later (day19), 4 out of 6 TCR2.5D6-treated mice relapsed. The remaining mice relapsed at day 32 and day 36 after T-cell injection, respectively. The control group treated with not transduced T cells showed tumor growth continuously over the entire period.

The median survival of mice treated with not transduced T cells was 22 day, for TCR-F5.4-treated mice 28 days and for TCR2.5D6-treated mice 46 days. Each group is significantly different from the others with the TCR2.5D6 group showing superior overall survival (Figure 38).

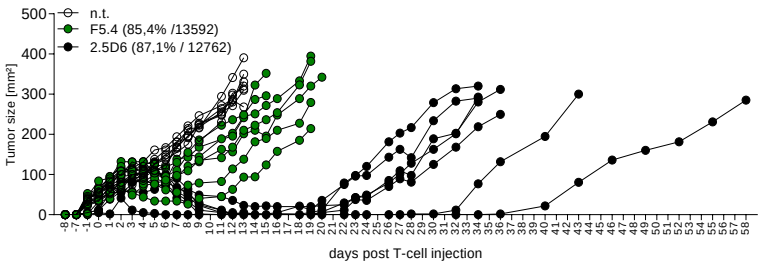

Figure 37: Subcutaneous growth of NB4-derived tumors after adoptive transfer of TCR-transduced $CD8^{+}T_{CM}$ in long-term NSG-mice experiment. Growth of NB4-B7 derived tumors at indicated days is shown for TCRF5.4-and TCR2.5D6-treated mice compared to not transduced controls. Tumor size is indicated in mm^2. Not transduced, TCRF5.4 and TCR2.5D6 n = 7 animals. Adapted from [102].

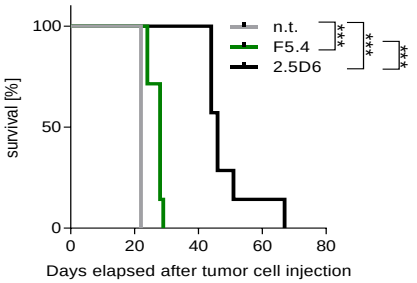

Figure 38: Survival curve of TCRF5.4- or TCR2.5D6-treated NSG mice. Median survival: Not transduced T cell-treated mice = 22 days, TCR.F5.4-treated mice = 28 days, TCR2.5D6-treated mice = 46 days. Statistical analysis was done using the Log-rank (Mantel-Cox) test ***p<0.001 [102].

For a better overview and to compare the results to the previous experiment (see chapter 3.4.3), Figure 39 displays the same data set as shown in Figure 37 only with the mean of each group together with the standard deviation. For the reason of data integrity, the growth curves are only displayed until the last time point with all mice being still alive in each group. This procedure shortened the displayed period for the TCRF5.4 cohort from 20 days to 15 days and for the TCR2.5D6 cohort from 58 days to 34 days. Compared to the growth curves shown in the short-term in-vivo experiment for the NB4-mouse model, there is an astonishing similarity of both TCR-transduced groups until day 6 to 7. Day 7, in turn, is the point of inflection between TCRF5.4- and TCR2.5D6-treated mice. While the TCR2.56 cohort showed ongoing tumor reduction down to the limit of detection, all tumors in the TCRF5.4 cohort indicate either an early tumor escape mechanism or a loss

of T-cell functionality after an initial period of immunogenicity. The tumors in the TCR2.5D6 cohort relapsed later around day 20.

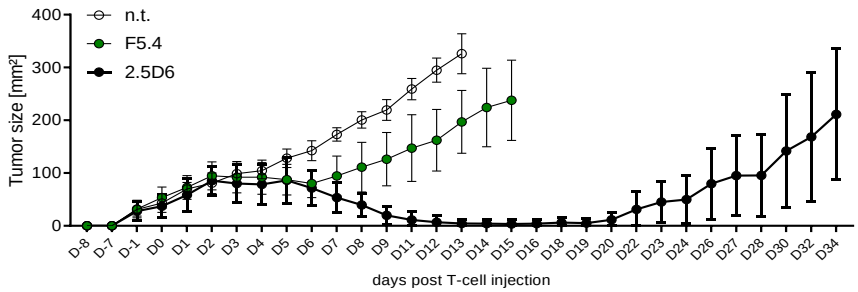

Figure 39: Long-term growth of subcutaneous NB4 tumors after adoptive transfer of TCR-transduced $CD8^+T_{CM}$. Growth of NB4-B7 derived tumors at indicated days is shown for TCRF5.4- and TCR2.5D6-treated mice compared to not transduced controls. Mean ± s.d. of tumor size in mm^2. Not transduced, TCRF5.4 and TCR2.5D6: each n = 7 animals.

Considering the first derivatives of the mean tumor growth (Figure 40), the initial course of growth rates for both TCR-treated cohorts was again very similar. However, around day 6 to 7 it became apparent that the TCRF5.4-treated mice did not enter a sustained tumor reduction phase (green line stays above the dashed horizontal line). Afterward, the tumor growth rates increased again. In contrast, the TCR2.5D6-treated mice entered a prolonged tumor reduction phase of 11 days starting at day 7 (black curve below the dashed horizontal line) before the tumors displayed again increased growth rates and tumor progression. Taken together, day 6 to 7 after T-cell injection is a turning point in the NB4-tumor model that revealed visible differences in tumor killing efficacy between the TCRF5.4- and TCR2.5D6-T-cells populations.

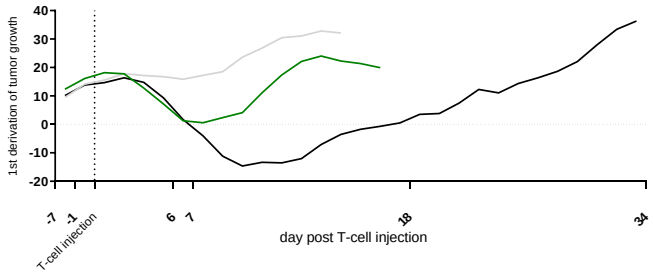

Figure 40: Analysis of tumor growth rates of NB4-derived tumors in NSG mice: The first deviation of tumor growth is shown for TCRF5.4- (green) and TCR2.5D6-treated mice (black) against the control of mice treated with not transduced T cells (gray). The determination of tumor growth equations and their first deviation was calculated using GraphPad Prism 8's smoothing and differentiating analysis tools (smoothing: numbers of neighbors to average = 5 and order of the smoothing polynomial = 2). X-axis: Starting 7 days before T-cell injection (-7) to 34 days after T-cell injection, vertical dashed line = time point of T-cell injection; Y-axis: Growth rates/slopes of tumors (1st deviation of tumor growth).

At day 13, the last time point where in the three cohorts all mice were still alive, the tumor sizes were compared to each other (Figure 41). The tumors were significant different with median sizes of 320 mm^2 for the not transduced cohort, 210 $mm^2$for the TCRF5.4-treated cohort and 2 mm^2 for the TCR2.5D6-treated cohort. Summarized, the TCR2.5D6-treated mice showed a superior tumor response after T-cell injection.

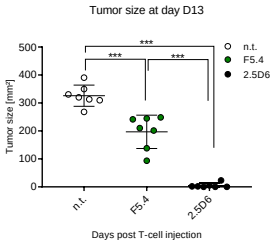

Figure 41: Tumor sizes of NB4-derived tumors at day 13 after T-cell injection. Not TCR-transduced T cells (n.t.), TCRF5.4 and TCR2.5D6: n = 7. The Mann-Whitney test was used for statistical analysis: ***p<0.001.

To assess if a loss of HLA-B7 expression was responsible for the tumor escapes within the different TCR-groups, single cell suspensions of ex vivo tumors were analyzed by flow cytometry for HLA-B7- and GFP-expression (Figure 42). The results show, that the

tumors of the TCRF5.4 group still expressed the HLA-B7 restriction element on the surface of the cells, while tumors of the TCR2.5D6 group had a loss of HLA-B7 expression.

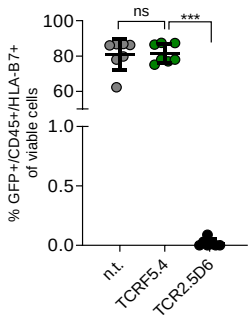

Figure 42: Loss of transgenic HLA-B7 expression in TCR2.5D6-treated mice. Percentage of viable $GFP^+CD45^+HLA\text{-}B7^+$ in extracted tumor material of mice treated with not transduced (n.t.), TCRF5.4- or TCR2.5D6-transduced T cells analyzed by flow cytometry. n = 7 for all three groups of mice. The Mann-Whitney test was used for statistical analysis: ***p<0.001. Adapted from [102].

Similar to the previous mouse experiment (see chapter 3.4.3), the lungs of mice treated with TCRF5.4-transduced T cells showed higher infiltration of $TCRm^+$ T cells compared to mice treated with TCR2.5D6-transduced T cells (Figure 43). This time, also the blood and the spleen showed significant higher infiltration of $TCRm^+$ T cells in TCRF5.4-treated mice compared to the TCR2.5D6-treated group. Of note, each mouse was analyzed at individual time of death or the need to sacrifice it. The data points for the TCR2.5D6-treated mice were collected substantially later because of the prolonged survival of this group. The absence of TCR-2.5D6-transduced mice in these cases could not directly be compared to the TCRF5.4-treated mice. The number of TCR2.5D6 T cells may decreased after tumor eradication and absence of pro-survival stimuli since the relapsed tumor cells were negative for the correct HLA-B7 restriction elements. Furthermore, the prolonged period of TCR2.5D6-transduced T cells in the mice without supportive T-cell milieu together with the challenging tumor conditions may have exhausted the T cells.

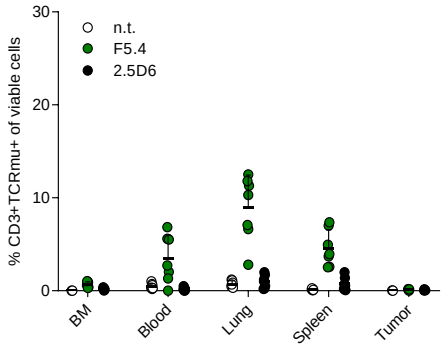

Figure 43: T-cell infiltration in bone marrow, blood, lung, and spleen of NSG mice after T-cell injection. Percentage of viable $CD3^{+}TCRmu^{+}$ T cells in indicates samples of mice treated with not TCR-transduced T cells (n.t.), TCRF5.4- or TCR2.5D6-transduced T cells analyzed by flow cytometry. For samples and groups n = 7. Adapted from [102].

3.5 Characterization of MPO_{145} and MPO_{466}

The observed differences in survival and tumor growth in the long-term in-vivo experiment (see chapter 3.4.4) despite the similarity between both TCR regarding k_{off}-rate, functional avidity and cytotoxicity in-vitro, turned the focus to the characterization of the peptide-MHC complexes. The goal was to characterize the impact of biochemical differences of both peptide-MHC complexes on the observed in-vivo and in-vitro results. First, the IFN-γ release of TCR-transduced T cells after co-stimulation with IFN-γ pretreated AML-cell lines was analyzed in order to estimate the impact of IFN-γ on HLA-expression and proteasome composition in target cells. In parallel, the MPO-peptide surface presentation on the same set of AML-cell lines was analyzed by mass spectrometry using an immunopeptidomics approach. In a second step, prolonged peptide variants of MPO_{145} were examined to exclude that also a nonameric variants might be responsible for the observed TCRF5.4 T-cell responses. Following this, UV-mediated peptide exchanges and differential scanning fluorimetry assays were performed to compare the stability of the MPO-MHC complexes. In a last step, detailed p-MHC modeling was done in cooperation with the group of Iris Antes from the Center for Integrated Protein Science at the Technical University Munich in Freising to visualize critical binding characteristics of the MPO-peptides to HLA-B7 and to describe the results observed in the amino acid substitution assays.

3.5.1 IFN-γ release and cytotoxicity of T cells after co-incubation with IFN-γ pretreated target cells

The four AML-cell lines NB4, HL60, ML2 with transgenic HLA-B7 expression and the SiG-M5 cell line with endogenous HLA-B7 expression were pretreated for 24h with graded amounts of IFN-γ to analyze the effect of IFN-γ on the target cell line and the immune response of TCR-transduced T cells in consecutive co-culture experiments.

TCRF5.4-transduced T cells showed an IFN-γ dose-dependent response to all four IFN-γ pretreated AML-cell lines. The most potent effect could be observed for the ML2 cell line with disrupted IFN-γ release by TCRF5.4-transduced T cells starting from 250 U/ml down to 7.8 U/ml IFN-γ used for the pretreatment. The cytotoxicity of the TCRF5.4 T cells was affected accordingly and reduced to 20% for the highest IFN-γ pretreatment concentrations (Figure 44A). Both effects were also observed for the other AML-cell lines NB4-B7, HL60-B7 and SiG-M5 but to a lower extent (Figure 44 B-D). Ranging the AML-cell lines according to their immunogenicity after IFN-γ pretreatment gives the following order: NB4< SiG-M5<HL60<ML-2. Interestingly, the effects of reduced IFN-γ release and reduced cytotoxicity for TCR2.5D6-transduced T cells could only be observed for the SiG-M5 cell line (Figure 44D). In all other cell lines, the effect was either absent or marginally low.

Taken together, both TCR-transgenic T cells showed different kinds of quantitative and qualitative immune responses against IFN-γ pretreated AML-cell lines. TCRF5.4-transduced T cells showed partially high sensitivity and substantial diminished immune responses against a part of IFN-γ pretreated target cells. The HLA-B7 transgenic AML-cell lines revealed no significant changes in HLA-B7 expression while it was slightly elevated on the SiG-M5 cell line with endogenous HLA-B7 expression after IFN-γ pretreatment.

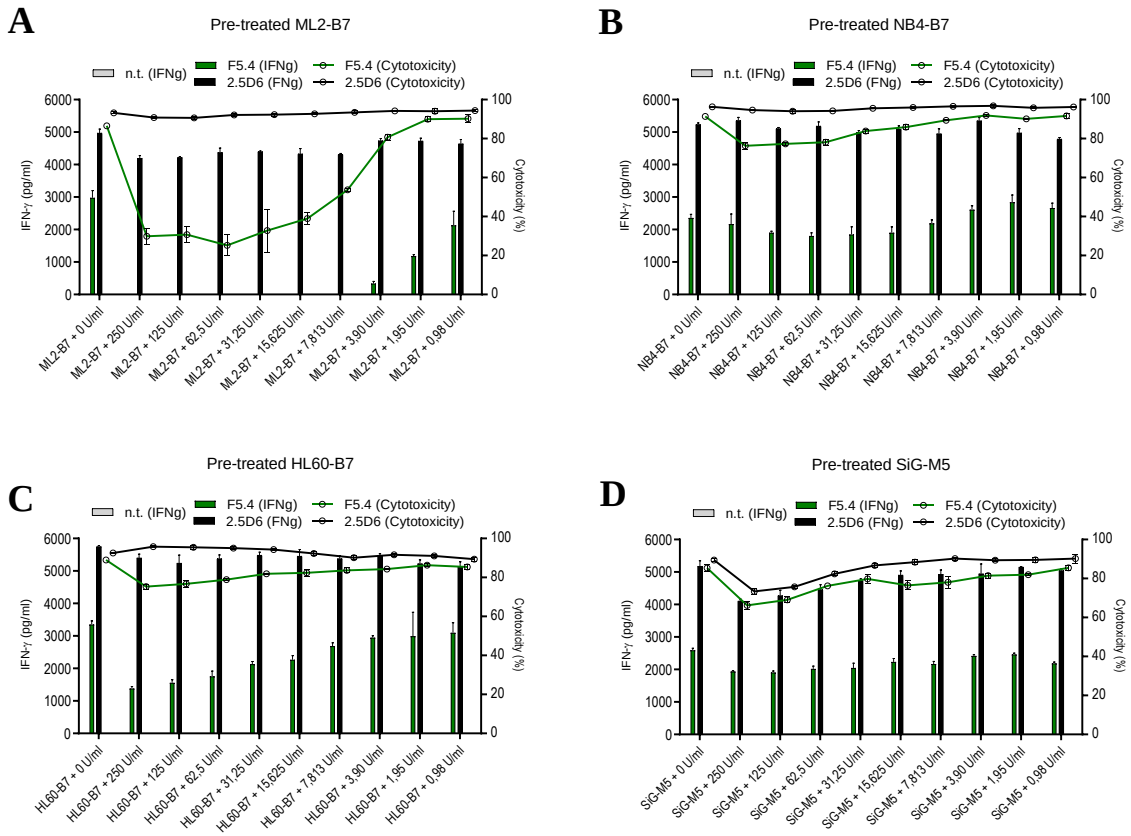

Figure 44: T-cell responses against IFN-γ pretreated AML-target cell lines. IFN-γ release (bar plot) of either TCRF5.4- or TCR2.5D6-transduced T cells measured by IFN-γ ELISA and cytotoxicity (line) evaluated by flow cytometry of remaining target cells after 24h of co-incubation with four different AML cell lines. The target cell lines ML2-B7 (A), NB4-B7 (B), HL60-B7 (C) and SiG-M5 (D) were treated with indicated amounts of IFN-γ for 24h before the co-stimulation with TCR-transduced T cells. Not transduced T cells and non-treated AML target cells were used as a negative control and as a baseline for IFN-γ release of T cells, respectively. The results are shown for one representative experiment (n = 2) and the mean ± s.d. is shown for each data point in triplicates.

Because of nearly unchanged HLA-B7 expressions in the IFN-γ pretreated AML-cell lines, reduced immune responses of TCRF5.4-transduced T cells may not be explained sufficiently by this mechanism. To test whether a change in the immune proteasome composition and a changed peptide processing could be the reason for the observed difference in immune response after IFN-γ pretreatment, the mRNA levels of the three proteasome subunits PSMB 8, PSMB 9 and PSMB 10 were analyzed. Additionally, the MPO_{145}- and MPO_{466}-peptide presentation on the surface of the target cells was relatively quantified

by mass spectrometry to estimate a change in peptide levels after IFN-γ pretreatment (see chapter 3.5.2).

As described, the proteasomal subunits PSMB 8, PSMB 9 and PSMB 10 are assembled to the immunoproteasome triggered by IFN-γ [106]. This assembly can result in an enhanced and more diverse peptide processing and HLA-dependent peptide presentation on the surface of cells [107]. The IFN-γ pretreatment for 24h with 200 U/ml resulted in a substantial increase of mRNA for all three PSMB subunits in the AML-cell line panel compared to not treated controls (Figure 45). The Jurkat76 cell line served as a positive control for the immunoproteasome after IFN-γ induction. The ML2-B7 cell line showed the highest increase in all three PSMB subunits after the IFN-γ treatment followed by the SiG-M5, NB4-B7, and HL60-B7 cell line. Notably, the proportional distribution of the subunits differed between these cell lines. In all cell lines, especially in SiG-M5 and NB4, PSMB 8 had the smallest proportion while PSMB 10 was highly expressed mainly in the ML2-B7 cell line after IFN-γ treatment. This observation seems to correlate in several aspects with the results of the co-stimulation experiments with IFN-γ pretreated target cells as described above. (i) Both cell lines (NB4 and SiG-M5) with the lowest increase in PSMB 8 expression after IFN-γ pretreatment, showed only marginal effects on TCRF5.4-transduced T-cell responses indicating no significant changes in MPO_{145} peptide presentation and points PSMB 8 as a limiting factor for sufficient immunoproteasome activity. (ii) HL60 and ML2 with higher PSMB 8 expression also showed the most substantial effects in reduction of IFN-γ release and cytotoxicity of TCRF5.4-transduced T cells after IFN-γ pretreatment of these cell lines (Figure 44A, C). In contrast, TCR2.5D6-transduced T cells showed nearly no difference in responses after co-stimulation with IFN-γ pretreatment ML2, HL60, and NB4 cells. Thus, the MPO_{145} processing and presentation machinery is more affected by changes of the PSMB 8-10 subunits than MPO_{466} in the tested cell line panel.

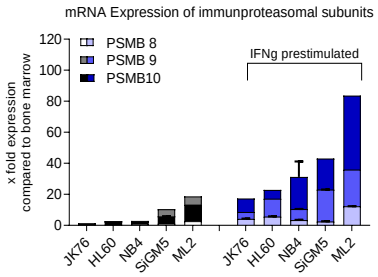

Figure 45: mRNA expression of immunoproteasome subunits after IFN-γ exposure. The expression of PSMB8, 9 and 10 was analyzed by semi-quantitative real-time PCR normalized to the three housekeeping genes GAPDH, HMBS, and HPRT1 after IFN-γ (200 U/ml) pretreatment for 24h. The expression of the cell lines HL60, NB4, SiG-M5, and ML2 was calculated relative to the expression of the Jurkat76 cell line (JK76).

3.5.2 Determination of MPO-peptide levels by LC-MS/MS

The relative quantification of MPO-peptide intensities presented on the surface of the cells by mass spectrometry was done in collaboration with Matteo Pecoraro from the Max Planck Institute for Biochemistry. The results indicate a substantial higher intensity of MPO_{466} on the surface of each AML-cell line compared to MPO_{145} (Figure 46). Within the MPO_{466} panel, the cell line NB4-B7 displayed the highest MPO_{466} intensity followed by ML2-B7, HL60-B7 and SiG-M5. For MPO_{145}, the cell lines NB4-B7 and ML2-B7 are similar in their peptide intensity levels followed by HL60-B7 and SiG-M5. Although the detectable levels of surface presented MPO_{466} and MPO_{145} seems to differ substantially and imply much higher MPO_{466} presentation on the surface of all cell lines compared to MPO_{145}, it is important to point out that both peptides are biochemically very different. These differences, however, led also to different recoveries of the peptides during the MS measurements. Thus, it needs to be considered that a direct comparison of both peptides might not be adequate.

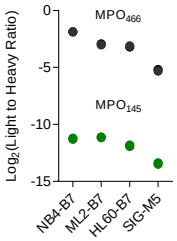

Figure 46: Intensity distribution of MPO_{145} and MPO_{466} on the surface of AML cell lines. The occurrences of logarithmic intensities of the MPO_{145}- (green) and MPO_{466}-peptides (black) on the surface of the NB4-B7, ML2-B7, HL60-B7, and SiG-M5 cell lines. The detection of the MPO-peptides was done using heavy labeled Leucine counterparts as controls. The mean of duplicates is shown for one representative measurement out of two (n = 2). Adapted from [102].

In a second run, the experiment was repeated with the IFN-γ pretreated AML-cell line panel. The results were compared to the untreated controls separately for both MPO-peptides. Except for the HL60-B7 cell line with increased MPO_{466} surface intensities, the intensities decreased for all the other cell lines ML2-B7, NB4-B7 and SiG-M5 after the IFN-γ pretreatment (Figure 47A). The intensities for the MPO_{145}-peptide were slightly elevated in HL60-B7 and ML2-B7 after the IFN-γ pretreatment while a decrease was observed for NB4-B7 and SiG-M5 (Figure 47B). The IFN-γ pretreatment results showed a distinct effect of IFN-γ on the peptide presentation machinery of the AML-cell lines. Partially the results are ambiguous if dragged on the observations made for the IFN-γ pretreatment co-cultivation experiments (Figure 44). As an example, the ML2-B7 cell line was hardly detected by TCRF5.4-transduced T cells after IFN-γ pretreatment (Figure 44A) although higher MPO_{145} intensity levels have been detected by mass spectrometry on the surface of the cells. Taken together, the outcome of the examined IFN-γ treatment experiment remain controversial and the observed results in-vitro could not be conclusively explained by mass spectrometry.

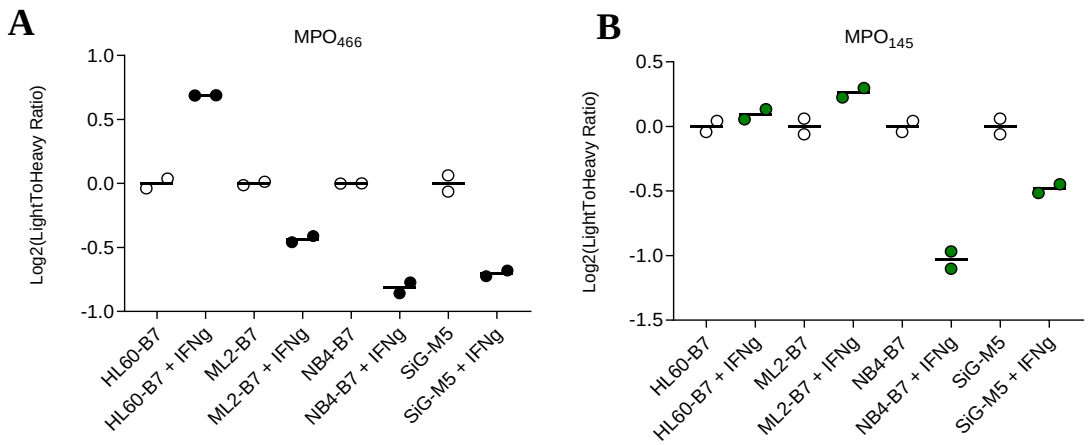

Figure 47: MPO-peptide surface intensities after IFN-γ pretreatment of AML cell lines. The occurrences of logarithmic intensities of the MPO_{466}- (A) and MPO_{145}-peptides (B) on the surface of the NB4-B7, ML2-B7, HL60-B7, and SiG-M5 cell lines with (closed circles) or without (open circles) IFN-γ pretreatment (200 U/ml) for 24h. Values of cell lines without IFN-γ pretreatment were set as a baseline to display the ratio of peptide intensities for IFN-γ treated samples. Results for the MPO_{466} peptide are shown in (A), for the MPO_{145}-peptide in (B), respectively. The detection of the MPO-peptides was done using heavy labeled Leucine counterparts as controls. The mean is shown for duplicates of one representative measurement (n = 2).

3.5.3 Prolonged peptide variants of MPO_{145}

MHC-peptide binding prediction tools using peptide-sequence based algorithms are mostly trained for nonameric peptides on MHC-I alleles. The same applies to the HLA-B7 allele implemented in the NetMHC database. To be sure that no nonameric version of the MPO_{145}-peptide (octamer) is responsible for the observed immune responses of TCRF5.4-transduced T cells, the nonameric versions LTPAQLNVL (MPO_2+L1) and TPAQLNVLS (MPO_2+S9) were synthesized (Genscript) and tested in peptide pulsing experiments using HLA-B7 transgenic KG-1a cells (Figure 48).

No IFN-γ release of TCRF5.4-transduced T cells could be observed for the MPO_2+S9 variant. However, the variant MPO_2+L1 showed nearly the same IFN-γ release of TCRF5.4-transduced T cells as shown for the control peptide MPO_{145}.

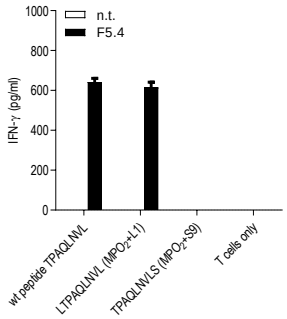

Figure 48: T-cell responses against nonameric MPO_{145}-peptide variants. IFN-γ release of TCRF5.4-transduced T cells measured by IFN-γ ELISA after co-incubation with either MPO_{145}- (wt), MPO_{145}+L1- or MPO_{145}+S9-pulsed LCL cells with endogenous HLA-B7 expression for 20h. Not transduced T cells and T cells without target cell incubation served as controls. The mean ± s.d. of triplicates is shown for n=2 [102].

Although it cannot be excluded that HLA-B7-bound MPO_2+L1 is a naturally presented T-cell epitope, this peptide was not detected by immunopeptidomics so far (see chapter 3.1). Furthermore, MPO_2+L1 peptide modeling revealed that the additional N-terminal leucine might have no positive contribution to the HLA-B7 complex binding (see chapter 3.5.6).

3.5.4 UV-mediated peptide exchange

With the technique of the UV-mediated peptide exchange, the potential of the MPO-peptides was assessed to rescue the HLA-B7 complex once the UV-sensitive placeholder peptide had been cleaved by UV-light. Figure 49A shows the results of the experiments and revealed that MPO_{466} was the peptide with the lowest V_{50} value (-5.204) compared to the MPO_{145}- (-4.610) and MPO_2+L1 (-4.143) peptides. Thus, a significant reduced half-maximal MPO_{466}-peptide concentration was necessary to rescue the HLA-B7 complexes compared to MPO_{145} (Figure 49B). This result indicates either a stronger HLA-binding affinity, HLA-stabilizing potential or faster complex association (k_{on}-rate) of MPO_{466} peptide to the HLA-B7 molecule compared to MPO_{145}.

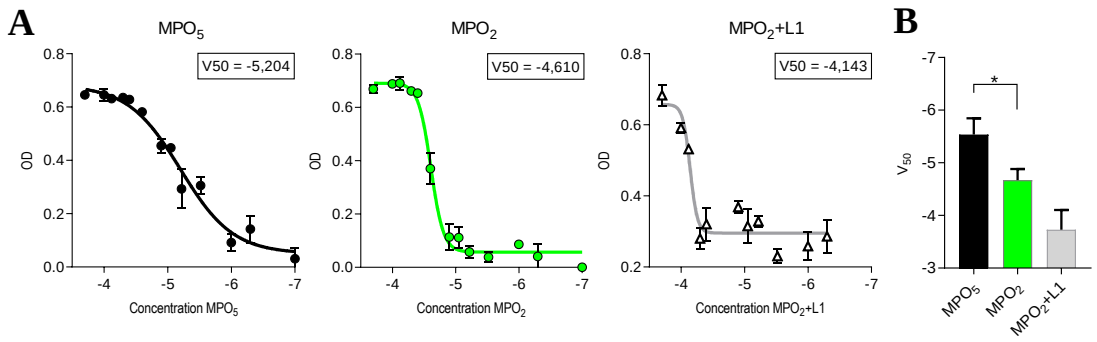

Figure 49: p-MHC stability of MPO_{145} and MPO_{466} HLA-molecules after UV-mediated peptide exchange. (A) Representative results of UV-mediated peptide exchanges of HLA-B7 monomers for the peptides (l.t.r.) MPO_{466}, MPO_{145}, and MPO_{145}+L1. MPO-peptide exchange efficiency was measured by beta-2-microglobulin (B2M)-ELISA for graded amounts of peptides followed by calculation of V_{50} values using Boltzmann curve fitting algorithms of GraphPad Prism 8. The mean ± s.d of triplicates is shown for each peptide. (B) Pooled results of V_{50} values for MPO_{466} n=4, MPO_{145} n=4 and MPO_{145}+L1 n=3. The Mann-Whitney test was used for statistical analysis: *p<0.05 [102].

3.5.5 Differential Scanning Fluorimetry of MPO-peptides

For further analysis of p-MHC complex stability, the differential scanning fluorimetry (thermal shift assay) method was used. This technique uses the property of a protein to denature at a specific temperature in dependence of its stability. The more stable the complex is, the higher temperature it can withstand. In addition, a stable protein denatures later than an unstable protein at constant temperatures. For the monitoring of denaturation SYPRO Orange was used. This dye attaches to hydrophobic amino acid residues that become accessible during denaturation and directly correlates with the degree of denaturation.

Interestingly, the two HLA-peptide complexes MPO_{466} and MPO_{145} displayed nearly the same temperatures necessary to denature ½ of all p-MHC complexes at around 46°C (Figure 50A). The high-affinity CMV peptide-$pp65_{(416-427)}$-HLA-B7 complex was used as a control and showed the highest p-MHC complex stability with a half-maximal temperature of 50°C. In contrast, the MPO_2+L1 complex denatured at a half-maximal temperature of 44°C and displayed the weakest p-MHC stability.

In a second experiment, the temperature was adjusted constantly to 37°C, and the denaturation of the p-MHC complexes was monitored over time (Figure 50B). Again, the pp65-MHC complex showed the most robust complex stability with a half-life of 5.6h and the MPO_2+L1-MHC complex the weakest complex stability with a half-life of 2.9 h. This time, the MPO_{145}- and MPO_{466}-MHC complexes clearly showed differences in complex stability. With a half-life of 4.1 h, the MPO_{466} complex was longer stable than the MPO_{145} complex (3.5 h). To conclude, the results of thermal shift assays provide the following order of MPO p-MHC complex stabilities: MPO_{466} > MPO_{145} > MPO_2+L1.

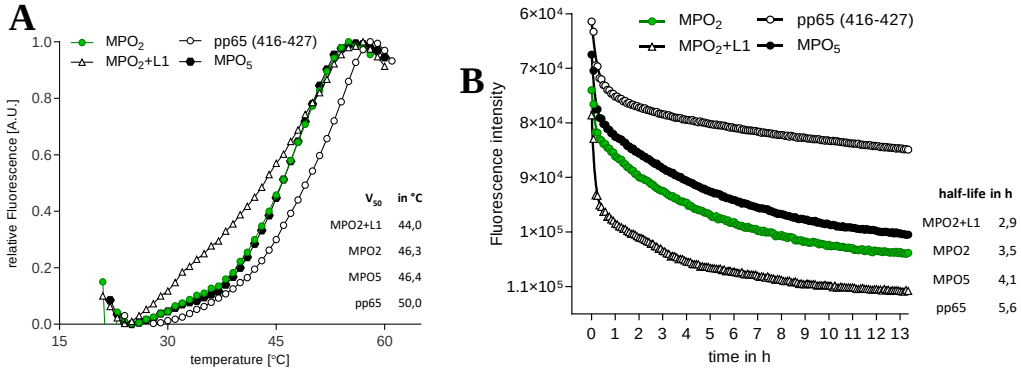

Figure 50: Thermal shift assay of MPO_{466}-, MPO_{145}- and MPO_{145}+L1- UV-exchanged HLA-B7 monomers. (A) HLA-B7 monomer denaturation was monitored during continuos heating starting from 21°C to 95°C simultaneously for all three MPO-MHC complexes compared to the pp65-MHC complex (pp65 = CMV-derived and also HLA-B7 restricted). The half-maximal denaturation (V_{50} in °C) was calculated by Boltzmann fitting algorithms using GraphPad Prism 8. (B) Stability of MPO-peptide-HLA-B7 monomers over time at constant temperature of 37°C compared to the pp65-HLA-B7 complex. The half-life of each peptide-MHC complexes was calculated by GraphPad Prism 8 using the two-phase exponential decay algorithm selecting the slowest constant rates. The means of quadruplicates are shown for both figures (n=2). The increasing fluorescence during denaturation or decay of the peptide-HLA complexes was monitored by SYPRO orange. Adapted from [102].

3.5.6 Characterization of MPO-MHC complexes by structural modeling

For more insights into the binding properties, especially on a structural basis, the MPO-peptide complexes were modeled and underwent molecular dynamic simulations performed by Manuel Glaser and Iris Antes from the Center for Integrated Protein Science at the Technical University Munich in Freising, Germany. Detailed results can be found

in the PhD-thesis related publication [102]. In brief, molecular dynamic simulations revealed a much higher conformational stability of MPO_{466} compared to the MPO_{145}-peptide with higher flexibility within the MHC-binding cleft. The results support the weaker MPO_{145} HLA-stability observed in the UV-mediated peptide exchange (see chapter 3.5.4) and differential scanning fluorimetry assays (see chapter 3.5.5). Subsequent comparisons to prediction results using the NetMHC4.0- and the SYFPEITH platforms showed excellent correlations and verified the higher HLA-affinity of MPO_{466} compared to MPO_{145} (Table 27). Conclusively, the weaker HLA-binding affinity of the MPO_{145}-peptide lowers the cell surface presentation compared to MPO_{466} (see chapter 3.5.2) because of more competitive MPO_{466}-peptide loading of HLA-B7 molecules. Furthermore, alanine and threonine variants of the MPO_{145}- and MPO_{466}-peptides were modeled and their in-silico p-MHC flexibility was compared to the experimental results of amino acid substitution assays (see chapter 3.2.7). Regarding this, the most important insight was a correlation between higher HLA-B7 binding affinities of single MPO_{466} variants and increased IFN-γ release of TCR2.5D6-transduced T cells in co-stimulation experiments. Taken together, the structural modeling of the MPO-HLA-complexes strongly support our experimental in-vitro data of MPO_{466} superiority regarding HLA-binding affinity and quality compared to the MPO_{145}-peptide.

4 Discussion

4.1 The selection of methods for TCR-p-MHC characterization

4.1.1 Only a small proportion of selected target antigens leads to promising TCR

In this work, MHC-mismatched allorestricted T-cell responses against diverse MPO-derived peptide ligands were investigated that had been identified by immunopeptidomics of tumor samples derived from patients with MPN [43]. The primary goal was to establish a TCR library specific for MPO-peptides to treat these diseases in an advanced stage with TCR-transgenic T cells. Such a therapy may be used in the context of allogeneic stem cell transplantation [108, 109] in a haplo- or sHLAm setting as well as alternatively within a conditioning regimen. The promising potential of adoptive transfers of immunoreceptor transgenic T cells, has been shown in the case of chimeric antigen receptors targeting B-cell malignancies [110, 111] or in the case of TCRs targeting melanomas [5]. However, only a small proportion of experimentally identified immunoreceptors enters the stage of clinical translation. In case of the six different MPO-peptides used for T-cell stimulation, only one novel allorestricted TCR (TCRF5.4) with high specificity for the HLA-B7-restricted MPO-derived peptide MPO_{145} could be identified. All other TCR candidates were excluded as potential candidates for clinical translation after meeting different kinds of stopping criteria indicating major hurdles for clinical translation. Major hurdles were for instance the lack of isolation and expansion of specific T-cell clones targeting MPO_{266}, MPO_{357} and MPO_{67}, failure in TCR expression after retroviral transfer of a TCR construct specific for MPO_{603} and peptide-independent recognition of target cells after TCR transfer in case of MPO_{368}. The insufficient surface expression or missing peptide specificity might be related to the composition of the TCR itself as it was shown before for other TCRs [112].

For the successful isolation and expansion of MPO_{145}-specific T cells within sHLAm-(HLA-B7) stimulated T-cell pools, the combination of a general depleting step of $CD137^+$ HLA-B7 alloreactive T-cells [113] followed by multimer-based sorting [114] was successfully applied. Without exception, all expanded T-cell clones after isolation showed distinct MPO_{145} specificity and shared the same sequences for the TCR alpha and beta chains.

4.1.2 Does a well-defined selection process for TCR identification exist?

One aim of this work was to define key in-vitro or in-silico characteristics for the selection of MHC-binding peptides and respective TCRs to facilitate future screening approaches of allorestricted TCRs to reduce or even to skip laborious in-vivo experiments. For that reason, the newly identified TCRF5.4 was compared to the previously characterized TCR2.5D6 [43] in side by side experiments in order to reveal both shared characteristics and differences. Therefore, the allorestricted TCR2.5D6 was ideal for in-depth analyses since this TCR shares the same HLA-B7 restriction element as well as the same target protein MPO with TCRF5.4. The choice of most in-vitro experiments was aligned to literature that reflects a connection between strong T-cell responses and anti-tumor capacity in-vivo [27, 80-82, 84-86, 115]. Consequently, for both TCRs, the expression, functional avidity, dissociation from the p-MHC complex (k_{off}-rate), cytokine release after stimulation, cytotoxicity against cell lines as well as cross-reactivity in-vitro was analyzed. Additionally, T-cell responses against target cell lines were analyzed that have been pre-treated with different concentrations of IFN-γ to mimic the release of IFN-γ by T cells during T-cell / target cell engagement in immune responses [116].

Among all these methods, functional differences of both TCRs were limited and mainly observed in TCR expression, quality and quantity of cytokine release as well as cross-

reactivity. In contrast, no significant differences were seen for target cell lysis, dissociation time of TCRs from p-MHC complex and functional avidity. Thus, these functional analyses failed to describe the proposed correlation of in-vivo outcome and strength of TCRs. Similar applies to TCR-p-MHC off-rates. Although reported as a critical factor, it failed to predict the different qualities of TCRF5.4- and TCR2.5D6-related immune responses [117] after adoptive transfer of T cells [81] into the chosen NB4 in-vivo model. The same applies to the functional avidity of TCRs towards the cognate MHC-peptide complexes which is reported to be a preferential selection criterion [84]. Specific features of MHC-mismatched TCRs could explain the lack of significant differences between both TCRs in k_{off}-rate and functional avidity. As reported elsewhere, allogeneic TCRs might have alternative binding features to the mismatched MHC involving CDR1 and CDR2 domains [118] potentially compensating for lower p-MHC as well as TCR-p-MHC affinity. Thus, functional avidity, as well as k_{off}-rate analyses, seem not to be predictive to identify allorestricted TCRs with high potential for clinical translation.

Although both TCRs are codon optimized [98], murinized [97] and the translation of the TCRα- and ß-chains was improved by bi-cistronic vectors using a 2A self-cleaving element [96] with insertion of an additional cysteine bridge similar to a previous report [119], the TCRF5.4 showed a reduced surface expression and MFI in transgenic T cells. It would be conceivable for further analyzes to harmonize the TCR expression between both TCRs in order to ensure better comparability of results that depend on TCR expression levels. To achieve this, micro RNAs or DNA cleaving nucleases can be used to silence the expression of the endogenous TCRs [120] or intersect the sequence within a TCR gene locus [121], respectively. State of the art approach uses the CRISPR-Cas technology to do both, disruption of endogenous TCR expression and simultaneous insertion of the transgenic

TCR or CAR sequence into the TCR gene locus [48, 49]. However, although TCR expression might be relevant, as also shown for the MPO_{603}-specific HLA-A2-TCR within this work with insufficient surface presentation, TCRF5.4 indicates that minor differences of generally well-expressed TCRs may not be critical in some cases. Additionally, precisely because the expression of both TCRs have not been additionally manipulated, it was possible to examine TCR- and recipient cell-related influences on TCR surface expression levels, as they are present in clinical application. TCRF5.4-transduced T cells were competitive in cytotoxicity in-vitro which may, however, not represent the most sensitive test for strong T-cell responses as previously described [122]. The results presented here also indicate that TCRF5.4 might have a higher functional avidity compared to TCR2.5D6 because of similar performance in these experiments despite lower TCR presentation quality and quantity as determined by flow cytometry. In contrast, the TCRF5.4 was inferior concerning qualitative and quantitative cytokine secretion in comparison to TCR2.5D6-transduced T cells possibly explaining inferiority in tumor rejection in-vivo [123-125]. However, considering the high functional avidity of the TCR, compensation of inferior in-vitro cytokine secretion of TCRF5.4-transgenic T cells after co-culture with peptide-pulsed targets indicates either inferior MPO_{145} peptide presentation or reduced p-MHC potency.

Regarding the differences in peptide presentation, MS-based results may support an inferior MHC presentation of MPO_{145} compared to MPO_{466}. Unfortunately, it cannot be excluded that the reduced detection of MPO_{145} using the immunopeptidomic approach could also rely on its biochemical nature possibly not optimal accessible for MS analyses. The two leucine and the valine within the MPO_{145}-peptide sequence make it very hydrophobic leading to fractions with high high-performance liquid chromatography (HPLC) retention times of often lower quality. Additionally, the absence of typical ionizable amino acids

in the MPO_{145} sequence prevents an efficient peptide ionization important for high quality mass spectra. In contrast, although MPO_{466} also contains a hydrophobic leucine, it has two compensating hydrophilic arginines, one of them very close to the C-terminal end, making it nearly ideal for MS analysis.

Other efforts to confirm the differences in MPO_{145} and MPO_{466} peptide presentation levels could not be applied for different reasons. It has been tried to assess the MFI of fluorescently labeled MPO-peptides pulsed on HLA-B7 transgenic target cells. However, the fluorescent labels themselves diminished proper peptide binding to the HLA-molecules as confirmed by control assays testing for functional recognition of respective target cells with labelled peptides by both TCR constructs.

Regarding p-MHC potency, a reduced MPO_{145}-MHC stability was observed in a UV exchange assays compared to MPO_{466}-MHC indicating overall lower p-MHC affinity. The lower MPO_{145}-MHC stability might significantly contribute to the experimental inferior tumor rejection of TCRF5.4. Indeed, our observations of improved in-vivo outcome for T cells with specificity for the peptide MPO_{466} with higher p-MHC stability and affinity are in line with reports about tumor reactive TCRs in the autologous MHC environment [27]. Furthermore, the quality of cytokine secretion [86, 122] was confirmed to be most sensitive in detecting potent in-vitro TCR responses also for allorestricted TCRs. Unfortunately, a direct comparison of our experimentally determined HLA-stability values with HLA-affinities of peptides presented by Engels et al., assessed by radiolabeled competitive peptide assays, was not possible due to different assays formats. Net-MHC 4.0 algorithms [68, 103] for affinity prediction of both MPO-peptides revealed predicted HLA-binding affinities of 36.75 nM for MPO_{466} and 305 nM for MPO_{145}. Therefore, values for both peptides lie above the proposed threshold of 10 nM peptide affinity necessary for relapse-free tumor eradication in-vivo [27]. For clear comparison, either the MPO-peptides need to be analyzed by the same competitive radiolabeled peptide approach [126]

as performed by Engels and colleagues or their peptides need to be analyzed by the UV-exchange approach. Alternatively, novel and cutting-edge technologies as for instance thermophoresis, measuring binding affinities of small molecules to protein complexes, might be a third possibility to precisely determine binding affinities of p-MHCs once adapted to this purpose [127].

Apart from the missing direct comparability of the MPO-peptides to peptides used in other studies, the presented dependency of peptide-binding quality and individual T-cell activity positively correlates as reported previously [128].

Another feature that should be investigated in subsequent work is TCR-p-MHC affinity determination. While we extensively investigated the dissociation of the TCR-p-MHC complexes, the k_{on}-rates of TCRs might be another suitable parameter for the screening to identify appropriate TCRs.

The TCR-affinity is reported to be highly relevant for adequate triggering of intracellular immune responses [129]. However, recent models also revealed that low affinity values, meaning longer k_{on}-rates, might induce even higher T-cell responses compared to TCRs with shorter TCR-p-MHC association times [79]. Therefore, similar to our TCR dissociation analyzes, the sole consideration of either k_{on}- or k_{off}-rate for the prediction of T-cell responses may not be sufficient [79]. In addition, there is not necessarily a positive correlation between affinity prediction and experimental outcome [130, 131]. Therefore, in addition to prediction, experimental validation seems to be indispensable.

4.1.3 In-vivo experiments revealed substantial differences in tumor rejection

As peptide presentation on the surface of tumor cells was identified as a critical factor and as the TCRs target different peptides, an in-vivo test model contrary to Engels et al., 2013 was chosen for several reasons. There, the impact of different antigen expression

levels on single TCR performances was estimated by evaluating eGFP expression coupled to the whole antigen [27]. Such comparison, however, does not consider downstream antigen processing and peptide presentation. This limitation would not be appropriate for the analysis of different TCRs targeting different p-MHC molecules. Although the MPO antigen expression in this work was every time identically for both TCR conditions as the targeted tumor cell lines were the same, the MPO-derived target peptide presentation for MPO_{145} and MPO_{466} was fundamentally different. Even approaches using MPO minigene transduced tumor cell lines would not have led to comparable surface presentation levels between both MPO-peptides. As a fundamental reason for this, endogenous peptide processing- and presentation machinery leads to different amounts of presented peptides conditioned by the peptide quality itself. In contrast, using the described NB4 tumor model with different presentation levels of both MPO-peptides as indicated in the respective analysis mimics a close to the clinic's situation where peptide presentation levels are also not harmonized. Furthermore, the NB4 cell line with transgenic HLA-B7 expression was selected because this cell line elicited almost equal in-vitro functionality in cytokine release and cytotoxicity before and after IFN-γ pre-stimulation of both TCR-transgenic T-cell populations. This characteristic is important to estimate the possible loop impact of IFN-γ release by the adoptively transferred T-cells on the peptide processing and presentation of both MPO-peptides in NB4-derived tumors. In this regard, T-cell responses against different IFN-γ pretreated target cell lines with endogenous MPO expression were analyzed. Additionally, these target cell lines were analyzed for different immunoproteasome subunits. However, a single correlation between proteasome subunit beta (PSMB) 8, 9 and 10 expression in target cells and alterations of T-cell responses could not be observed. One hint might be the inferior PSMB 9 expression in NB4 cells compared to the other AML-cell lines that might be not enough to disrupt the MPO_{145}

processing machinery even at high IFN-γ conditions. Here, further experiments would be necessary to clarify this causality.

As TCR-transgenic T-cell conditions from a donor and transduction with comparable transduction efficacies as well as TCR-density surface expression for both TCR were selected for the long-term in-vivo study, the superior outcome of the TCR2.5D6 group was initially unexpected. Thereby, both TCRs differed sharply in their tumor rejection capacity. Mice treated with TCR2.5D6-transduced T cells showed significantly longer survival compared to those treated with TCRF5.4-transduced T cells. Of note, all mice in the group of TCR2.5D6 also relapsed after apparent tumor eradication. However, tumor escape mechanisms were different in both groups. Whereas tumors in mice treated with TCR2.5D6-transduced T cells lacked HLA-B7 and lost all TCR-transgenic T cells, TCRF5.4-transgenic T cells could be detected in all examined tissues except in the still HLA-B7-expressing tumors. Loss of HLA-B7 indicates an intense immunogenic pressure by strong tumor reactivity and resembles observations made with CD19-CAR T cells [132] although this may happen more easily in case of an HLA-B7 transgene as present in target cells in this model. In contrast, although TCRF5.4-transgenic T cells have well engrafted, our experiments indicate that tumor escape relies more on peptide and TCR-intrinsic features failing to provide complete tumor eradication. Furthermore, increased infiltration of TCRF5.4-T cells into the lung compared to TCR2.5D6-T cells could be observed and might be a hint for TCRF5.4-releated cross-reactivity. Taken together, our findings underline that the most critical differences seen in-vitro, comprising cytokine release quality and quantity as well as peptide quality itself, might be key selection criteria to identify superior TCR-p-MHC combinations.

4.1.4 TCRF5.4 revealed higher cross-reactivity compared to TCR2.5D6

For the identification and isolation of TCRF5.4, the same sHLAm stimulation approach was applied as for the TCR2.5D6. However, both TCR differ in their cross-reactivity pattern analyzed by a set of typical experiments comprising the screening of randomly chosen cognate and non-cognate peptides for HLA-B7 [43], screening of LCL cell lines with common HLA [94] and amino acid substitution assays [133]. Here, TCRF5.4 revealed different TCR-binding motifs in dependence which amino acid, either alanine or threonine, was used for the substitution. Although each motif, analyzed separately in ScanProsite analyses [92], led to only one different protein containing this specific motif, the combined pattern of the alanine- and threonine scan revealed numerous hits. Thus, these results indicating very high peptide promiscuity and a higher risk for more unspecific TCR-binding compared to TCR2.5D6 with a consolidated TCR-binding motif for both alanine- and threonine scan. These differences might be explained by a rather HLA-focused binding of TCRF5.4 with an only minor contribution of the MPO_{145} peptide to a stable TCR-binding and a vice versa for TCR2.5D6. It might be precisely this binding quality of TCRF5.4 that could explain the observed MPO_{145}-peptide independent cross-reactivity against HLA-B51 as described previously [118]. Detailed analyses of the ScanProsite hits for MPO_{145} would make it necessary to apply sequence and structure-based in-silico predictions as well as statistical tools to narrow down the hits to a manageable quantity of potential cross-reactive peptides to be tested in experimental assessments before further clinical translation of TCRF5.4.

4.1.5 Structure-based p-MHC modeling support key results and might substitute laborious peptide screening in future

Structure-based modeling and molecular-dynamic simulations done in cooperation with the group of Iris Antes for both p-MHC complexes revealed the molecular basis of experimental peptide stability results measured by UV exchange assays and give explanations for the observed TCR-binding motifs derived from the amino acid substitution assays. Furthermore, the results of the structure-based p-MHC modeling are in line with sequence-based predictions calculating the p-MHC binding affinity.

Experimentally, MPO_{466}-peptide variants (substituted by alanine or threonine at position six) induced enhanced IFN-γ release of TCR2.5D6-transduced T-cells leading to higher T-cell activity because of improved p-MHC binding quality compared to the wildtype MPO_{466}-peptide. In contrast, the higher in-silico determined peptide flexibility of MPO_{145} within the MHC-binding cleft seems to allow a more flexible binding of TCRF5.4 as observed in the alanine and threonine amino acid substitution assays. Additionally, the experimentally observed differences in TCRF5.4-binding motifs for either alanine or threonine MPO_{145}-peptide variants could be an indication for TCRs with higher risk for unspecific binding. Therefore, it is proposed to use several different amino acids for the analysis of the TCR-binding motif. Taken together, these observations combined with the individual assessed cross-reactive potential of both TCR strongly supports a correlation of TCR specificity, peptide flexibility and cross-reactivity. The TCR2.5D6 targeting the more stiff peptide of higher affinity, probably leading to the favorable TCR-recognition motif, revealed a very promising cross-reactive profile [43]. For TCRF5.4, it seems to be exactly the opposite. Here, the peptide is more flexible within the MHC-binding cleft, the TCR displayed a complex TCR-binding motif and revealed a higher cross-reactive potential as observed in our experimental measurements. Consequently, molecular dynamic simulations and structure-based p-MHC modeling together with amino acid substitution

experiments in combination with cross-reactivity analyses may be a suitable set of tools to identify TCRs with insufficient specificity or risky cross-reactive potential early in the TCR characterization workflow.

4.1.6 Conclusion and Outlook

The presented in-depth analyses of p-MHC binding and TCR functionality leads to the conclusion that characteristics of cytokine release and p-MHC binding are the most appropriate features to discriminate time-efficiently between allogeneic TCRs that are suitable for further clinical translation and TCRs that might carry a higher risk of potential cross-reactivity or ineffectiveness in clinical applications. Based on our discoveries, we propose a curtailed set of methods (Figure 51) for the characterizations of allorestricted TCRs that might help researchers to be able to decide early on in TCR screening whether a TCR is worth it to go on with or not. Thereby we have taken care of practicability and time-efficiency of selected methods in order to empower high-efficacy immunotherapies using transgenic TCR with a favorable safety profile. However, further analyses of new available TCRs or retrospectively of already well characterized TCRs are urgently needed to proof our concept for TCRs identified in the MHC-mismatched allogeneic repertoire.

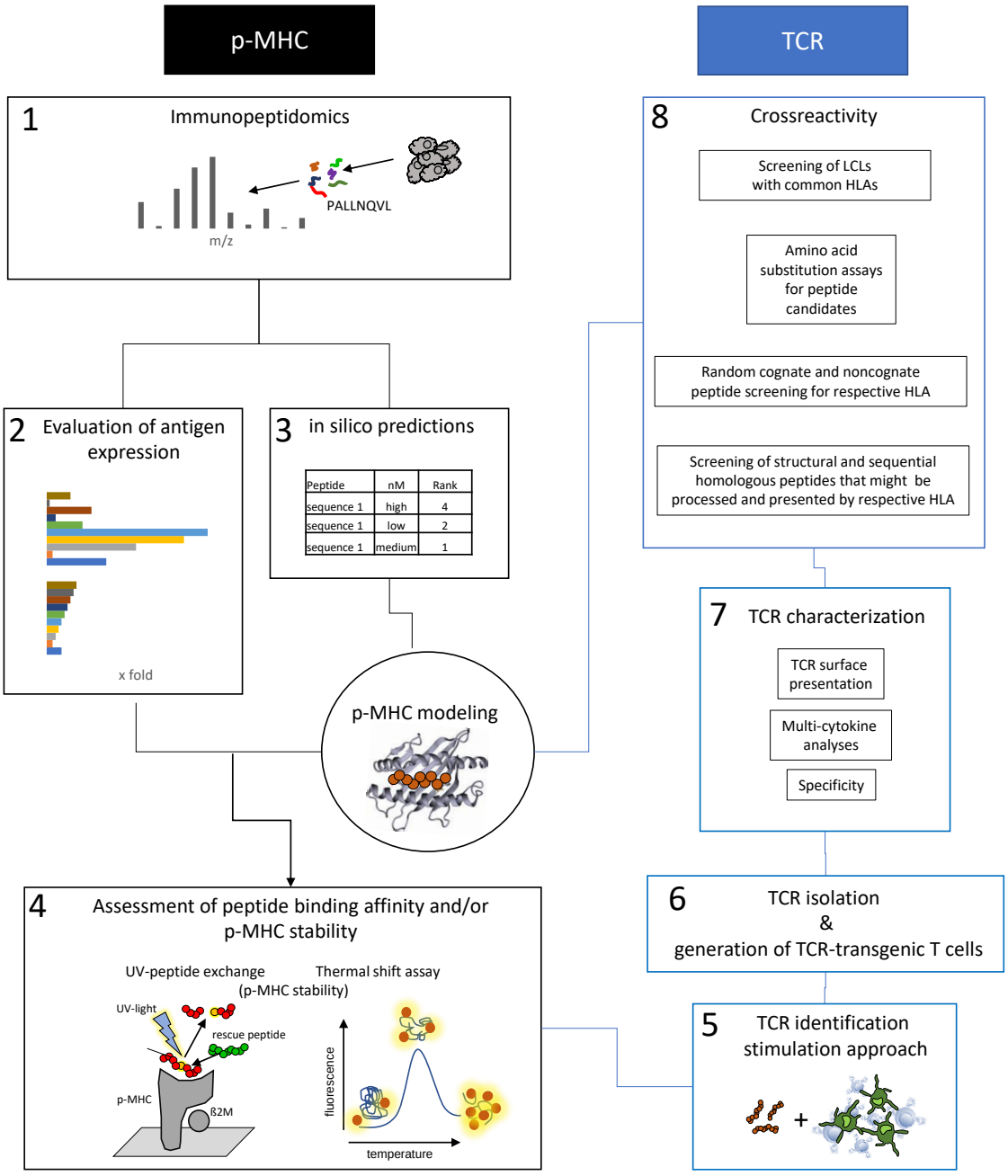

Figure 51: Proposed workflow for allorestricted TCR selection: (1) Immunopeptidomics of tumor samples; (2) Analysis of antigen expression on various human tissues; (3, 4) Prediction based ranking of candidate peptides in combination with experimental HLA-affinity and/or HLA-stability assays assisted by p-MHC modeling; (5, 6) Identification and isolation of TCR; (7) TCR assessment regarding induction of cytokine secretion, TCR surface presentation and specificity; (8) Characterization of cross-reactivity assisted by structure-based modeling.

References

1. Rosenberg, S.A., et al., *Use of tumor-infiltrating lymphocytes and interleukin-2 in the immunotherapy of patients with metastatic melanoma. A preliminary report.* N Engl J Med, 1988. **319**(25): p. 1676-80.
2. Audehm, S. and A.M. Krackhardt, *Specific Adoptive Cellular Immunotherapy in Allogeneic Stem Cell Transplantation.* Oncol Res Treat, 2017. **40**(11): p. 691-696.
3. Maude, S.L., et al., *Chimeric antigen receptor T cells for sustained remissions in leukemia.* N Engl J Med, 2014. **371**(16): p. 1507-17.
4. Cruz, C.R., et al., *Infusion of donor-derived CD19-redirected virus-specific T cells for B-cell malignancies relapsed after allogeneic stem cell transplant: a phase 1 study.* Blood, 2013. **122**(17): p. 2965-73.
5. Morgan, R.A., et al., *Cancer regression in patients after transfer of genetically engineered lymphocytes.* Science, 2006. **314**(5796): p. 126-9.
6. Kolb, H.J., et al., *Donor leukocyte transfusions for treatment of recurrent chronic myelogenous leukemia in marrow transplant patients.* Blood, 1990. **76**(12): p. 2462-5.
7. Horowitz, M.M., et al., *Graft-versus-leukemia reactions after bone marrow transplantation.* Blood, 1990. **75**(3): p. 555-62.
8. Chapuis, A.G., et al., *Transferred WT1-reactive CD8+ T cells can mediate antileukemic activity and persist in post-transplant patients.* Sci Transl Med, 2013. **5**(174): p. 174ra27.
9. Heslop, H.E., et al., *Long-term restoration of immunity against Epstein-Barr virus infection by adoptive transfer of gene-modified virus-specific T lymphocytes.* Nat Med, 1996. **2**(5): p. 551-5.
10. Walter, E.A., et al., *Reconstitution of cellular immunity against cytomegalovirus in recipients of allogeneic bone marrow by transfer of T-cell clones from the donor.* N Engl J Med, 1995. **333**(16): p. 1038-44.
11. Perruccio, K., et al., *Transferring functional immune responses to pathogens after haploidentical hematopoietic transplantation.* Blood, 2005. **106**(13): p. 4397-406.
12. Zhang, C., et al., *Engineering CAR-T cells.* Biomark Res, 2017. **5**: p. 22.
13. Brown, C.E., et al., *Regression of Glioblastoma after Chimeric Antigen Receptor T-Cell Therapy.* N Engl J Med, 2016. **375**(26): p. 2561-9.
14. Jamnani, F.R., et al., *T cells expressing VHH-directed oligoclonal chimeric HER2 antigen receptors: towards tumor-directed oligoclonal T cell therapy.* Biochim Biophys Acta, 2014. **1840**(1): p. 378-86.
15. Maus, M.V. and C.H. June, *Making Better Chimeric Antigen Receptors for Adoptive T-cell Therapy.* Clin Cancer Res, 2016. **22**(8): p. 1875-84.
16. Kalos, M., et al., *T cells with chimeric antigen receptors have potent antitumor effects and can establish memory in patients with advanced leukemia.* Sci Transl Med, 2011. **3**(95): p. 95ra73.
17. Brentjens, R.J., et al., *CD19-targeted T cells rapidly induce molecular remissions in adults with chemotherapy-refractory acute lymphoblastic leukemia.* Sci Transl Med, 2013. **5**(177): p. 177ra38.
18. Turtle, C.J., et al., *CD19 CAR-T cells of defined CD4+:CD8+ composition in adult B cell ALL patients.* J Clin Invest, 2016. **126**(6): p. 2123-38.

19. Porter, D.L., et al., *Chimeric antigen receptor T cells persist and induce sustained remissions in relapsed refractory chronic lymphocytic leukemia.* Sci Transl Med, 2015. **7**(303): p. 303ra139.
20. Davila, M.L., et al., *Efficacy and toxicity management of 19-28z CAR T cell therapy in B cell acute lymphoblastic leukemia.* Sci Transl Med, 2014. **6**(224): p. 224ra25.
21. Murphy, K.M., et al., *Janeway Immunologie*. Vol. Auflage 7. 2009: Spektrum Akademischer Verlag.
22. Davis, M.M. and P.J. Bjorkman, *T-cell antigen receptor genes and T-cell recognition.* Nature, 1988. **334**(6181): p. 395-402.
23. Grotzke, J.E., et al., *The ongoing saga of the mechanism(s) of MHC class I-restricted cross-presentation.* Curr Opin Immunol, 2017. **46**: p. 89-96.
24. Engelhard, V.H., *Structure of peptides associated with class I and class II MHC molecules.* Annu Rev Immunol, 1994. **12**: p. 181-207.
25. Vasmatzis, G., et al., *TcR recognition of the MHC-peptide dimer: structural properties of a ternary complex.* J Mol Biol, 1996. **261**(1): p. 72-89.
26. Reinherz, E.L., et al., *The crystal structure of a T cell receptor in complex with peptide and MHC class II.* Science, 1999. **286**(5446): p. 1913-21.
27. Engels, B., et al., *Relapse or eradication of cancer is predicted by peptide-major histocompatibility complex affinity.* Cancer Cell, 2013. **23**(4): p. 516-26.
28. Gajewski, T.F., H. Schreiber, and Y.X. Fu, *Innate and adaptive immune cells in the tumor microenvironment.* Nat Immunol, 2013. **14**(10): p. 1014-22.
29. Johnson, L.A., et al., *Gene transfer of tumor-reactive TCR confers both high avidity and tumor reactivity to nonreactive peripheral blood mononuclear cells and tumor-infiltrating lymphocytes.* J Immunol, 2006. **177**(9): p. 6548-59.
30. Parkhurst, M.R., et al., *T cells targeting carcinoembryonic antigen can mediate regression of metastatic colorectal cancer but induce severe transient colitis.* Mol Ther, 2011. **19**(3): p. 620-6.
31. Robbins, P.F., et al., *A pilot trial using lymphocytes genetically engineered with an NY-ESO-1-reactive T-cell receptor: long-term follow-up and correlates with response.* Clin Cancer Res, 2015. **21**(5): p. 1019-27.
32. Robbins, P.F., et al., *Tumor regression in patients with metastatic synovial cell sarcoma and melanoma using genetically engineered lymphocytes reactive with NY-ESO-1.* J Clin Oncol, 2011. **29**(7): p. 917-24.
33. Rosenberg, S.A., et al., *Durable complete responses in heavily pretreated patients with metastatic melanoma using T-cell transfer immunotherapy.* Clin Cancer Res, 2011. **17**(13): p. 4550-7.
34. Cameron, B.J., et al., *Identification of a Titin-derived HLA-A1-presented peptide as a cross-reactive target for engineered MAGE A3-directed T cells.* Sci Transl Med, 2013. **5**(197): p. 197ra103.
35. Linette, G.P., et al., *Cardiovascular toxicity and titin cross-reactivity of affinity-enhanced T cells in myeloma and melanoma.* Blood, 2013. **122**(6): p. 863-71.
36. Morgan, R.A., et al., *Cancer regression and neurological toxicity following anti-MAGE-A3 TCR gene therapy.* J Immunother, 2013. **36**(2): p. 133-51.
37. Kato, T., et al., *Effective screening of T cells recognizing neoantigens and construction of T-cell receptor-engineered T cells.* Oncotarget, 2018. **9**(13): p. 11009-11019.
38. Saini, S.K., N. Rekers, and S.R. Hadrup, *Novel tools to assist neoepitope targeting in personalized cancer immunotherapy.* Ann Oncol, 2017. **28**(suppl_12): p. xii3-xii10.

39. Bassani-Sternberg, M., et al., *Direct identification of clinically relevant neoepitopes presented on native human melanoma tissue by mass spectrometry.* Nat Commun, 2016. **7**: p. 13404.
40. Trolle, T., et al., *The Length Distribution of Class I-Restricted T Cell Epitopes Is Determined by Both Peptide Supply and MHC Allele-Specific Binding Preference.* J Immunol, 2016. **196**(4): p. 1480-7.
41. Harndahl, M., et al., *Peptide-MHC class I stability is a better predictor than peptide affinity of CTL immunogenicity.* Eur J Immunol, 2012. **42**(6): p. 1405-16.
42. Abelin, J.G., et al., *Mass Spectrometry Profiling of HLA-Associated Peptidomes in Mono-allelic Cells Enables More Accurate Epitope Prediction.* Immunity, 2017. **46**(2): p. 315-326.
43. Klar, R., et al., *Therapeutic targeting of naturally presented myeloperoxidase-derived HLA peptide ligands on myeloid leukemia cells by TCR-transgenic T cells.* Leukemia, 2014. **28**(12): p. 2355-66.
44. Berlin, C., et al., *Mapping the HLA ligandome landscape of acute myeloid leukemia: a targeted approach toward peptide-based immunotherapy.* Leukemia, 2015. **29**(3): p. 647-59.
45. Walz, S., et al., *The antigenic landscape of multiple myeloma: mass spectrometry (re)defines targets for T-cell-based immunotherapy.* Blood, 2015. **126**(10): p. 1203-13.
46. Rapoport, A.P., et al., *NY-ESO-1-specific TCR-engineered T cells mediate sustained antigen-specific antitumor effects in myeloma.* Nat Med, 2015. **21**(8): p. 914-921.
47. Deniger, D.C., et al., *Stable, Nonviral Expression of Mutated Tumor Neoantigen-specific T-cell Receptors Using the Sleeping Beauty Transposon/Transposase System.* Mol Ther, 2016. **24**(6): p. 1078-1089.
48. Eyquem, J., et al., *Targeting a CAR to the TRAC locus with CRISPR/Cas9 enhances tumour rejection.* Nature, 2017. **543**(7643): p. 113-117.
49. Albers, J.J., et al., *Gene editing enables T-cell engineering to redirect antigen specificity for potent tumor rejection.* Life Sci Alliance, 2019. **2**(2).
50. van Loenen, M.M., et al., *Mixed T cell receptor dimers harbor potentially harmful neoreactivity.* Proc Natl Acad Sci U S A, 2010. **107**(24): p. 10972-7.
51. Ahmadi, M., et al., *CD3 limits the efficacy of TCR gene therapy in-vivo.* Blood, 2011. **118**(13): p. 3528-37.
52. Hart, D.P., et al., *Retroviral transfer of a dominant TCR prevents surface expression of a large proportion of the endogenous TCR repertoire in human T cells.* Gene Ther, 2008. **15**(8): p. 625-31.
53. Wilde, S., et al., *Dendritic cells pulsed with RNA encoding allogeneic MHC and antigen induce T cells with superior antitumor activity and higher TCR functional avidity.* Blood, 2009. **114**(10): p. 2131-9.
54. Aleksic, M., et al., *Different affinity windows for virus and cancer-specific T-cell receptors: implications for therapeutic strategies.* Eur J Immunol, 2012. **42**(12): p. 3174-9.
55. Jahn, L., et al., *TCR-based therapy for multiple myeloma and other B-cell malignancies targeting intracellular transcription factor BOB1.* Blood, 2017. **129**(10): p. 1284-1295.
56. Parkhurst, M., et al., *Isolation of T-Cell Receptors Specifically Reactive with Mutated Tumor-Associated Antigens from Tumor-Infiltrating Lymphocytes Based on CD137 Expression.* Clin Cancer Res, 2017. **23**(10): p. 2491-2505.

57. Cohen, C.J., et al., *Recognition of fresh human tumor by human peripheral blood lymphocytes transduced with a bicistronic retroviral vector encoding a murine anti-p53 TCR.* J Immunol, 2005. **175**(9): p. 5799-808.
58. Davis, J.L., et al., *Development of human anti-murine T-cell receptor antibodies in both responding and nonresponding patients enrolled in TCR gene therapy trials.* Clin Cancer Res, 2010. **16**(23): p. 5852-61.
59. Li, L.P., et al., *Transgenic mice with a diverse human T cell antigen receptor repertoire.* Nat Med, 2010. **16**(9): p. 1029-34.
60. Larsen, M.V., et al., *Large-scale validation of methods for cytotoxic T-lymphocyte epitope prediction.* BMC Bioinformatics, 2007. **8**: p. 424.
61. Nielsen, M., et al., *The role of the proteasome in generating cytotoxic T-cell epitopes: insights obtained from improved predictions of proteasomal cleavage.* Immunogenetics, 2005. **57**(1-2): p. 33-41.
62. Roider, J., et al., *Comparison of experimental fine-mapping to in-silico prediction results of HIV-1 epitopes reveals ongoing need for mapping experiments.* Immunology, 2014. **143**(2): p. 193-201.
63. Hunt, D.F., et al., *Pillars article: Characterization of peptides bound to the class I MHC molecule HLA-A2.1 by mass spectrometry. Science 1992. 255: 1261-1263.* J Immunol, 2007. **179**(5): p. 2669-71.
64. Khodadoust, M.S., et al., *Antigen presentation profiling reveals recognition of lymphoma immunoglobulin neoantigens.* Nature, 2017. **543**(7647): p. 723-727.
65. Dahal, U.P., et al., *Small molecule quantification by liquid chromatography-mass spectrometry for metabolites of drugs and drug candidates.* Drug Metab Dispos, 2011. **39**(12): p. 2355-60.
66. Jorgensen, K.W., et al., *NetMHCstab - predicting stability of peptide-MHC-I complexes; impacts for cytotoxic T lymphocyte epitope discovery.* Immunology, 2014. **141**(1): p. 18-26.
67. Lundegaard, C., O. Lund, and M. Nielsen, *Accurate approximation method for prediction of class I MHC affinities for peptides of length 8, 10 and 11 using prediction tools trained on 9mers.* Bioinformatics, 2008. **24**(11): p. 1397-8.
68. Nielsen, M., et al., *Reliable prediction of T-cell epitopes using neural networks with novel sequence representations.* Protein Sci, 2003. **12**(5): p. 1007-17.
69. Rammensee, H., et al., *SYFPEITHI: database for MHC ligands and peptide motifs.* Immunogenetics, 1999. **50**(3-4): p. 213-9.
70. Peters, B., et al., *Examining the independent binding assumption for binding of peptide epitopes to MHC-I molecules.* Bioinformatics, 2003. **19**(14): p. 1765-72.
71. Andreatta, M. and M. Nielsen, *Bioinformatics Tools for the Prediction of T-Cell Epitopes.* Methods Mol Biol, 2018. **1785**: p. 269-281.
72. Han, Y. and D. Kim, *Deep convolutional neural networks for pan-specific peptide-MHC class I binding prediction.* BMC Bioinformatics, 2017. **18**(1): p. 585.
73. O'Donnell, T.J., et al., *MHCflurry: Open-Source Class I MHC Binding Affinity Prediction.* Cell Syst, 2018. **7**(1): p. 129-132 e4.
74. Wang, S., et al., *Improving the prediction of HLA class I-binding peptides using a supertype-based method.* J Immunol Methods, 2014. **405**: p. 109-20.
75. Antunes, D.A., et al., *Structure-based Methods for Binding Mode and Binding Affinity Prediction for Peptide-MHC Complexes.* Curr Top Med Chem, 2018. **18**(26): p. 2239-2255.
76. Morimoto, S., et al., *Establishment of a novel platform cell line for efficient and precise evaluation of T cell receptor functional avidity.* Oncotarget, 2018. **9**(75): p. 34132-34141.

77. Moore, T.V., et al., *Relationship between CD8-dependent antigen recognition, T cell functional avidity, and tumor cell recognition.* Cancer Immunol Immunother, 2009. **58**(5): p. 719-28.
78. Stone, J.D., A.S. Chervin, and D.M. Kranz, *T-cell receptor binding affinities and kinetics: impact on T-cell activity and specificity.* Immunology, 2009. **126**(2): p. 165-76.
79. Gálvez, J., J.J. Gálvez, and P. García-Peñarrubia, *Is TCR/pMHC Affinity a Good Estimate of the T-cell Response? An Answer Based on Predictions From 12 Phenotypic Models.* Frontiers in Immunology, 2019. **10**(349).
80. Nauerth, M., et al., *Flow cytometry-based TCR-ligand Koff -rate assay for fast avidity screening of even very small antigen-specific T cell populations ex vivo.* Cytometry A, 2016. **89**(9): p. 816-25.
81. Nauerth, M., et al., *TCR-ligand koff rate correlates with the protective capacity of antigen-specific CD8+ T cells for adoptive transfer.* Sci Transl Med, 2013. **5**(192): p. 192ra87.
82. Alexander-Miller, M.A., G.R. Leggatt, and J.A. Berzofsky, *Selective expansion of high- or low-avidity cytotoxic T lymphocytes and efficacy for adoptive immunotherapy.* Proc Natl Acad Sci U S A, 1996. **93**(9): p. 4102-7.
83. Presotto, D., et al., *Fine-Tuning of Optimal TCR Signaling in Tumor-Redirected CD8 T Cells by Distinct TCR Affinity-Mediated Mechanisms.* Front Immunol, 2017. **8**: p. 1564.
84. Zeh, H.J., 3rd, et al., *High avidity CTLs for two self-antigens demonstrate superior in-vitro and in-vivo antitumor efficacy.* J Immunol, 1999. **162**(2): p. 989-94.
85. Zhong, S., et al., *T-cell receptor affinity and avidity defines antitumor response and autoimmunity in T-cell immunotherapy.* Proc Natl Acad Sci U S A, 2013. **110**(17): p. 6973-8.
86. Gottschalk, R.A., et al., *Distinct influences of peptide-MHC quality and quantity on in-vivo T-cell responses.* Proc Natl Acad Sci U S A, 2012. **109**(3): p. 881-6.
87. Speiser, D.E., et al., *Discrepancy between in-vitro measurable and in-vivo virus neutralizing cytotoxic T cell reactivities. Low T cell receptor specificity and avidity sufficient for in-vitro proliferation or cytotoxicity to peptide-coated target cells but not for in-vivo protection.* J Immunol, 1992. **149**(3): p. 972-80.
88. Scott, D.R., et al., *Disparate degrees of hypervariable loop flexibility control T-cell receptor cross-reactivity, specificity, and binding mechanism.* J Mol Biol, 2011. **414**(3): p. 385-400.
89. Wooldridge, L., et al., *A single autoimmune T cell receptor recognizes more than a million different peptides.* J Biol Chem, 2012. **287**(2): p. 1168-77.
90. Birnbaum, M.E., et al., *Deconstructing the peptide-MHC specificity of T cell recognition.* Cell, 2014. **157**(5): p. 1073-87.
91. Liang, X., et al., *A single TCR alpha-chain with dominant peptide recognition in the allorestricted HER2/neu-specific T cell repertoire.* J Immunol, 2010. **184**(3): p. 1617-29.
92. de Castro, E., et al., *ScanProsite: detection of PROSITE signature matches and ProRule-associated functional and structural residues in proteins.* Nucleic Acids Res, 2006. **34**(Web Server issue): p. W362-5.
93. Obenaus, M., et al., *Identification of human T-cell receptors with optimal affinity to cancer antigens using antigen-negative humanized mice.* Nat Biotechnol, 2015. **33**(4): p. 402-7.

94. Heemskerk, M.H., et al., *Dual HLA class I and class II restricted recognition of alloreactive T lymphocytes mediated by a single T cell receptor complex.* Proc Natl Acad Sci U S A, 2001. **98**(12): p. 6806-11.
95. Engels, B., et al., *Retroviral vectors for high-level transgene expression in T lymphocytes.* Hum Gene Ther, 2003. **14**(12): p. 1155-68.
96. Leisegang, M., et al., *Enhanced functionality of T cell receptor-redirected T cells is defined by the transgene cassette.* J Mol Med (Berl), 2008. **86**(5): p. 573-83.
97. Cohen, C.J., et al., *Enhanced antitumor activity of murine-human hybrid T-cell receptor (TCR) in human lymphocytes is associated with improved pairing and TCR/CD3 stability.* Cancer Res, 2006. **66**(17): p. 8878-86.
98. Scholten, K.B., et al., *Codon modification of T cell receptors allows enhanced functional expression in transgenic human T cells.* Clin Immunol, 2006. **119**(2): p. 135-45.
99. Livak, K.J. and T.D. Schmittgen, *Analysis of relative gene expression data using real-time quantitative PCR and the 2(-Delta Delta C(T)) Method.* Methods, 2001. **25**(4): p. 402-8.
100. Rodenko, B., et al., *Generation of peptide-MHC class I complexes through UV-mediated ligand exchange.* Nat Protoc, 2006. **1**(3): p. 1120-32.
101. Niesen, F.H., H. Berglund, and M. Vedadi, *The use of differential scanning fluorimetry to detect ligand interactions that promote protein stability.* Nat Protoc, 2007. **2**(9): p. 2212-21.
102. Audehm, S., et al., *Key Features Relevant to Select Antigens and TCR From the MHC-Mismatched Repertoire to Treat Cancer.* Frontiers in Immunology, 2019. **10**(1485).
103. Andreatta, M. and M. Nielsen, *Gapped sequence alignment using artificial neural networks: application to the MHC class I system.* Bioinformatics, 2016. **32**(4): p. 511-7.
104. Rammensee, H.G., T. Friede, and S. Stevanoviic, *MHC ligands and peptide motifs: first listing.* Immunogenetics, 1995. **41**(4): p. 178-228.
105. Mall, S., et al., *Immuno-PET Imaging of Engineered Human T Cells in Tumors.* Cancer Res, 2016. **76**(14): p. 4113-23.
106. Vigneron, N. and B.J. Van den Eynde, *Proteasome subtypes and regulators in the processing of antigenic peptides presented by class I molecules of the major histocompatibility complex.* Biomolecules, 2014. **4**(4): p. 994-1025.
107. Arellano-Garcia, M.E., et al., *Interferon-gamma induces immunoproteasomes and the presentation of MHC I-associated peptides on human salivary gland cells.* PLoS One, 2014. **9**(8): p. e102878.
108. Thomas, E.D., et al., *Intravenous infusion of bone marrow in patients receiving radiation and chemotherapy.* N Engl J Med, 1957. **257**(11): p. 491-6.
109. Copelan, E.A., *Hematopoietic stem-cell transplantation.* N Engl J Med, 2006. **354**(17): p. 1813-26.
110. Brudno, J.N., et al., *Allogeneic T Cells That Express an Anti-CD19 Chimeric Antigen Receptor Induce Remissions of B-Cell Malignancies That Progress After Allogeneic Hematopoietic Stem-Cell Transplantation Without Causing Graft-Versus-Host Disease.* J Clin Oncol, 2016. **34**(10): p. 1112-21.
111. Ghosh, A., et al., *Donor CD19 CAR T cells exert potent graft-versus-lymphoma activity with diminished graft-versus-host activity.* Nat Med, 2017. **23**(2): p. 242-249.
112. Sommermeyer, D., et al., *Designer T cells by T cell receptor replacement.* Eur J Immunol, 2006. **36**(11): p. 3052-9.

113. Wehler, T.C., et al., *Targeting the activation-induced antigen CD137 can selectively deplete alloreactive T cells from antileukemic and antitumor donor T-cell lines.* Blood, 2007. **109**(1): p. 365-73.
114. Altman, J.D., et al., *Phenotypic analysis of antigen-specific T lymphocytes.* Science, 1996. **274**(5284): p. 94-6.
115. Chen, W., et al., *Determinant selection of major histocompatibility complex class I-restricted antigenic peptides is explained by class I-peptide affinity and is strongly influenced by nondominant anchor residues.* J Exp Med, 1994. **180**(4): p. 1471-83.
116. Yang, X.W., et al., *Coordinated regulation of the immunoproteasome subunits by PML/RARalpha and PU.1 in acute promyelocytic leukemia.* Oncogene, 2014. **33**(21): p. 2700-8.
117. Kalergis, A.M., et al., *Efficient T cell activation requires an optimal dwell-time of interaction between the TCR and the pMHC complex.* Nat Immunol, 2001. **2**(3): p. 229-34.
118. Colf, L.A., et al., *How a single T cell receptor recognizes both self and foreign MHC.* Cell, 2007. **129**(1): p. 135-46.
119. Kuball, J., et al., *Facilitating matched pairing and expression of TCR chains introduced into human T cells.* Blood, 2007. **109**(6): p. 2331-8.
120. Clauss, J., et al., *Efficient Non-Viral T-Cell Engineering by Sleeping Beauty Minicircles Diminishing DNA Toxicity and miRNAs Silencing the Endogenous T-Cell Receptors.* Hum Gene Ther, 2018. **29**(5): p. 569-584.
121. Provasi, E., et al., *Editing T cell specificity towards leukemia by zinc finger nucleases and lentiviral gene transfer.* Nat Med, 2012. **18**(5): p. 807-815.
122. Valitutti, S., et al., *Different responses are elicited in cytotoxic T lymphocytes by different levels of T cell receptor occupancy.* J Exp Med, 1996. **183**(4): p. 1917-21.
123. Braumuller, H., et al., *T-helper-1-cell cytokines drive cancer into senescence.* Nature, 2013. **494**(7437): p. 361-5.
124. Johansson, A., et al., *Tumor-targeted TNFalpha stabilizes tumor vessels and enhances active immunotherapy.* Proc Natl Acad Sci U S A, 2012. **109**(20): p. 7841-6.
125. Kammertoens, T., et al., *Tumour ischaemia by interferon-gamma resembles physiological blood vessel regression.* Nature, 2017. **545**(7652): p. 98-102.
126. Assarsson, E., et al., *A quantitative analysis of the variables affecting the repertoire of T cell specificities recognized after vaccinia virus infection.* J Immunol, 2007. **178**(12): p. 7890-901.
127. Seidel, S.A., et al., *Microscale thermophoresis quantifies biomolecular interactions under previously challenging conditions.* Methods, 2013. **59**(3): p. 301-15.
128. Bowerman, N.A., et al., *Different strategies adopted by K(b) and L(d) to generate T cell specificity directed against their respective bound peptides.* J Biol Chem, 2009. **284**(47): p. 32551-61.
129. Zhang, S.Q., et al., *Direct measurement of T cell receptor affinity and sequence from naive antiviral T cells.* Sci Transl Med, 2016. **8**(341): p. 341ra77.
130. Wang, S., et al., *Analyzing the effect of peptide-HLA-binding ability on the immunogenicity of potential CD8+ and CD4+ T cell epitopes in a large dataset.* Immunol Res, 2016. **64**(4): p. 908-18.
131. Schmidt, J., et al., *In-silico and cell-based analyses reveal strong divergence between prediction and observation of T-cell-recognized tumor antigen T-cell epitopes.* J Biol Chem, 2017. **292**(28): p. 11840-11849.

132. Grupp, S.A., et al., *Chimeric antigen receptor-modified T cells for acute lymphoid leukemia.* N Engl J Med, 2013. **368**(16): p. 1509-1518.
133. Chen, W., et al., *Changes at peptide residues buried in the major histocompatibility complex (MHC) class I binding cleft influence T cell recognition: a possible role for indirect conformational alterations in the MHC class I or bound peptide in determining T cell recognition.* J Exp Med, 1993. **177**(3): p. 869-73.

Appendix

TCRF5.4 Nucleotide Sequence

TCRF5.4

DNA Sequence: Variable beta chain; codon optimized; murine constant beta chain

ATGGGATTTCGCCTGCTGTGCTGCGTGGCATTCTGCCTGCTGGGAGCAGGACCAGTTGATAGCGGCGTCACCCAGACACC
CAAACACCTGATTACTGCTACCGGGCAGCGCGTGACCCTGCGTTGTAGTCCACGGTCAGGAGACCTGTCAGTTTATTGGTA
CCAGCAGAGCCTGGATCAGGGTCTGCAGTTCCTGATCCAGTATTACAACGGGGAAGAGCGTGCAAAGGGAAATATTCTG
GAGCGGTTTTCCGCGCAGCAGTTCCCCGACCTGCATTCTGAACTGAACCTGTCCTCTCTGGAGCTGGGGGATAGTGCCCTG
TATTTTTGCGCTAGTTCAGTCGTCCGCAGCACTGACACCCAGTACTTCGGCCCGGGTACTAGACTGACAGTGCTGGAAGAT
CTACGCAACGTGACCCCACCCAAAGTCAGCCTGTTTGAACCGTCCAAGGCCGAGATTGCTAACAAACAGAAGGCCACCCT
GGTGTGCCTGGCTCGCGGCTTTTTCCCTGACCACGTGGAACTGTCCTGGTGGGTTAACGGCAAAGAGGTGCATAGCGGTG
TTTCCACAGATCCACAGGCCTACAAGGAATCTAATTATAGTTACTGCCTGAGCTCCCGGCTGAGAGTGTGCGCTACCTTCTG
GCACAACCCAAGAAATCATTTTCGCTGTCAGGTTCAGTTCCACGGCCTGAGTGAAGAGGACAAATGGCCCGAAGGTTCAC
CGAAGCCTGTTACACAGAATATCAGCGCAGAGGCATGGGGAAGAGCAGATTGTGGTATTACTTCAGCGAGCTATCATCAG
GGCGTGCTGAGCGCAACCATCCTGTACGAGATTCTGCTGGGTAAAGCGACACTGTATGCGGTCCTGGTCAGCGGGCTGGT
CCTGATGGCAATGGTCAAAAAGAAAAATAGC

DNA Sequence: Variable alpha chain; codon optimized; murine constant alpha chain

ATGATGAAATCACTGAGGGTCCTGCTGGTCATCCTGTGGCTGCAGCTGTCCTGGGTGTGGAGTCAGCAGAAAGAGGTCGA
GCAGAACTCAGGACCACTGAGCGTGCCAGAGGGAGCAATCGCTAGCCTGAACTGCACATACTCCGATCGGGGATCTCAGA
GTTTCTTTTGGTACAGACAGTATAGTGGCAAGTCACCAGAGCTGATCATGAGCATCTACTCCAACGGGGACAAGGAAGAT
GGAAGGTTCACCGCTCAGCTGAACAAGGCATCCCAGTACGTGAGCCTGCTGATTCGCGACTCTCAGCCCTCAGATAGCGC
CACTTACCTGTGCGCTGTGGTCAGCGGCGGGTATCAGAAGGTGACCTTTGGAACCGGCACAAAACTGCAGGTCATCCCCA
ACATTCAGAATCCCGAGCCTGCCGTGTACCAGCTGAAAGACCCTCGATCTCAGGATAGCACCCTGTGCCTGTTCACAGACT
TTGATTCTCAGATCAATGTGCCTAAGACCATGGAAAGTGGGACATTCATTACTGACAAAACCGTCCTGGATATGAAGGCCA
TGGACTCCAAATCTAACGGCGCAATCGCCTGGAGTAATCAGACATCATTCACTTGTCAGGATATCTTCAAGGAAACAAACG
CATGCTATCCTAGCTCCGACGTGCCATGTGATGCCACTCTGACCGAGAAAAGCTTCGAAACTGACATGAACCTGAATTTTC
AGAATCTGTCCGTCATGGGCCTGAGAATCCTGCTGCTGAAGGTCGCTGGGTTTAATCTGCTGATGACTCTGCGGCTGTGGT
CCTCC

Acknowledgments

An erster Stelle möchte ich Prof. Dr. med. Angela Krackhardt für die ausgezeichnete Betreuung und Ihre großartige Unterstützung während dieser aufregenden Zeit danken. Besonders auch dafür, dass Sie neben Ihrer klinischen Arbeit immer Zeit gefunden hat mir mit inspirierendem Rat und Tat zur Seite zu stehen.

Danke auch an Prof. Dr. med. Christian Peschel für die Bereitstellung der notwendigen Infrastruktur innerhalb der III. Medizinischen Klinik.

Weiteren Dank möchte ich auch Prof. Iris Antes und Dr. Manuel Glaser für die großartige Zusammenarbeit, besonders am Ende des Projects, aussprechen. Zahlreiche intensive Treffen, Anregungen und Diskussionen haben die exzellente Qualität der Modelling Ergebnisse erst möglich gemacht.

Großer Dank gilt auch Prof. Dr. med. Dirk Busch und seinem Labor. Hier danke ich besonders Manuel Effenberger für die Zusammenarbeit und die zahlreichen wissenschaftlichen, aber auch persönlichen Gespräche.

Danken möchte ich auch Matteo Pecoraro vom Max-Planck-Institut für Biochemie für die angenehme Zusammenarbeit und die Durchführung der Massenspektrometrie und Josef Mautner vom Helmholtz-Zentrum für das freundliche Mentoring.

Vielen Dank auch an Nicole Abbrederis und Almut Barden für die freundliche Unterstützung und das Beantworten zahlloser Fragen rund um das PhD-Programm.

Ein ganz herzlicher Dank geht an das gesamte Team der AG Krackhardt. Besonders möchte ich Stephanie Rämisch, Richard Klar, Sabine Mall und Eva Bräunlein für Ihre wertvolle Unterstützung und Freundschaft danken.

Abschließend möchte ich meiner Familie für die unendliche Geduld und Rücksichtnahme während der Promotion danken und dafür, dass Sie immer für mich da waren.